UNIVERSITÄT
DUISBURG
ESSEN

Offen im Denken

Assessment of the impact of deregulated signal transduction pathways on the radiotherapy response of non-small-cell lung cancer

Inaugural-Dissertation

zur

Erlangung des Doktorgrades

Dr. rer. nat.

der Fakultät für Biologie

an der Universität Duisburg-Essen

vorgelegt von

Sarah Alexandra Wieczorek

aus Bochum

November 2015

Die der vorliegenden Arbeit zugrunde liegenden Experimente wurden im Labor für Molekulare Onkologie der Inneren Klinik (Tumorforschung) am Universitätsklinikum Essen durchgeführt.

1. Gutachter: Prof. Dr. Martin Schuler
2. Gutachter: Prof. Dr. George Iliakis

Vorsitzende des Prüfungsausschusses: Prof. Dr. Verena Jendrossek

Tag der mündlichen Prüfung: 18.01.2016

Results of this thesis work are part of a manuscript, which has been submitted for publication.

Table of contents

1 Abstract

Lung cancer is the leading cause of cancer-related death worldwide. Approximately 85 % of all lung cancers are histologically grouped as non-small-cell lung cancer (NSCLC). Besides surgery and chemotherapy, radiotherapy is firmly established as an important modality in curative treatment of localized as well as locally advanced NSCLC and in palliative care. Nevertheless, systemic and localized relapse is frequently observed. Recent developments have led to a more refined typing of advanced NSCLC by incorporating biomarkers of oncogenic pathway activation. This has allowed the successful introduction of "targeted pharmacotherapies" that are better tailored towards biological differences between histologically uniform NSCLC entities. In contrast, radiotherapy still does not take advantage of biological disease heterogeneity, and radiosensitization protocols are empirically derived, rather than based on validated biomarkers.

Against this background, it was hypothesized that an improved understanding of the modulation of the radiotherapy response of NSCLC by signal transduction pathways may open new avenues for the development of more specific protocols to combine radiotherapy with pharmacotherapies. To this end, a systematic assessment of the functional impact of selected regulators of apoptosis, oncogenes, and signal transduction mediators on irradiation-induced cell death was initiated in a small-scale screen of lung cancer models.

Anti-apoptotic members of the BCL-2 family have been selected as the first group of potential biomarkers for the radiotherapy response in NSCLC. BCL-xL as well as MCL-1 conferred resistance against irradiation in A431 cells. Expression of both modulators led to decreased radiation-induced cell death and additionally gave a competitive edge in clonogenic survival *in vitro*. Studies obtained by radiation therapy of tumor-bearing mice *in vivo* supported the relevance of BCL-xL for radioresistance in an organismal context. Surprisingly, these findings were not convincingly explained by BCL-xL and MCL-1 mediating radioresistance by inhibition of apoptosis, as radiotherapy induced only negligible amounts of apoptosis. Also no impact of BCL-xL on cell cycle kinetics following irradiation was observed. Studying the influence of BCL-xL on deoxyribonucleic acid (DNA) double-strand break (DSB) repair pathways as a potential effector mechanism revealed that BCL-xL-mediated radioresistance relied on functional homologous

recombination repair (HRR) and involved enhanced repair through error-prone alternative end-joining (alt-EJ). This led to the propagation of cells with gross chromosomal aberrations, possibly promoting survival of more resistant and aggressive lung cancer subclones. To circumvent this, combining irradiation with targeted therapies against anti-apoptotic BCL-2 family members was suggested as a useful strategy. Thus, BCL-xL and/or MCL-1 were antagonized on a genetic or functional level. These strategies, including shRNA-mediated knockdown, conditional overexpression of pro-apoptotic BAK, as well as pharmacological treatment with BH3-mimetics, sensitized lung cancer cells to radiotherapy. Based on this, it is proposed to select patients with high expression of the respective drug targets in recent tumor biopsies for clinical proof-of-principle studies combining radiotherapy with pharmacologic antagonists of the BCL-2 family such as Navitoclax.

The signal transduction mediator RAF-1 was identified as the second potential biomarker for the radiotherapy response in NSCLC. Conditional activation of RAF-1 reduced the number of irradiation-induced cell death significantly. Clonogenic survival could not be evaluated as RAF-1 activation itself inhibited colony formation in general, possibly due to induction of a cell cycle arrest or senescence. It was further shown that activation of RAF-1 even after irradiation had still radioprotective effects. The underlying mechanisms remain to be elucidated in technically more appropriate models, in particular *in vivo*.

In conclusion, two modulators of the radiotherapy response in NSCLC were identified and functionally validated. In addition, targeting non-apoptotic functions of BCL-2 family proteins was nominated as a novel strategy for biologically rational radiosensitization protocols.

2 Introduction

Every year, about 1.8 million people are diagnosed with lung cancer. Therewith, it is the most common type of cancer worldwide with highest estimated age-standardized incidence rates in Central and Eastern Europe as well as Eastern Asia (Ferlay et al. 2013). Furthermore, lung cancer is the leading cause of cancer-related death worldwide, estimated to be responsible for nearly one in five (Ferlay et al. 2013). Approximately 85 % of all lung cancers are histologically grouped as non-small-cell lung cancer (NSCLC) with adenocarcinoma being the predominating subtype. The 5-year survival rate for lung cancer is 17 % on average. Localized stages have a 5-year survival of 54 %, but only 15 % are diagnosed at those stages. 57 % of all cases are diagnosed at distant stages and have a 5-year survival rate of only 4 % (American Cancer Society 2015). This emphasizes the significance of research in the field of lung cancer treatment.

The following chapters present current treatment concepts for NSCLC and the molecular basics for radiotherapy. Here, radiation physics, the significance of double-strand breaks (DSBs), and different mechanisms for repairing those lethal lesions are outlined. This provides the theoretical framework for this thesis. In addition, two modulators of radiotherapy response that have been identified in this work, namely members of the BCL-2 family and the regulator of signaling RAF-1, are described in detail.

2.1 Current treatment of non-small-cell lung cancer (NSCLC)

Current treatment of NSCLC includes surgery, radiotherapy, chemotherapy, and/or targeted therapies. Surgery is usually the treatment of choice for NSCLC diagnosed at an early stage (stages I/II and IIIA), and is often combined with adjuvant chemotherapy. Inoperable early stage tumors are typically treated with radiotherapy (Goeckejan et al. 2010). Advanced stages of NSCLC are usually treated with multimodal strategies including chemotherapy, radiotherapy, and targeted drugs (American Cancer Society 2015; Goeckejan et al. 2010). Combined chemoradiotherapy protocols are frequently applied, as some chemotherapeutics (e.g. platinum derivates) were shown to have radiosensitizing effects (reviewed in Kvols 2005). These combined chemoradiotherapy strategies can lead to response

rates of up to 50 %, however they are often accompanied by increased acute or chronic side effects, and relapse is frequently observed. Consequently, the 5-year survival rate is only marginally increased (Wagner & Yang 2010).

Molecular stratification of individual tumors has become an important topic in NSCLC in the last years. Several driver mutations determining multiple subgroups have been identified by comprehensive genomic analyses (Weir et al. 2007; Ding et al. 2008; Pao & Girard 2011). These findings led to the successful introduction of targeted pharmacotherapies as an important modality in NSCLC treatment (Paez et al. 2004; Kwak et al. 2010; Mok et al. 2009; Stöhlmacher-Williams 2012). Thus, therapy decisions are not only based on staging, additional diseases, and the overall condition of a patient any more (Ausborn et al. 2012), but molecular characteristics of tumors define the application of targeted drugs.

One example for treatment based on molecular characteristics are tumors with activating mutations in the epidermal growth factor receptor (EGFR), which are found in 10 - 40 % of all NSCLC patients (Kosaka et al. 2004; Paez et al. 2004; Shigematsu et al. 2005). In 2004, Paez and colleagues demonstrated that response to the EGFR tyrosine kinase inhibitor (TKI) gefitinib is associated with mutations in EGFR (Paez et al. 2004). Even more impressively, it was not only shown that patients with EGFR mutations in their tumors have a better outcome when treated with EGFR TKI (like gefitinib, erlotinib), but patients which are negative for EGFR mutations show a better survival when treated with standard carboplatin-paclitaxel chemotherapy (Mok et al. 2009; Maemondo et al. 2010; Mitsudomi et al. 2010; Fukuoka et al. 2011; Rosell et al. 2012). This is an excellent example for the importance of molecular stratification for treatment decisions.

Besides impressive initial responses of stratified tumors to targeted therapies, tumor control is only transient and localized as well as systemic relapse are frequently observed. This has been linked to acquisition of additional mutations in the drug target, thereby making the drug ineffective, or activation of other signaling pathways, which promote tumor progression (Yu et al. 2013). Thus, there is an urgent need to develop new, more efficient treatment strategies, which also provide a long-term survival benefit.

2.1.1 Strategies to improve radiotherapy with targeted drugs

Radiotherapy is an important modality for curative treatment of localized and locally advanced NSCLC as well as in palliative care. For curative treatment, either conventional radiotherapy (> 60 Gy total dose, 1.8 to 2 Gy per day, 5 fractions per week) or continuous, hyperfractionated, accelerated radiotherapy (CHART, 54 Gy total dose, 3 x 1.5 Gy per day on 12 consecutive days) are applied. In palliative care, conventional as well as different hypofractionated radiotherapy protocols are used depending on general condition and symptoms of the patient (Goeckejan et al. 2010). Major limitations of current radiotherapy lie in normal tissue toxicity and standard protocols are already administered at the maximum-tolerated doses (Morgan et al. 2014). Two strategies are feasible to improve radiotherapy: either protecting normal tissue, or sensitizing tumor cells. Both approaches are expected to broaden the therapeutic window.

As radiotherapy response of several tumor entities, including NSCLC, is highly heterogeneous, even in clinically and histologically similar tumors, it was hypothesized that genetic and epigenetic processes define the tumor's radiosensitivity (Das et al. 2010). In the last decade, molecular signatures of radiation response have been investigated tremendously. However, there are no validated biomarkers available in NSCLC, yet (Ausborn et al. 2012). Most present pre-clinical strategies target either DNA damage response (e.g. via CHK-1 or PARP-1) or signaling pathways, with EGFR being extensively investigated. Inhibition of EGFR by ZD1839 (Iressa, TKI), erlotinib (TKI) or cetuximab (antibody) mediated radiosensitization of tumor cells *in vitro* and *in vivo* (Bianco et al. 2002; Chinnaiyan et al. 2005; Wang et al. 2011). However, initial clinical trials have rather not been successful. Combination of chemoradiotherapy and anti-EGFR monoclonal antibodies (e.g. cetuximab) did not result in survival benefit and similarly, the combination with EGFR TKI (e.g. gefitinib, erlotinib) only showed marginal advantages which were partially accompanied by severe side effects (reviewed in Zhuang et al. 2014).

The major issues of clinical trials with combined treatment modalities are patient selection, scheduling and dose of applied therapies, as well as therapy duration. Thus, preclinical testing of those parameters and also understanding the molecular

mechanisms of radioresistance are a prerequisite of successful future clinical trials for biomarker-driven protocols.

2.2 Ionizing radiation, DNA damage, and double-strand break (DSB) repair

DNA damage is one major issue a cell has to cope with every day, as cellular survival highly depends on the integrity of the carrier of genetic information. Modifications and lesions in the DNA occur from physical as well as chemical environmental agents, intracellular oxidative stress (as a product of metabolism), and scheduled biological processes like DNA replication or V(D)J recombination (Mladenov & Iliakis 2011a). The steady-state background of endogenous DNA lesions is thought to be at least 50,000 in every cell per day (Swenberg et al. 2011). To ensure survival nonetheless, cells have evolved a variety of mechanisms to repair those modifications and lesions (reviewed in Sancar et al. 2004). As the majority of those damages are abasic sites or base modifications (Swenberg et al. 2011), there is still an undamaged complementary strand in the DNA double helix available, which can serve as a template for repair and facilitates rather easy repair.

Ionizing radiation (IR) exposure with a dose of 1 Gy results in only 1000 single-strand breaks (SSBs), a similar number of base lesions, and about 20 - 40 double-strand breaks (DSBs) per cell (Ward 1990). In contrast to the everyday DNA damage, this number of lesions is rather small. Nevertheless, normal cells frequently die from this damage. The reason for this is that those damages are not homogenously distributed among the whole genome, but occur as clustered and complex damage sites. This is a unique characteristic of IR (Mladenov & Iliakis 2011a) and is caused by its physical features.

2.2.1 Physical background of ionizing radiation (IR)

Radiation is defined as energy that was emitted from a source and travels through space or mass of matter. If the energy of radiation is enough to free electrons from atoms and molecules, this radiation is termed ‚ionizing', as a target becomes

charged or ionized by this type of radiation (Hall & Giaccia 2006). Chemically, emerging electron loss is equivalent to oxidation (Mladenov & Iliakis 2011a). The unit of IR is Gray (Gy) with 1 Gy corresponding to 1 J/kg (Hall & Giaccia 2006).

IR is generated by either electromagnetic waves of short wave length and high frequency (like X-rays and γ-rays, which were used in this thesis) or particles (like electrons, protons, α-particles, neutrons, or heavy ions). IR is subclassified into 'directly ionizing' and 'indirectly ionizing'. Only electrically charged particles are directly ionizing, meaning that they carry enough energy to directly interact with atomic electrons through coulombic forces, thereby disrupting the atomic structure of the absorber and producing chemical or biological changes (Hall & Giaccia 2006). Radiation that is indirectly ionizing is not able to directly interact with atomic electrons, as it is electrically neutral. However, collision with atomic nuclei produces charged particles, which cause ionization in a second step. This process is called linear energy transfer (LET). LET is defined as energy of an ionizing particle transferred to material along the track (keV/µm) (Seltzer et al. 2011). The main target for LET is water producing hydroxyl radicals (OH•). Two types of LET are distinguished: low LET (sparsely ionizing) and high LET (densely ionizing). X-rays and γ-rays show mostly low LET, in contrast to this e.g. α-particles possess high LET features (Hall & Giaccia 2006). In general, high LET causes more biological effects than low LET (Kadhim et al. 2006). A reason for this might be that radiation with high LET produces very large energy depositions in target structures, which is unachievable by x- and γ-rays (Goodhead & Nikjoo 1989). This indicates that IR with low and high LET differ in their track structures (Figure 1). Densely ionizing charged particles as well as electrons at the end of their track show increased ionization events in a rather small volume (Nikjoo et al. 1994; Nikjoo & Goodhead 1991).

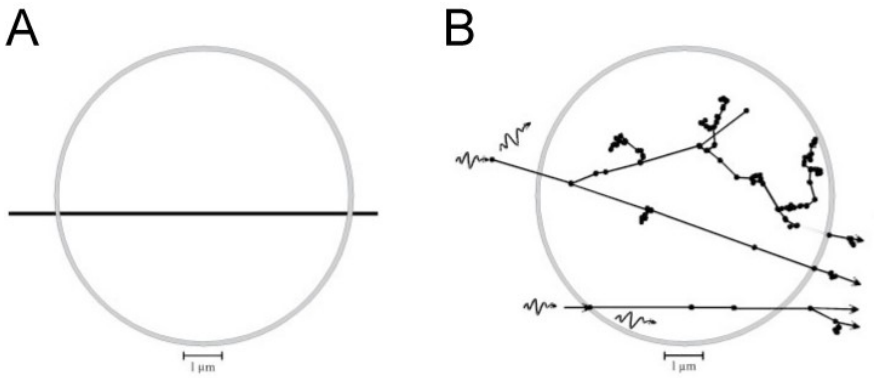

Figure 1: Schematic drawing of IR tracks through a cell nucleus. (A) High LET track (e.g. from α-particles). A dose of 1 Gy corresponds to 3 to 4 tracks. **(B)** Low LET tracks (e.g. from X-ray or γ-rays). A dose of 1 Gy corresponds to about 1000 tracks (modified from Kadhim et al. 2006).

2.2.2 Double-strand breaks (DSBs) and their repair

As described above, the unique characteristic of IR is the generation of complex and clustered DNA damage. Severity of those clustered lesions comes from their reduced reparability compared to individual lesions (Lomax et al. 2013; Eccles et al. 2011) and from the finding that multiple lesions affecting both DNA strands and localizing in close proximity (within one helical turn) are highly prone to generate additional DSBs. Early studies already termed DSBs to be the 'lesions most likely to be the cause of lethal effects of ionizing radiation' (Ward 1990). This type of lesions is defined as a break in the phosphodiester backbone of both DNA strands separated by about 10 base pairs or less (Lomax et al. 2013; Hanai et al. 1998). Three main scenarios are known that contribute to DSB formation: 1) close proximity of two SSBs, which form DSBs promptly, 2) chemical processing of sugar lesions, which in their initial form do not disrupt the sugar-phosphate backbone, and 3) enzymatic processing of nearby base damage (Mladenov & Iliakis 2011a). DSBs are the most severe form of DNA damage for two reasons: first, because they are difficult to repair due to the lack of an intact template strand, and second, because they disrupt the continuity of the DNA molecule, thereby also destabilizing surrounding chromatin and endangering loss of genetic information (Mladenov & Iliakis 2011a).

To allow efficient removal of those complex lesions, repair has to be coordinated with other cellular processes. This coordination is triggered by the DNA damage response (DDR) and is essential for genomic stability as well as cell survival

(Kastan 2008). It comprises a multistep process of sensing DNA damage (especially DSBs), signaling damage to downstream pathways, and mediating cellular response (Zhou & Elledge 2000). The major players in sensing DNA damage are phosphatidylinositol 3-kinase-related kinases (PIKK) including DNA-dependent protein kinase (DNA-PK), ataxia telangiectasia-mutated (ATM), and ATM and Rad3-related (ATR), which are recruited to damage sites by protein-protein interactions (Sirbu & Cortez 2013). All downstream processes are regulated by posttranslational modifications (like acetylation, ubiquitinylation, and especially phosphorylation) and protein-protein interactions. DDR includes local as well as global changes within the cell and provides an environment for efficient repair. It induces chromatin-remodeling to create a permissive local environment around the damage to enable repair. Additionally, it impacts several components of global cell metabolism, thereby changing transcription, chromosome mobility, and deoxynucleotide (dNTP) levels (Sirbu & Cortez 2013). However, the major contribution of DDR is inhibition of cell cycle progression and induction of programmed cell death (apoptosis), if damaged sites cannot be repaired.

Repair of DSBs comprises highly sophisticated machineries. This is necessary as unrepaired or misrepaired DSBs entail severe consequences for the cell. Unrepaired DSBs can induce permanent cell cycle arrest, apoptosis, or another type of cell death (Olive 1998), while misrepair can cause mutations, chromosome rearrangements, and carcinogenesis (Jackson 2002). Currently, three major repair pathways for DSBs, namely homologous recombination repair (HRR), classical non-homologous end-joining (c-NHEJ), and alternative end-joining (alt-EJ) are known and will be described in a simplified form in the next sections.

2.2.2.1 Homologous recombination repair (HRR)

As already indicated by its name, HRR utilizes homologous DNA strands to repair, which enables error-free repair (Mladenov & Iliakis 2011a). It operates in a cell cycle dependent manner, because it uses the sister chromatid as the homologous segment and this is only available during late S and G2 phase of the cell cycle (Lee et al. 1997; Krüger et al. 2004). There is evidence that HRR does not only repair DSBs, but is also involved in other processes such as repair of DNA-protein

crosslinks (Ide et al. 2008) as well as restart and repair of stalled replication forks (Petermann et al. 2010).

The HRR pathway operates with rather slow kinetics (Mao et al. 2008) and consists of five major steps: 1) DNA end-resection to form single-stranded DNA (ssDNA) overhangs, 2) stabilization of ssDNA, 3) search for the homologous segment and subsequent invasion into the intact strand to form a 'Holiday junction', 4) DNA synthesis, and 5) final resolution of the strands. Figure 2 presents those steps in detail including the involved proteins.

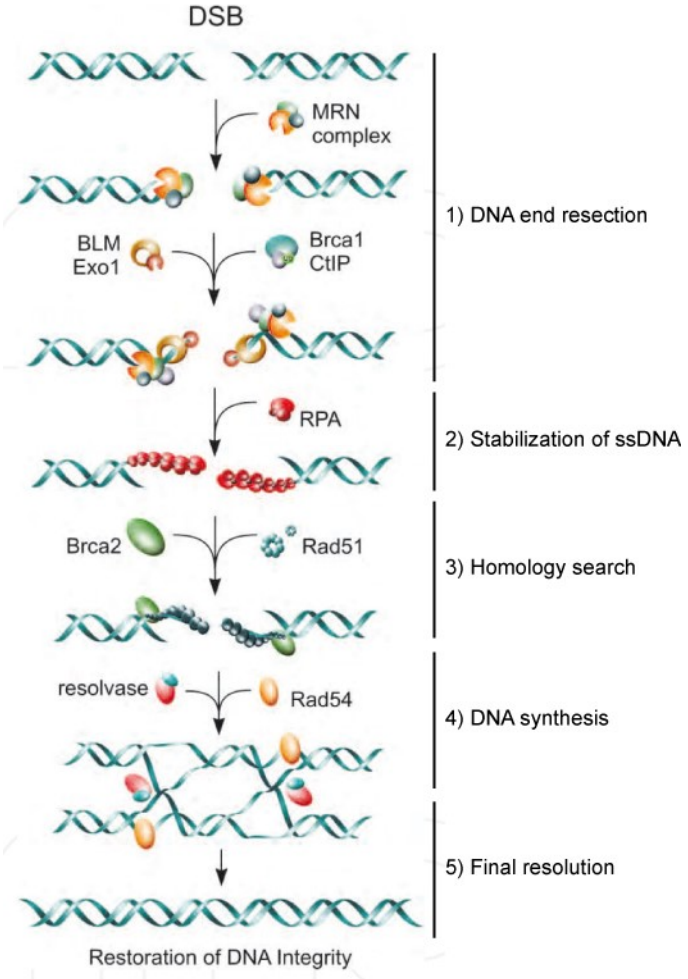

Figure 2: Schematic drawing of HRR pathway. The five key steps of HRR are presented including proteins involved in these processes (modified from Mladenov & Iliakis 2011b).

1) DNA end-resection

The first step of HRR is mediated by binding of the MRN complex to the break (reviewed in Stracker & Petrini 2011). This complex comprises meiotic recombination 11 (MRE11), RAD50, and Nijmegen breakage syndrome 1 (NBS1).

It induces recruitment of C-terminal binding interacting protein (CtIP) (Sartori et al. 2007), Bloom's syndrome protein (BLM) (Nimonkar et al. 2008), exonuclease 1 (Exo1) (Nimonkar et al. 2008), and breast cancer 1 (BRCA1) (Moynahan et al. 1999). The conjunction of all those proteins removes terminal nucleotides at the 5'-ends on both sides of the break, thereby producing long 3'-ssDNA overhangs (Paull & Gellert 1998).

2) Stabilization of ssDNA

To stabilize the processed ssDNA, replication protein A (RPA) heterodimers bind to the 3'-overhangs. This protects ssDNA from degradation and prevents formation of secondary structures (Wold 1997; Sleeth et al. 2007; Fanning et al. 2006). Besides its direct function in HRR, RPA also initiates the DNA damage response (DDR) by recruiting the ATR / ATR-interacting protein (ATRIP) complex, which induces cell cycle arrest (Cimprich & Cortez 2008; Zegerman & Diffley 2009).

3) Homology search

The search for the homologous strand during HRR is mainly promoted by RAD51. Therefore, RAD51 has to be recruited to RPA-covered ssDNA overhangs. To this end, BRCA1, which has bound to the break in the first step, recruits BRCA2, which confers RAD51 loading (Thorslund & West 2007). This process is supported by RAD51 paralogs, like RAD52 (Mortensen et al. 2009). By this, a RAD51 nucleoprotein filament is formed and serves as the basis for the homology search reaction. After finding the homologous DNA strand, the filament, in interaction with RAD54, promotes chromatin remodeling, unwinding of duplex DNA, and strand invasion to form a 'Holliday junction' (Mazin et al. 2010).

4) DNA synthesis

In the created Holiday junction, the RAD51 loaded strand displaces the original strand from the homologous duplex and builds a displacement loop (D-loop) (Jackson 2002; Heyer et al. 2010). This primes for DNA synthesis catalyzed by polymerases, which copy sequence information from the undamaged to the damaged molecule.

5) Final resolution

In the last step of HRR, resolvase protein complexes resolve the holiday junction, anneal the new strand with the original strand (Symington & Holloman 2008; West 2009), and promote ligation, potentially in conjunction with ligases. However, this is still not completely understood. During the final process, gene conversion or crossing over can occur (Mladenov & Iliakis 2011a).

2.2.2.2 Classical non-homologous end-joining (c-NHEJ)

C-NHEJ, which is also often called canonical or DNA-PK-dependent NHEJ (D-NHEJ), is the predominant pathway for DSB repair in mammals (Rothkamm et al. 2003; Mao et al. 2008). Although, it operates with lower fidelity than HRR as it mainly just ligates two locally available DNA ends. However, c-NHEJ accepts a wide range of DNA end substrate configurations, which makes it quite flexible on a mechanistic level (Lieber 2010).

As it does not depend on homologous sequences, it is able to operate throughout the whole cell cycle, but it is not capable to ensure sequence restoration or ligation of the ends of the original DNA. This makes it quite error-prone. Regarding kinetics, c-NHEJ is much faster than HRR with typical half times of 15 - 30 min (Mladenov & Iliakis 2011a; Mao et al. 2008).

C-NHEJ consists of 3 steps: 1) recognition of the break, 2) processing of damaged DNA, and 3) ligation. For a detailed description of involved proteins see Figure 3.

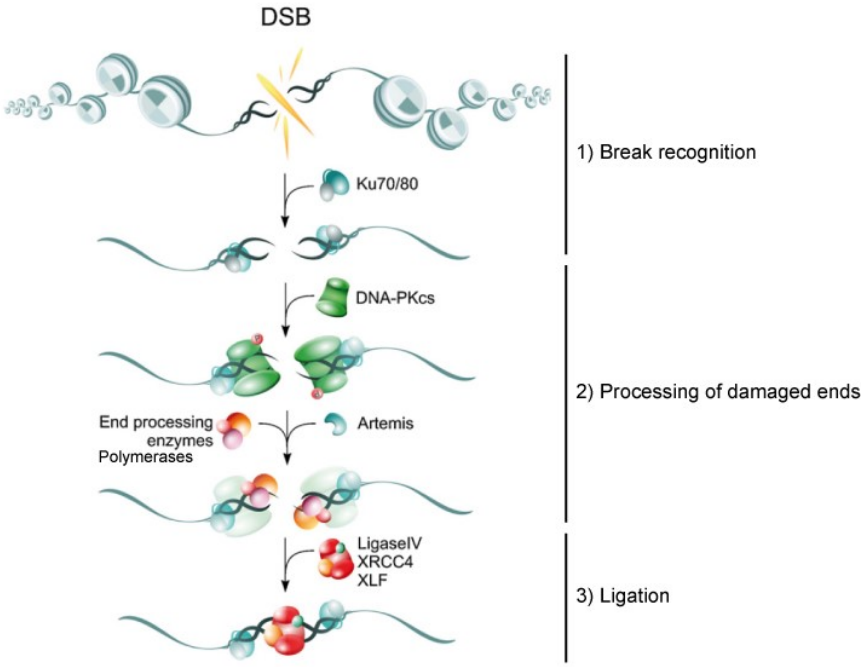

Figure 3: Schematic drawing of c-NHEJ. The three key steps of c-NHEJ are presented including the involved proteins (modified from Mladenov & Iliakis 2011a).

1) Break recognition

C-NHEJ is initiated by binding of the Ku heterodimer, consisting of Ku70 and Ku80, to the DNA ends surrounding the DSB (Mimori & Hardin 1986; Lieber et al. 1997; Lieber 2010).

2) Processing of damaged ends

The Ku heterodimer recruits the catalytic subunit of DNA-dependent protein kinase (DNA-PKcs) to form the active holoenzyme DNA-PK (Gottlieb & Jackson 1993; Meek et al. 2004). This complex attracts and phosphorylates end-processing enzymes, like Artemis, and other substrates. The complex with Artemis possesses nuclease activity to process damaged overhangs (Ma et al. 2002). Additionally, polymerases are recruited to the break to fill in new DNA to generate blunt DNA ends. Polymerases λ and μ seem to be of major importance here, as both are able to bind Ku and are quite flexible in template-dependent as well as -independent DNA synthesis (Lieber 2010).

3) Ligation

In the last step of c-NHEJ, a complex of ligase IV (LigIV), XRCC4, and XRCC4-like factor (XLF) ligate the processed ends to reconstitute integrity of the DNA double-strand (Leber et al. 1998; Ahnesorg et al. 2006).

2.2.2.3 Alternative end-joining (alt-EJ)

In recent years, a third pathway for DSB repair, which seems to function as backup, has been described. This pathway is based on end-joining activities and is therefore often termed alternative end-joining (alt-EJ) pathway. The major finding contributing to this new pathway was that c-NHEJ mutants were still able to repair DSBs although HRR-related proteins were not active (Dibiase et al. 2000; Wang et al. 2003; Iliakis et al. 2004). C-NHEJ and possibly also HRR suppress alt-EJ (Perrault et al. 2004). Thus, alt-EJ seems to gain functional relevance when these standard repair processes fail, globally or locally (Dueva & Iliakis 2013), which provides its backup character.

Alt-EJ is operating much slower than c-NHEJ with typical half times of 0.5 to 20 h. Theoretically, alt-EJ is able to operate throughout the whole cell cycle as homologous sequences are not required. However, it was shown that repair of DSBs by alt-EJ is enhanced in G2 and reduced or abrogated in G1 and resting cells, respectively (Wu, Wang, Mussfeldt, et al. 2008; Wu, Wang, Wu, et al. 2008). Additionally, there are some studies that claim preferential use of microhomologies by alt-EJ pathways (Kabotyanski et al. 1998; Verkaik et al. 2002). As c-NHEJ mutants show increased levels of irradiation-induced chromosomal aberrations, alt-EJ is suggested to be highly error-prone (Virsik-Köpp et al. 2003).

Several factors contributing to alt-EJ have been identified, which gave rise to the hypothesis that there are several sub-pathways, which compete at each DSB by yet undefined parameters (Dueva & Iliakis 2013). Figure 4 presents one concept of alt-EJ, which consists of a two-step process including 1) recognition of the break and 2) ligation. However, further research is needed to define the precise mechanisms of alt-EJ.

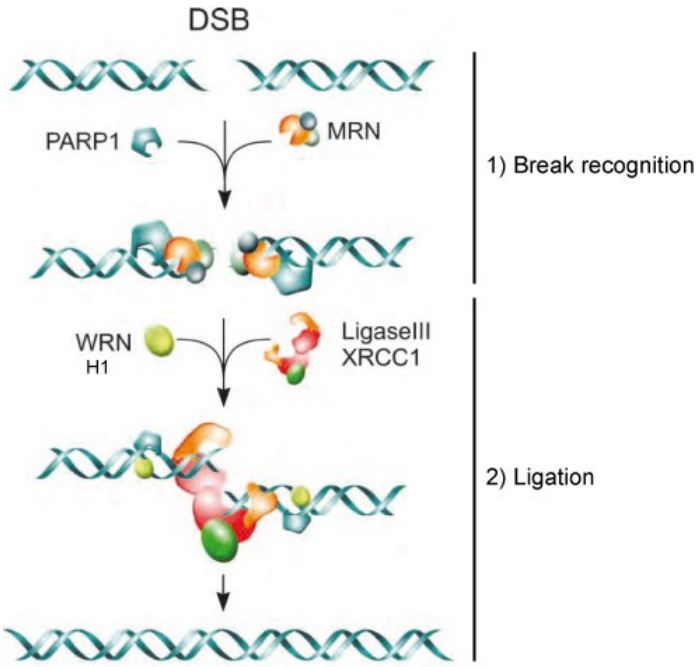

Figure 4: Schematic drawing of alt-EJ. The two key steps of alt-EJ are presented including the known main players (modified from Mladenov & Iliakis 2011b).

1) Break recognition

During alt-EJ, PARP-1 recognizes and binds DSBs in the first step (Wang et al. 2006; Audebert et al. 2006; Audebert et al. 2008). Potentially, also the MRN complex is involved here, as inhibition of MRE11 in c-NHEJ mutants decreases end-joining frequency (Dinkelmann et al. 2009; Rass et al. 2009). Those factors might promote DNA end processing before ligation.

2) Ligation

The ligation step is executed by a complex of XRCC1 and Ligase III, which is regulated by PARP-1 (Audebert et al. 2004; Della-Maria et al. 2011). There is also evidence for involvement of histone 1 (H1), which enhances PARP-1 activity (Rosidi et al. 2008), and Werner syndrome proteins (WRN) (Sallmyr et al. 2008).

2.2.2.4 Determinants for DSB repair pathways choice

Pathway choice for DSB repair is an important topic of current research and only the surface of this research area will be touched in the following section.

As described above, there are three main pathways (HRR, c-NHEJ, and alt-EJ) that compete for DSB repair. However, contribution of each pathway for overall

repair of DSBs is not equal and depends on several factors, like expression and phosphorylation of repair proteins, chromatin modulation for repair factor accessibility, availability of homologous templates, and probably also complexity of the damage. Furthermore, there are also differences in pathway choice among different species and cell types. However, in many cell types of higher eukaryotic cells, the major repair pathway is c-NHEJ (Shrivastav et al. 2008; Rothkamm et al. 2003; Mao et al. 2008).

The most obvious determinant of pathway choice is the cell cycle as HRR needs a homologous template for its repair processes. Thus, HRR is upregulated during S and G2 phase when a sister chromatid is available. Nevertheless, end-joining pathways also remain active in those phases of the cell cycle (Shrivastav et al. 2008; Takata et al. 1998). In contrast, both end-joining pathways repair homology-independently and can operate theoretically throughout the whole cell cycle.

Besides physical determination of pathway choice throughout the cell cycle, the main cell cycle regulators, cyclin-dependent kinases (CDKs), were also shown to regulate repair pathways. For example, BRCA2 gets phosphorylated at Ser3291 by CDKs in M phase, which blocks the interaction between BRCA2 and RAD51 leading to downregulation of HRR (Esashi et al. 2005). However, mechanisms of DDR are able to bypass this cell cycle dependent phosphorylation of BRCA2 after irradiation (Shrivastav et al. 2008). c-NHEJ is also phosphorylated in a cell cycle dependent manner. For example, irradiation-induced autophosphorylation of Ser2056 and Thr2609, which is essential for c-NHEJ, is reduced in S phase cells (B. P. C. Chen et al. 2005).

Additionally, direct competition and protein interaction are suggested as other determinants of pathway choice. In line with the competition model is the finding that cells with mutant c-NHEJ are still able to repair DSBs, yet with slower kinetics and repair defects (Dibiase et al. 2000), which was later found to be executed by alt-EJ (Wang et al. 2003). Other groups also observed an increase in HRR in c-NHEJ defective cells (Shrivastav et al. 2008; Pierce et al. 2001; Delacôte et al. 2002). Another study presents direct competition of PARP-1 (involved in alt-EJ) and Ku (involved in c-NHEJ) for DSB ends (Wang et al. 2006). As Ku has a higher affinity to DSBs than PARP-1, c-NHEJ wins this competition under normal conditions and provides the kinetic basis for the backup character of alt-EJ (Mladenov & Iliakis 2011a). Moreover, the main players of alt-EJ (e.g. PARP-1 and

LigIII) are also involved in repair of other lesions (e.g. SSBs, base damage), which are induced upon irradiation to a much higher extent than DSBs (Mladenov & Iliakis 2011a) and therewith might be an explanation for the non-dominating role of alt-EJ.

Another suggested central regulator of pathway choice is DNA-PKcs. Controversially, elimination of DNA-PKcs increases HRR (Allen et al. 2002), while inhibition of DNA-PKcs decreases HRR (Allen et al. 2003). An explanation for this could be that inhibited DNA-PKcs is still capable of binding to DNA ends and therewith, blocking access of other repair factors (Shrivastav et al. 2008).

Other potential contributors to pathway choice are highly suggest to exist, but will go beyond the scope of this thesis. In summary, pathway choice seems to be performed by a complex network of different determinants, and the exact mechanisms are not yet understood.

2.3 BCL-2 family

Programmed cell death (apoptosis) is an essential cellular process for development, tissue homeostasis, and immunity (Czabotar et al. 2014). Deregulation of this process can result in degenerative conditions (if cell death is increased) or cancer as well as autoimmune diseases (if cell death is prevented) (Cory et al. 2003). The central regulators of apoptosis are proteins of the B-cell lymphoma 2 (BCL-2) family (Danial & Korsmeyer 2004). This protein family comprises death-promoting as well as death-inhibiting factors and the interplay between those opposing family members defines cellular susceptibility to undergo apoptosis upon insults (Lee et al. 1999; Cory et al. 2003; Danial & Korsmeyer 2004). Three different subgroups, which share a varying degree in structural and sequence homology, are known: BCL-2-like survival factors, pro-apoptotic effector proteins, and pro-apoptotic BCL-2 homology 3 (BH3)-only proteins (for details see 2.3.1, 2.3.2, and 2.3.3, respectively). The first two subgroups share four BCL-2 homology (BH) domains (BH1 - BH4), while BH3-only proteins just have the BH3 domain in common with other family members (e.g. Boyd et al. 1995) (Figure 5). Additionally, all BCL-2 family members share a transmembrane (TM) region, which targets those proteins to the outer mitochondrial membrane (Moldoveanu et al. 2014).

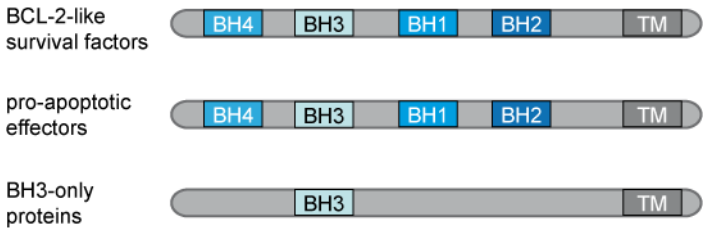

Figure 5: Schematic drawing of sequence homology of different BCL-2 subgroups. All BCL-2 family members share the transmembrane-targeting domain (TM) and the BCL-2 homology 3 domain (BH3). Additionally, BCL-2-like survival factors and pro-apoptotic effectors have BH1, BH2, and BH4 domains in common (modified from Moldoveanu et al. 2014).

The four BH domains build the BCL-2 core, which folds into a hydrophobic pocket (Muchmore et al. 1996; Suzuki et al. 2000; Petros et al. 2001). This is essential for interaction with other family members (Sattler et al. 1997; Moldoveanu et al. 2006; Czabotar et al. 2014) via binding either the BH3 domain of binding partners or the TM region (Moldoveanu et al. 2014).

2.3.1 BCL-2-like survival factors

The *BCL-2* gene was identified by cloning the chromosome breakpoint of t(14;18) chromosome translocation in neoplastic B cells (Tsujimoto et al. 1984) and was associated with early steps of tumorigenesis. Later, other family members educed especially from homology studies. To date, six BCL-2-like survival factors are known: BCL-2, B-cell lymphoma extra-large (BCL-xL, also known as BCL2L1), BCL-w (also known as BCL2L2), myeloid cell leukemia 1 (MCL-1, also known as BCL2L3), BCL-2-related protein A1 (also known as BFL1, BCL2L5), and BCL-B (also known as Boo, Diva, BCL2L10).

Mouse genetic studies revealed overlapping functions of different anti-apoptotic BCL-2 family members. However, some of them operate in a tissue-specific manner, and inactivation of individual genes leads to diverse phenotypes (summarized in Ranger et al. 2001; Cory et al. 2003). In general, survival of every cell type depends on one or more pro-survival family members, with BCL-xL or MCL-1 often being crucial (Czabotar et al. 2014).

BCL-2-like survival factors promote their anti-apoptotic feature by binding either pro-apoptotic BH3-only proteins (Cheng et al. 2001) or activated effector proteins to control their pro-apoptotic activity (Fletcher et al. 2008) (for detailed information about functional interplay, see 2.3.4). While all anti-apoptotic proteins bind BAX, BAK only interacts with BCL-xL, MCL-1, and A1 (Willis et al. 2005; Simmons et al. 2008).

2.3.1.1 BCL-xL *and* MCL-1

Studying chicken lymphoid cells in terms of *bcl-2*-related genes discovered bcl-x as having 44 % amino acid identity with murine and human BCL-2 (Boise et al. 1993). Screening for human *BCL-x* discovered two different splice variants of this gene: BCL-xL, which has a similar size and structure as BCL-2 (Boise et al. 1993; Petros et al. 2004), and BCL-xS, which lacks the BH1 and BH2 domains (Boise et al. 1993). While BCL-xL inhibits cell death after growth factor deprivation, its shorter counterpart antagonizes the anti-apoptotic function of BCL-2 and BCL-xL (Kirkin et al. 2004). BCL-xL is targeted to the outer mitochondrial membrane by its C-terminal transmembrane helix (Zamzami et al. 1998) and seems to be essential

for survival, as bcl-x-deficient mice die at around day 13 of gestation having anomalies in the development of the brain and hematopoietic tissue due to massive apoptosis (Motoyama et al. 1995).

MCL-1 was originally discovered in maturing human myeloid leukemia cells (ML-1) and was proofed to have high sequence similarity with *BCL-2* (Kozopas et al. 1993). MCL-1 expression is critical for multiple myeloma cells (Zhang et al. 2002) and like BCL-xL, MCL-1 is also essential for survival as *MCL-1* deficiency results in peri-implantation lethality (E3.5 - 4) in mice (Rinkenberger et al. 2000). MCL-1 shares only three BH domains (BH1 - BH3) and the TM domain with other anti-apoptotic family members. Additionally, it contains a large N-terminal region with several confirmed and putative regulatory motifs (Germain & Duronio 2007; Thomas et al. 2010). Some of these motifs (like PEST enrichment and arginine pairs) are associated with protein lability (Yang et al. 1995). Indeed, MCL-1 has a much shorter half-life than BCL-2 and BCL-xL (< 1 h compared to 16 - 24 h) (Yang et al. 1995; Maurer et al. 2006). Thus, MCL-1 seems to be tightly regulated in terms of transcription, translation, and protein stability (reviewed in Thomas et al. 2010).

2.3.2 Pro-apoptotic effector proteins

The group of pro-apoptotic effector proteins comprises BCL-2-associated X protein (BAX, also known as BCL2L4), BCL-2 antagonist / killer (BAK, also known as BCL2L7), and BCL-2-related ovarian killer (BOK, also known as BCL2L9) with BAX and BAK being the main apoptosis effectors. They share sequence homology with BCL-2 in all four BH domains and also hold a TM domain, which targets them to the outer mitochondrial membrane. However, while BAK is permanently located at mitochondria (Griffiths et al. 1999), BAX is kept in the cytosol in the absence of apoptotic stimuli, as its TM domain is hided in its hydrophobic groove (Suzuki et al. 2000). Upon cytotoxic signals, BAX and BAK undergo an activating conformational change, which uncovers the TM domain of BAX and leads to mitochondrial localization of BAX (Gross et al. 1998). Furthermore, the conformational change induces homo-oligomerization of both proteins (Gross et al. 1998; Dewson et al. 2008) and therewith, permeabilization of the outer mitochondrial membrane by

either forming channels themselves (Schlesinger et al. 1997), interacting with channel-forming proteins (Tsujimoto & Shimizu 2000; Zamzami & Kroemer 2001) or forming supramolecular openings different from discrete protein channels (Kuwana et al. 2002). The detailed mechanism of BCL-2 family protein interaction and apoptosis-induction is described in 2.3.4.

2.3.3 Pro-apoptotic BH3-only proteins

In mammalian cells, ten or more BH3-only proteins have been identified (Kirkin et al. 2004) and serve as upstream sentinels that convert specific, proximal death and survival signals into cellular outcome (Danial & Korsmeyer 2004). Some examples are: BCL-2-associated agonist of cell death (BAD, also known as BCL2L8), NOXA (also known as PMAIP1), BIM (also known as BCL2L11), BH3 interacting domain death agonist (BID), and BCL2 binding component 3 (BBC3, also known as PUMA). They are often described as ‘sensors’ or ‘mediators’ of apoptosis (Kirkin et al. 2004) as they are not able to induce apoptosis in the absence of effector proteins (Zong et al. 2001). Moreover, most of them have dual functions by activating BAX and BAK upon death signals and neutralizing BCL-2-like survival factors (Wei et al. 2000; Letai et al. 2002; Cory et al. 2003; L. Chen et al. 2005; Kuwana et al. 2005; Willis et al. 2007).

Transcriptional control or posttranslational modifications normally constrain the pro-apoptotic activity of BH3-only proteins (Zha et al. 1996; Oda et al. 2000; Nakano & Vousden 2001). Different cytotoxic signals induce transcriptional upregulation, posttranslational modifications and/or relocalization of particular BH3-only proteins, which then extend their full pro-apoptotic potential (reviewed in Adams & Cory 2007; Happo et al. 2012). For example, BIM is upregulated in response to kinase inhibitors and microtubule-stabilizing drugs (Happo et al. 2012).

BH3-only proteins interact with pro-survival proteins via the BH3 amphipathic helix and the hydrophobic groove, respectively (Czabotar et al. 2014). Minor differences in BH3 domains and grooves lead to different binding affinities. While some BH3-only proteins (like BIM, tBID (cleaved active form of BID) and PUMA) can interact and neutralize all BCL-2-like proteins, other BH3-only proteins (like BAD and

NOXA) selectively bind only specific pro-survival factors (L. Chen et al. 2005; Kuwana et al. 2005; Happo et al. 2012).
Individual BH3-only proteins seem to be not essential for survival, as loss of them (except of BIM), does not change a cellular phenotype, at least in the absence of stress signals (Happo et al. 2012).

2.3.4 Complex interaction network regulating apoptosis

The net balance between BCL-2-like pro-survival proteins and pro-apoptotic BH3-only proteins decides about survival and death (Kirkin et al. 2004). Consequently, it seems to be a simple competition model that regulates apoptosis mediated by diverse interactions (Czabotar et al. 2014). Several studies have developed different models of interaction processes contributing to apoptosis.
In the ‘direct activation model’ (Letai et al. 2002; Kuwana et al. 2005; Chipuk et al. 2010), BH3-only proteins are grouped into ‘activators’ and ‘sensitizers’. Activators (e.g. BIM, tBID) are thought to directly bind effector proteins like BAX and BAK, which triggers their conformational change resulting in homo-oligomerization and induction of apoptosis. Sensitizers (e.g. BAD) interact with BCL-2-like survival factors, which sequester BAX and BAK in the absence of stress signals. Binding of sensitizers leads to release of BAX and BAK resulting in their activation.
This second sensitizer role of BH3-only proteins, is thought to be their essential function in the ‘indirect activation model’ According to this model, BCL-2-like proteins antagonize BAK and BAX by binding them, and this antagonism is abrogated by BH3-only proteins similarly binding to survival factors (L. Chen et al. 2005; Willis et al. 2005; Willis et al. 2007; Uren et al. 2007).
Recently, a ‘unified model’, which describes the complex network of interactions, was designed (Llambi et al. 2011; Moldoveanu et al. 2014) and is presented in Figure 6. In the unified model, the interaction equilibrium of pro-survival proteins, BH3-only proteins, and pro-apoptotic effector proteins defines an anti-apoptotic threshold. In the absence of stress signals, effector proteins are inhibited by pro-survival factors, which also interact with BH3-only proteins leading to reciprocal inhibition. In the presence of cytotoxic conditions, BH3-only proteins get upregulated or posttranslationally activated. If this exceeds the threshold, anti-

apoptotic interactions get out of the equilibrium and change into a pro-apoptotic state. In this state, BAX and BAK are released from BCL-2-like factors as BH3-only proteins sequester those. Additionally, binding of BH3-only proteins to BAX and BAK further activates them. Activation of effector proteins triggers the so-called MOMP (mitochondrial outer-membrane permeabilization). MOMP leads to release of apoptogenic factors, especially cytochrome c, which activate the downstream caspase cascade leading to apoptosis (Zou et al. 1997; Kluck et al. 1997; Li et al. 1997).

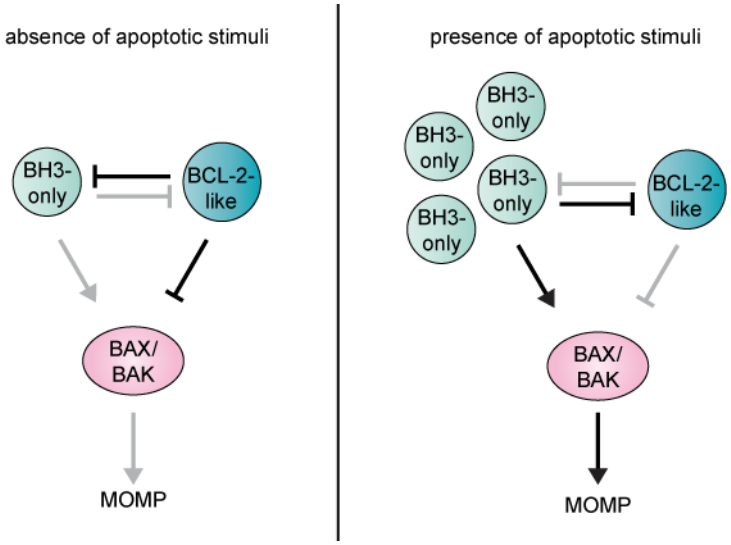

Figure 6: Schematic drawing of interaction of BCL-2 family members in the unified model. The balance between BH3-only and BCL-2-like proteins determines the threshold for induction of apoptosis. In the absence of apoptotic stimuli (left), BLC-2-like proteins inhibit BH3-only proteins as well as effector proteins (BAX/BAK), thereby preventing mitochrondrial outer-membrane permeabilization (MOMP). In the presence of apoptotic stimuli (right), BH3-only proteins get upregulated or post-translationally activated. This leads to increased inhibition of BCL-2-like proteins, which release BAX/BAK, and additional activation of BAX/BAK. This promotes MOMP and subsequent caspase cascade activation leading to apoptosis. Black arrows: predominantly active, gray arrows: predominantly inactive (modified from Moldoveanu et al. 2014).

2.3.5 BCL-2 family and cancer

Evasion of programmed cell death (apoptosis) is one of the hallmarks of cancer (Hanahan & Weinberg 2000) and tumor cells evolve a variety of strategies to circumvent cell death (Hanahan & Weinberg 2011). One of those circumvention strategies is deregulation of BCL-2 family members, which is frequently observed during tumorigenesis (Strasser et al. 1997). In several types of cancer, BCL-2-like pro-survival factors are upregulated and function as oncoproteins, while anti-apoptotic family members are downregulated or lost and therewith, have tumor

suppressor features. Both contribute to tumor initiation and progression (Kirkin et al. 2004; Amundson et al. 2000). However, not only direct mutations of *BCL-2* family genes lead to deregulation, also a variety of other deregulated signal transduction pathways results in deregulated expression of BCL-2 family members (Sherr 2001; Kirkin et al. 2004).

Activation of the BCL-2-regulated apoptosis pathway seems to be crucial for the therapeutic efficacy of most current therapies, including conventional cytotoxic agents as well as targeted therapies, although cancer treatments can induce different types of cell death (Czabotar et al. 2014). Accordingly, several studies have demonstrated that BCL-2 family deregulation entails development of resistance against diverse therapy strategies, including cytotoxic chemotherapy, antibody-based therapy, kinase inhibitors, and immunotherapy (Wesarg et al. 2007; Meiler et al. 2012; Stolz et al. 2008; Kasper, Breitenbuecher, Reis, et al. 2012; Kasper, Breitenbuecher, Heidel, et al. 2012; Huber et al. 2005; Ravi et al. 2006; Hähnel et al. 2008; Kutuk & Letai 2008). There are also few studies which show that BCL-2 family members, especially BCL-2, mediate radioresistance (Gilbert et al. 1996; Lee et al. 1999; Condon et al. 2002).

The most important deregulated factors seem to be BCL-xL and MCL-1, which are amplified in many different tumors (Beroukhim et al. 2010). In NSCLC, approximately one third of cases exhibits strong expression of anti-apoptotic BCL-2 and / or BCL-xL (Borner et al. 1999; Berrieman et al. 2005), and more than 50 % express high levels of MCL-1 (Wesarg et al. 2007; Borner et al. 1999; Zhang et al. 2011).

The finding that several cancer treatments converge at the integrity of the mitochondrial membrane, which is regulated by BCL-2 family members, provides the biological rationale for targeting this family and several compounds have been described in the last years. The most promising strategy implies BH3-mimetics and several drugs have been tested (pre-)clinically as single agents or in combination with conventional therapy (reviewed in Lessene et al. 2008).

2.3.6 BCL-2 family and DNA repair

Besides their unquestionable function in apoptosis regulation, there is emerging evidence that BCL-2 family members might have additional, non-canonical functions including impact on mitochondrial dynamics and energetics, regulation of transcription factor activities, cell cycle regulation, regulation of autophagy, calcium handling, and neuronal activity, as well as modulation of innate immunity during viral infections. Furthermore, some studies also predict an association of BCL-2 family members with DNA repair pathways (reviewed in Hardwick & Soane 2013; Laulier & Lopez 2012), which might be interesting in regard to radiotherapy.

Most of those studies analyzed BCL-2 itself and it was shown to inhibit all DNA repair systems (nucleotide excision repair (NER), base excision repair (BER), SSB repair, mismatch repair, DSB repair) (reviewed in Laulier & Lopez 2012). As DSBs are the most severe lesions after irradiation, the focus of the following section will be on this aspect.

Overexpression of BCL-2 leads to unrepaired DSBs as shown by persistence of γH2AX foci (Wang et al. 2008) and accumulation of aberrant chromosomes (Kumar et al. 2010). This is, at least in part, due to nuclear accumulation of BCL-2 and interaction with KU70, which prevents binding of Ku70 to DNA ends and disrupts the Ku/DNA-PKcs complex (Kumar et al. 2010; Wang et al. 2008). By this, BCL-2 affects effectiveness and fidelity of c-NHEJ (Wang et al. 2008; Laulier & Lopez 2012). However, there are also some contradictory studies, which showed increased c-NHEJ in the presence of BCL-2 (Sotiropoulou et al. 2010) and did not observe nuclear accumulation of BCL-2 (Laulier et al. 2011). BCL-2 was also linked to inhibition of HRR induced by various insults (Saintigny et al. 2001). Identification of BRCA1 as a target of BCL-2 confirmed this. BCL-2 can interact with BRCA1 and sequesters it in endomembranes. This in turn, leads to depletion of nuclear BRCA1 and a decrease in HRR (Laulier et al. 2011). Thus, BCL-2 is able to interfere with c-NHEJ as well as HRR. Additionally, BCL-2 can also interact with PARP1 and inhibit PARP1-dependent DNA repair (Dutta et al. 2012).

BCL-xL was also linked to HRR, however, the results are contradictory in terms of stimulation or inhibition of repair (Saintigny et al. 2001; Wiese et al. 2002). BID and MCL-1 were associated with coordination of DNA damage-mediated checkpoint response (Jamil et al. 2008; Jamil et al. 2010; Laulier & Lopez 2012) and BAX was

shown to affect several repair pathways like NER, c-NHEJ, and HRR (reviewed in Laulier & Lopez 2012).

In summary, the interaction between BCL-2 family members and DNA repair proteins seems to be complex, but it might allow very gradual responses to DNA damage (Laulier & Lopez 2012).

2.4 RAF-1

RAF-1 belongs to a protein family of serine / threonine kinases, which consists of three members: A-RAF, B-RAF, and RAF-1 (also known as C-RAF, c-RAF-1). This protein family was discovered as human homologues of the retroviral oncogene v-raf that was acquired by the murine retrovirus 3611-MSV (Rapp et al. 1983). In the same study, Rapp and colleagues also cloned RAF-1, while A-RAF as well as B-RAF were identified a few years later. The common structure of RAF proteins is made up of three conserved regions (CR1, CR2, and CR3) with an N-terminal regulatory domain (CR1 and CR2) and the C-terminal kinase domain (CR3) (Wellbrock et al. 2004). All three kinases participate in the RAS-RAF-MEK-ERK signal transduction pathway, which is also known as the mitogen-activated protein kinase (MAPK) cascade and transduces signals from cell surface to nucleus thereby mediating diverse biological functions (e.g. survival and differentiation) (Wellbrock et al. 2004). A-RAF, B-RAF as well as RAF-1 are essential for survival and do not have redundant functions in development as shown by genetic studies in mice (Mikula et al. 2001; Pritchard et al. 1996; Wojnowski et al. 1997).

2.4.1 Regulation and function of RAF-1

RAF-1 gets activated upon binding of extracellular ligands (e.g. growth factors, cytokines or hormones) to their receptors. Ligand-induced receptor stimulation activates the rat sarcoma (RAS) protein, which directly binds to CR1 in the N-terminal regulatory domain of RAF (Wittinghofer & Nassar 1996). This recruits RAF to the plasma membrane where RAS is predominantly located (Hancock 2003) and initiates activation of RAF in a phosphorylation-dependent manner (Marais et al. 1995). RAF kinases phosphorylate MEK1/2 (also known as

MAPK/ERK kinase), which in turn, activate ERK1/2. These effector kinases have more than 50 cytosolic or nuclear substrates (e.g. hypoxia-inducible factor (HIF), Ets-like transcription factor-1 (ELK-1), MDM2, p27kip, ARF) (Roskoski Jr. 2010; Gollob et al. 2006), which mainly regulate transcription, metabolism, and cytoskeletal rearrangements (Wellbrock et al. 2004).

Furthermore, recent studies have demonstrated MEK/ERK-independent functions of RAF-1. Mice genetic studies revealed that RAF-1 directly inhibits apoptosis by several mechanisms that require its translocation to mitochondria (Hüser et al. 2001; Gollob et al. 2006). This translocation can be mediated by p21-activated kinase (PAK)-1- or BCR-ABL-mediated phosphorylation, which then mediates BAD phosphorylation going along with its inactivation or BCL-2 activation (Jin et al. 2005; Salomoni et al. 1998). Additionally, RAF-1 was shown to inhibit MCL-1 degradation (Yoon et al. 2002). Other studies have also demonstrated that RAF-1 inhibits the pro-apoptotic proteins ASK-1 (Chen et al. 2001; Alavi et al. 2007) and MST2 (O'Neill et al. 2004). All this prevents induction of the apoptosis cascade. Besides its effects on apoptosis, RAF-1 has also been shown to interact with ROK (Ehrenreiter et al. 2005) and PLK1 (Mielgo et al. 2011) in a MEK-independent manner, thereby driving cell migration and G2 / M cell cycle checkpoint progression, respectively.

RAF kinases are regulated in a complex interplay of protein-protein interactions, phosphorylation as well as dephosphorylation, and conformational changes (Wellbrock et al. 2004) with all conserved regions contributing to this. As described above, CR1 mediates interaction with RAS, which promotes RAF activation. However, RAS does not activate RAF directly, but recruits it to the cell membrane, where it gets activated in a multi-step process involving dephosphorylation and phosphorylation (Gollob et al. 2006). CR2 mainly contributes to inhibitory regulation of the kinase via binding of the regulatory protein 14-3-3 in a phosphorylation-dependent manner (Kolch 2005). 14-3-3 binding blocks the interaction of RAF with RAS (Wellbrock et al. 2004).

All RAF kinases have numerous phosphorylation sites with inhibitory as well as stimulatory functions (Wellbrock et al. 2004). For activation of RAF-1, the most important phosphorylation sites are Ser338, Ser471 as well as Tyr341 (Marais et al. 1995; Fabian et al. 1993; Roskoski Jr. 2010; King et al. 1998). Two additional phosphorylation sites within the activation segment (Thr491, Ser494) have

stimulatory functions (Roskoski Jr. 2010). In contrast to this, phosphorylation at Ser259 suppresses RAF-1 kinase activity (Roskoski Jr. 2010).
RAF kinases dimerize to activate its kinase activity. All three family members can either form homo- or heterodimers (Rushworth et al. 2006) and activation occurs even when one monomer is kinase-dead (Roskoski Jr. 2010).

2.4.2 RAF-1 and cancer

The MAPK pathway is upregulated in approximately 30 % of all human cancers (Rushworth et al. 2006). Although RAF-1 has oncogenic potential and mutants have been shown to transform cells *in vitro*, RAF-1 mutations are rarely observed in human tumors (Gollob et al. 2006). However, several tumors demonstrate constitutive RAF-1 activation due to growth factor receptor overexpression, oncogenic mutations in receptor tyrosine kinases (RTK) or oncogenic RAS mutations, which are some of the most frequently detected genetic aberrations in human cancers (Downward 2003). All this is associated with onset and progression of tumors, like metastatic spread and therapy resistance (Gollob et al. 2006). Several strategies of targeting the MAPK-pathway via RAF-1 have been developed, including antisense oligonucleotides, RAF destabilizers, and small-molecule inhibitors (Gollob et al. 2006) and are currently under (pre-)clinical investigations.

2.4.3 RAF-1 and irradiation

The first reports on the impact of RAF-1 on radiotherapy response revealed contradictory results. While Kasid and colleagues demonstrated RAF-1-mediated radioresistance in several studies (Kasid et al. 1987; Kasid et al. 1989; Kasid et al. 1996), Warenius et al. rather showed that RAF-1 is associated with radiosensitivity (Warenius et al. 1994; Warenius et al. 1996; Warenius et al. 1998). The authors argue that the proto-oncogene and the activated oncogene may have different effects on radiosensitivity.
Later, other groups confirmed radioresistance-mediating effects of RAF-1. In an expression study of different squamous cell carcinoma of head and neck, RAF-1

overexpression was associated with resistance to radiotherapy (Riva et al. 1995) and furthermore, Grana et al. showed that RAF-1 contributes to RAS-mediated radioresistance (Grana et al. 2002). Some studies suggest targeting of RAF-1 for radiosensitization of human tumors (Pirollo et al. 1997; Kasid & Dritschilo 2003) and in the first phase I clinical trial this was also tested to be effective (Dritschilo et al. 2006). Here, a liposome-encapsulated RAF-1 anti-sense oligonucleotide (LErafAON) was used and tumor response was evaluated at completion of treatment. Four patients showed partial response and another four showed stable disease. However, four patients also experienced progressive disease. Furthermore, the authors claim that the liposomal composition has to be modified for future clinical trials, as there were dose-dependent and infusion-related reactions observed (Dritschilo et al. 2006).

In summary, RAF-1 has been associated with radioresistance, but the underlying mechanisms remain to be elucidated although MEK-independent mechanisms are already proposed to be responsible (Grana et al. 2002).

3 Aim of the study

Radiotherapy is an important modality in curative treatment of localized as well as locally advanced NSCLC and in palliative care. Simultaneous administration of radiation with cisplatin-based chemotherapy has moderately but consistently increased the curative potential of radiotherapy in locally advanced NSCLC. Recent improvements in treatment of metastatic NSCLC were achieved by taking the specific tumor biology into consideration. For example, molecularly targeted agents can be superior to cisplatin-based chemotherapy when patients are selected by genomic biomarkers detected in tumor tissues.

Radiotherapy still does not take advantage of biological disease heterogeneity, although the radiotherapy response of lung cancers is dramatically varying in the clinic and this might be, at least in part, due to molecular differences within the tumors. Against this background, it was hypothesized that combining radiation with biomarker-stratified targeted therapy could lead to better outcomes in curatively intended radiotherapy protocols. A better molecular understanding of targetable mechanisms of radiation resistance is a prerequisite for implementation of this strategy. An improved understanding of the modulation of the radiotherapy response by signal transduction pathways may open new avenues for the development of more specific therapy protocols combining targeted pharmacotherapies with radiotherapy to improve overall treatment efficacy in lung cancer. Thus, the overarching aim of this study was to identify potential modulators of the radiotherapy response in NSCLC.

To this end, the impact of selected regulators of apoptosis, oncogenes, and signal transduction mediators on irradiation-induced cell death was assessed. Candidates with the most striking effect (BCL-xL and RAF-1) were applied to further systematical experiments to validate them as modulators *in vitro* as well as *in vivo* and to characterize the underlying mechanisms. Additionally, targeting of the modulators was tested to provide the *in vitro* basis for the development of new personalized treatment protocols.

4 Methods

4.1 Cell culture methods

4.1.1 General cell line maintenance

Cells were cultured in medium containing 10 % fetal bovine serum (FBS, Biochrom), 1 % L-Glutamine (Gibco), and 1 % penicillin-streptomycin (Gibco) at 37 °C and 5 % CO_2. A431, FNX, and HEK293T cells were grown in Dulbecco's modified eagle medium (DMEM, Gibco), A549 as well as H1299 cells were maintained in Roswell Park Memorial Institute (RPMI) 1640 medium (Gibco).

Cells stably expressing different transgenes were generated by retroviral transduction (see 4.3.1; 4.3.3). Stable knockdown of specific genes was achieved by lentiviral transduction (see 4.3.2, 4.3.3). All stably transduced cell lines were maintained in the same growth medium as parental cells supplemented with 0.5 - 1 µg/ml puromycin (Calbiochem).

Cells were passaged twice or thrice weekly at a confluency of about 80 %. After washing once with Dulbecco's phosphate-buffered saline (DPBS, Gibco), cells were detached using Trypsin-Ethylenediaminetetraacetic acid (Trypsin-EDTA, Gibco) and seeded in fresh culture medium according to their individual growth rate. Cells were discarded after approximately 20 - 30 passages.

For a list of used cell lines see 8.2.1.

4.1.2 Freezing and thawing

For long term storage, cells were frozen in DMEM or RMPI 1640 supplemented with 25 % FBS and 7.5 % dimethyl sulfoxide (DMSO, Sigma-Aldrich) and stored at -80 °C or in liquid nitrogen. Frozen stocks were thawed in warm medium and centrifuged at 1,400 rpm for 5 min to remove DMSO. Supernatant was discarded and cells were cultured under standard conditions as described above. After thawing, cells were passaged at least two times before using them in experiments.

4.1.3 Cell counting

For all experiments, defined numbers of cells were seeded. For counting, cells were collected and resuspended in fresh culture medium. Cells were diluted 1:1 in 0.4 % Trypan blue (Invitrogen) to distinguish between dead (Trypan blue positive) and viable (Trypan blue negative) cells. Cell dilutions were applied to a Countess™ Cell Counting Chamber Slide (Invitrogen) and counted with a Countess™ Automated Cell Counter (Invitrogen). Only viable cell counts were used for calculation of cell numbers for seeding.

4.1.4 Induction of transgene activity

Some transgenes, namely AKT-ER^{tam} and ΔRAF1-ER^{tam}, were established as conditionally activatable systems (see 5.1). Those kinases were activated by adding 100 nM 4-hydroxytamoxifen (4OHT, Sigma-Aldrich) to the cell culture medium.

4.2 Plasmid DNA purification

For plasmid DNA purification, Escherichia coli (E. coli) bacteria of a glycerol stock were inoculated in 8 mL Circlegrow ® medium (MP Biomedicals) containing the suitable selective antibiotic and cultured at 32 °C and 200 rpm overnight. To increase bacterial yield, precultured bacteria were further grown in 140 mL Circlegrow ® medium supplemented with the suitable antibiotic under the same conditions.

Bacteria were pelleted by centrifugation at 6,000 x g for 10 min at 4 °C and supernatant was discarded completely. Plasmid DNA was purified using Plasmid Plus Maxi Kit (QIAGEN) according to the manufacturer's protocol. DNA was reconstituted in an appropriate volume of sterile Aqua destillatum (A. dest.) and plasmid yield was determined photometrically using a NanoDrop lite spectrophotometer (Thermo Scientific).

4.3 Establishment of stably transduced cells

In order to assess the impact of knockdown, overexpression or activation of different transgenes on the radiotherapy response of various cell lines, stably expressing cell lines were established by retro- or lentiviral transduction. First, retro- or lentiviral particles were generated. Second, parental target cells were transduced with those particles and third, cells that expressed transgenes were selected by maintaining them in appropriate selection medium.

4.3.1 Production of retroviral particles

All transgenes that were used for overexpression or conditional activation were established in retroviral vectors. Therefore, retroviral particles were generated to stably express those transgenes subsequently in target cells.

For the production of retroviral particles, FNX packaging cells were transfected with retroviral packaging plasmids and the plasmid of interest by a calcium-phosphate transfection method (see 8.2.3 for a list of plasmids). Transfection was performed 24 h after seeding. A total of 13 µg DNA (10 µg plasmid of interest, 1.5 µg polymerase plasmid, and 1.5 µg envelope plasmid) were diluted in 200 µl A. dest. and mixed with 50 µl $CaCl_2$ (2.5 M). After adding 250 µl 2x HBS buffer (see 8.2.11) while vortexing, the mix was incubated for 5 min at RT and added drop-wise to the packaging cells. 6 to 16 h after transfection, culture medium was changed to enhance cell viability and to avoid carryover of plasmid. Virus containing supernatants were collected at 48 h after transfection. To avoid carry-over of cells into the viral preparation, supernatants were centrifuged at 1,400 rpm for 5 min and filtered through a Minisart ® 0.2 µm filter (Sartorius Stedim Biotech). To monitor transfection efficiency, a control plate was always transfected with a green fluorescent protein (GFP) plasmid and the number of GFP positive cells was evaluated by flow cytometry 48 h after transfection (see 4.7.1). Viral preparations were either used immediately for transduction of target cells or stored in aliquots at -80 °C.

4.3.2 Production of lentiviral particles

Stable knockdown of different genes was established by lentiviral transduction of target cells, as all knockdown plasmids were of lentiviral origin (see 8.2.3 for a list of plasmids).

Lentiviral particles were produced by calcium-phosphate transfection of HEK293T cells with lentiviral packaging plasmids and the plasmid of interest. Transfection was conducted as for the production of retroviral particles (see 4.3.1).

4.3.3 Transduction of target cells

To stably express different transgenes or knockdown specific genes, parental cells were transduced using the retro- or lentiviral particles from sections 4.3.1 and 4.3.2, respectively. Retro- or lentiviral particles were added to target cells 24 h after seeding. 6 to 8 h later, fresh medium was added and cells were further incubated overnight. Medium was changed 24 h after transduction. Transduction efficiency was controlled using an Olympus CKX41 fluorescence microscope (Olympus). Selection of transgene expressing cells was started 48 to 72 h after transduction by maintaining cells in culture medium supplemented with 1 µg/ml puromycin.

4.4 Analysis of messenger ribonucleic acid (mRNA) expression

In order to examine the expression of some transgenes on the level of messenger ribonucleic acid (mRNA), total RNA was isolated from the cells and applied to quantitative real-time polymerase chain reaction (qRT-PCR) after converting mRNA into complementary DNA (cDNA).

4.4.1 RNA isolation and cDNA synthesis

Total RNA was extracted using High Pure RNA Isolation Kit (Roche) according to the manufacturer's protocol. RNA was eluted in 50 µL Elution Buffer.

Concentration and purity of extracted RNA was determined photometrically using a NanoDrop lite spectrophotometer (Thermo Scientific).

cDNA synthesis was performed using Transcriptor High Fidelity cDNA Synthesis Kit (Roche) following the manufacturer's guidelines. Briefly, 5 µg total RNA were diluted in 10.4 µL PCR grade A. dest. and mixed with 1 µl Anchored-oligo(dT)$_{18}$ Primer (final concentration 2.5 µM). For denaturation of RNA secondary structures, the mix was incubated at 65 °C for 10 min and subsequently cooled down to 4 °C. Afterwards, it was incubated with RT Mix containing Transcriptor High Fidelity Reverse Transcriptase Reaction Buffer, Protector RNase Inhibitor, Deoxynucleotide Mix, DTT, and Transcriptor High Fidelity Reverse Transcriptase using the following temperature protocol:

period	temperature
30 min	50 °C
5 min	85 °C
∞	4 °C

RNA and cDNA were stored at -20 °C.

4.4.2 Quantitative real-time polymerase chain reaction (qRT-PCR)

qPCR reactions were performed using the Light Cycler ® 480 SYBR Green Master Kit (Roche) according to the manufacturer's protocol. Briefly, 10 µl SYBR Green I Master were mixed with 1 µl sense primer, 1 µl antisense primer, and 3 µl A. dest.. cDNA was synthesized as described in 4.4.1 and diluted 1:5 in A dest.. For each qPCR reaction, 5 µL cDNA dilution were applied. qPCR reactions were performed in triplicates on 96 well qPCR plates (Roche) using the LightCycler® 480 System (Roche) on basis of the following temperature protocol:

procedure	period	temperature	cycle
initialization	5 min	95 °C	1 x
denaturation	10 s	95 °C	45 x
annealing	20 s	60 °C	
elongation	30 s	72 °C	
melting curve	5 s	95 °C	1 x
	60 s	65 °C	
	continuous	97 °C	
cooling	10 s	40 °C	1 x

The melting curve was used to analyze the specificity of the amplicon.

For normalization the housekeeping gene actin (P0) was used. Relative expression of a gene of interest (GOI) was determined as follows:

ΔCt = Ct (GOI) – Ct (P0)

$\Delta\Delta Ct$ = ΔCt (control sample) – ΔCt (treated sample)

$2^{\Delta\Delta Ct}$ = relative mRNA expression

qPCR primers were purchased from Eurofins MWG and are listed in 8.2.2.

4.5 Immunoblot analysis

Immunoblot analysis was used to control expression as well as activation of different transgenes and to evaluate knockdown efficiency on protein level. Proteins of whole cell extracts were separated by SDS-PAGE followed by immunoblotting.

4.5.1 Preparation of whole cell extracts

Cells were cultivated and treated in culture dishes as necessary. After removing the medium, all following steps were performed on ice to prevent protein degradation. Cells were washed once with cold PBS and appropriate volume of ice-cold NP40 lysis buffer (see 8.2.11) supplemented with cOmplete Protease Inhibitor Cocktail (Roche) and Phosphatase Inhibitor Cocktail 2 / 3 (Sigma-Aldrich) was added. After scraping cells with a Nunc® cell scraper (Thermo Scientific) and transferring them into a tube on ice, lysates were vortexed and incubated for at least 10 min on ice. To get rid of cell debris and unbroken cells, samples were spun down in a microcentrifuge at maximum speed (14,000 rpm) at 4 °C for 10 min. Protein containing supernatant was transferred to a fresh tube and stored at -80 °C.

4.5.2 Bradford assay to determine protein concentration

The Bradford assay is a colorimetric assay to quantify protein concentration of a sample. It is based on an absorbance shift of Coomassie Brilliant Blue G250 upon

binding of proteins (Bradford 1976). For the measurement, 2 µl cell lysate were mixed with 200 µl Protein Assay Dye Reagent Concentrate (BioRad) and 800 µl A. dest.. Absorbance of the samples was measured against a reference (only Protein Assay Dye Reagent Concentrate and A. dest.) at 595 nm wavelength using a Gene Quant Pro spectrophotometer (GE Healthcare). Protein concentrations were calculated in comparison to a standard curve.

4.5.3 SDS-PAGE

Equal protein amounts (30 - 50 µg) were supplemented with SDS loading buffer (see 8.2.11) and denaturated at 95 °C for 5 min. Separation of lysates was carried out using the Mini-PROTEAN electrophoresis system (BioRad) for SDS-PAGE. 10 µL PageRuler Prestained Protein Ladder (Thermo Scientific) and denaturated lysates were loaded and protein separation was performed at 10 mA in the stacking gel and 30 mA in the resolving gel.

4.5.4 Immunoblotting

SDS-PAGE was followed by subsequent immunoblotting. Therefore, two different strategies were performed: either wet blotting or semi-dry turbo blotting. For wet blotting, SDS-PAGE gels were blotted on Hybond ECL 0.45 µm nitrocellulose membranes (GE Healthcare) using the Mini-Trans Blot ® Cell tank blot system (BioRad). Blotting was performed at 350 mA for 70 min. For turbo blotting, SDS-PAGE gels were blotted on nitrocellulose membranes (BioRad) using the Trans-Blot® Turbo™ Transfer System (BioRad) according to the manufacturer's protocol. Blotting was performed with the settings for 1.5 mm mini gels (1.3 A, 25 V, 10 min). Transfer efficiency was analyzed by staining the membranes with Ponceau S (see 8.2.12).

Afterwards, membranes were blocked in gelatin-containing NET-G or Blotto (see 8.2.12) at RT for at least 1 h and incubated with primary antibodies (see list 8.2.4.1) at 4°C overnight. After washing thrice in NET-G or Blotto for 10 min, membranes were incubated with HRP-coupled secondary antibodies (see list 8.2.4.2) for at least 1 h at RT, followed by repeated washing as described above.

Chemiluminescence was determined using the Super Signal West Pico system (Thermo Fisher Scientific) and the ChemiSmart Imaging System (Vilber Lourmat, France).

4.5.5 Stripping of nitrocellulose membranes

To analyze proteins of similar size, it was required to dehybridize nitrocellulose membranes from former antibodies. Therefore, the membrane was incubated in stripping buffer (see 8.2.11) at 55°C for 30 min. After washing thrice for 10 min and blocking in NET-G or Blotto for at least 1 h, membranes were again incubated with primary antibodies as described above (see 4.5.4).

4.6 Irradiation

Cells were irradiated at room temperature using a Co-60 γ-ray machine (Philips) with a dose rate of 0.6 - 0.9 Gy/min. For DNA repair assays, cells were irradiated using an X-ray machine (GE-Healthcare) operated at 320 kV, 10 mA with a 1.6 mm aluminum filter. The dose rate was 3.6 Gy/min.

4.7 Flow Cytometry

Flow cytometry is a technique to analyze different cellular parameters (like cell size, granularity, and fluorescent staining) simultaneously on a single cell level within a population. This is achieved by suspending cells in a stream of fluid and passing them through an optical-to-electronic coupling system as single cells. The system detects how cells scatter incident laser light or emit fluorescence, and transfers this into information about the above mentioned cellular parameters.
Here, flow cytometry was used to analyze transfection efficiency (GFP measurement), to examine cell cycle profiles, and to study cell death as well as apoptosis.

4.7.1 GFP measurement

As described in 4.3, cell transfection was always accompanied by a control of GFP transfection to evaluate transfection efficiency. Expression of GFP in those cells was measured by flow cytometry.

Cells were collected 48 h after transfection and resuspended in an appropriate volume of PBS. GFP expression of single cells was detected in FL1 of the FC500 (Beckman Coulter). At least 5,000 cells per sample were analyzed. GFP transfected cells were compared with non-transfected cells to determine transfection efficiency.

4.7.2 Cell cycle profiling and subG1 measurement

The method to analyze cell cycle distribution by flow cytometry using propidium iodide (PI) staining was initially developed by Fried and colleagues (Fried et al. 1978) and was further developed by Nicoletti and colleagues (Nicoletti et al. 1991). PI is a fluorescent dye, which intercalates into DNA. The method is based on saturated PI staining of permeabilized cells. The PI fluorescence signal is detected flow cytometrically and is proportional to the DNA content of each single cell. During the cell cycle, DNA content changes: Cells in G0/G1 phase have a diploid set of chromosomes (2n). After replication (S phase), chromosomes are doubled and cells in G2 phase have twice as much DNA (4n) as G1 cells. Therewith, detecting DNA content by measuring fluorescence intensity allows to distinguish cells in different phases of the cell cycle (Figure 7). Furthermore, this method also allows measuring apoptotic cells (Nicoletti et al. 1991) as DNA is extensively fragmented into oligonucleosomal subunits during apoptosis (Wyllie et al. 1980). Therewith, apoptotic cells have a hypodiploid DNA content (subG1).

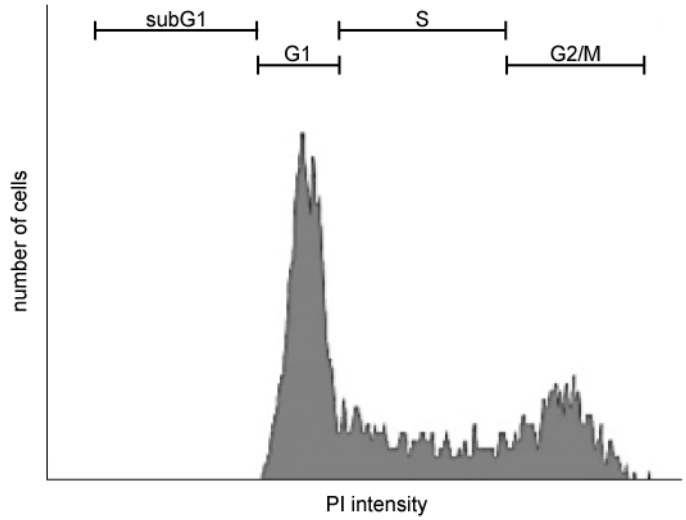

Figure 7: Representative image of cell cycle profile. Histogram is derived from flow cytometry measurement. Gates indicate different cell cycle phases (G1, S, and G2/M) and apoptotic cells (subG1).

For cell cycle and subG1 analysis, adherent cells as well as supernatants were collected at different time points after irradiation with γ-rays. Cells were incubated with HFS buffer (see 8.2.11) at 4 °C in the dark for at least 30 min to fix, permeabilize, and stain them with PI. Cell cycle distribution and subG1 content were analyzed by flow cytometry using FL3 of the FC500 (Beckman Coulter). For each sample, at least 5,000 cells were counted while doublets were excluded from analysis.

4.7.3 Cell death analysis by PI exclusion assay

To analyze cell viability, cells were stained with PI without fixing and permeabilizing them. Thus, PI can only enter dying cells as those lose integrity of the cell membrane. Therefore, only dead cells get stained with PI.

Cells were irradiated with different doses of γ-rays and incubated for 24 - 72 h. At different time points, adherent cells and supernatants were collected and stained with 0.5 µg/ml PI (Fluka, Sigma-Aldrich) on ice for 10 min. To determine the portion of dead cells, PI-positive cells were quantified by flow cytometry using FL2 of the FC500 (Beckman Coulter). The gate for PI-positive cells was adjusted to non-irradiated control cells and at least 5,000 cells per sample were counted.

4.7.4 Apoptosis analysis

Apoptosis is characterized by certain morphologic and molecular changes of cells. Loss of plasma membrane asymmetry is one of the earliest features in apoptotic cells. In viable cells, the phospholipid phosphatidylserine (PS) is only located at the inner leaflet of the plasma membrane. In apoptotic cells, PS is translocated to the outer leaflet (Fadok et al. 1992; Martin et al. 1995). This so-called flip is used here to follow apoptosis by flow cytometry. Cells were stained with FITC-conjugated Annexin V and PI. Annexin V is a phospholipid-binding protein with high affinity for PS and PI intercalates with DNA, but can only enter cells without intact membranes. The co-staining allows distinguishing between viable cells, early apoptotic cells, and late apoptotic / necrotic cells (Vermes et al. 1995). Viable cells exclude PI as well as FITC Annexin V, and represent as double negative (Annexin V^-, PI^-). Early apoptotic cells also have an impermeable membrane, however, they present PS on the cell surface and Annexin V can bind to it. Therewith, early apoptotic cells only stain for Annexin V (Annexin V^+, PI^-). Membranes of damaged or dead cells are permeable for PI and Annexin V, which leads to double positive stainings (Annexin V^+, PI^+). Following this method with time kinetics allows considering whether cells die via apoptosis or another mode of cell death.

At different time points after irradiation with γ-rays, apoptosis was analyzed using the FITC Annexin V Apoptosis Detection Kit (BD Biosciences) according to the manufacturer's guidelines. Briefly, cells were collected and stained with FITC Annexin V and PI in Annexin V Binding Buffer in the dark for 15 min. After diluting samples with additional Annexin V Binding Buffer, samples were kept on ice and analyzed by dual color flow cytometry using the FC500 (Beckman Coulter). FITC Annexin V was measured in FL1, PI was measured in FL3. At least, 5,000 cells per sample were counted. Cells stained for either FITC Annexin V only or PI only were used for compensation of fluorescence signals. Gates were adjusted to non-stained and non-irradiated controls.

4.8 MTT assay

Cell viability was measured with MTT assay, which is based on the cellular conversion of yellow tetrazolium salt 3-[4,5-dimethylthiazol-2-yl]-2,5-diphenyltetrazolium bromide (MTT) to blue formazan crystals in metabolically active, viable cells. Thus, the amount of produced formazan is directly proportional to the number of viable cells.

Appropriate numbers of cells were seeded in 96-well plates and treated with different substances. After indicated incubation, 10 µl of 0.5 % MTT solution (in PBS) were added per well and cells were incubated under standard conditions for additional 4 h. Cells were lyzed with 100 µl MTT solubilization buffer (see 8.2.11) overnight. The absorption of solubilized formazan crystals was measured with a spectrophotometer plate reader at 570 nm wavelength.

4.9 Clonogenic survival assay

The clonogenic survival assay is one of the most important assays to determine cellular radiosensitivity. It is based on the ability of a single cell to form a colony (at least 50 cells) due to unlimited cell division potential.

For clonogenic survival assay, appropriate numbers of cells were seeded in 60 mm petri dishes or 6-well plates allowing accurate counting of resulting colonies (about 100 colonies per dish / well). After 5 h, cells were irradiated with different doses and colonies were grown for 10 – 12 days, fixed with 70 % ethanol, and stained with colony staining solution (8.2.12). Colonies of more than 50 cells were counted. For each cell line in each experiment, the plating efficiency of non-irradiated control cells was calculated and used to normalize survival fractions of irradiated cells.

4.10 Analysis of DNA double-strand break repair

DNA double-strand breaks (DSBs) are the most severe lesions induced by irradiation and repair of those breaks is required for cell survival (see 2.2.2). Different techniques are available to analyze presence and repair of DSBs. On a

physical level, DSBs were analyzed by pulsed-field gel electrophoreses (PFGE). Furthermore, RAD51 foci formation and dissolution were examined to study DSBs on a biochemical level and metaphase analyses were included to evaluate chromosomal aberrations induced by DSBs.

4.10.1 Pulsed-field gel electrophoresis (PFGE)

The accumulation of DSBs leads to fragmentation of chromosomal DNA. This fragmentation can be detected by pulsed-field gel electrophoresis (PFGE). Here, asymmetric field inversion gel electrophoresis, a subtype of PFGE, was used. It was developed by Stamato and Denko in 1990 (Stamato & Denko 1990) and takes advantage of different mobility of intact and fragmented chromosomal DNA. Whereas, intact chromosomes are unable to move in an agarose gel due to their high molecular weight, fragmented DNA is able to move. The amount of DNA that moves from the well into the gel is linear to the fragmentation and therewith depends on the applied dose. In each PFGE experiment, dose response analyses were performed in parallel to repair kinetics. Dose response analyses were necessary to examine the induction of DSBs upon irradiation with different doses and facilitated the comparison of results obtained from different cell lines and different experiments.

For dose response analyses, cells were collected from 60 mm petri dishes after growing in these for two days. Cells originated from the same cell population as for repair kinetics. $3x10^6$ cells/ml were embedded in serum-free growth medium containing 0.5 % Low Melting Agarose (Roth) and pipetted into glass tubes with 3 mm diameter. After solidification on ice, cell-agarose suspension was extruded from the glass tubes and cut into 5 mm pieces (plugs). Plugs were irradiated with different X-ray doses (0, 5, 10, 15, 20 Gy) on ice and directly transferred to cold PFGE lysis buffer (see 8.2.13) in order to prohibit any repair of DSBs. Plugs were kept at 4 °C for 0.5 – 2 h. Hot lysis, washing and gel electrophoresis was performed in conjunction with repair kinetic plugs (see below).

For repair kinetics, cells were grown in 60 mm petri dishes for two days and irradiated with 20 Gy of X-rays. Pre-treatment with 10 µM NU7441 was performed 1 h before irradiation. Cells were collected at different time points and embedded

in serum-free growth medium containing 0.5 % Low Melting Agarose as described above. Cells were lysed in PFGE lysis buffer at 50 °C for 18 h. Then, agarose plugs were transferred to PFGE washing buffer (see 8.2.13) and incubated at 4 °C overnight. Afterwards, plugs were treated with washing buffer containing 0.1 mg/ml RNAse A (Sigma-Aldrich) at 37 °C for 1 h.

Gel electrophoresis was carried out in 0.5 % gels of SeaKem LE Agarose (Lonza) supplemented with 0.5 µg/ml ethidium bromide (Roth). Gels were run in 0.5x TBE (see 8.2.13) at 6 °C for 40 h with alternating cycles of 50 V for 900 s in forward direction and 200 V for 75 s in reverse direction. Gels were scanned using a Typhoon 9410 Imager (GE-Healthcare).

The fraction of DNA released (FDR) from the well into the lane, which reflects the amount of DSBs, was analyzed with Image-Quant (GE-Healthcare) (see Figure 8 A). FDR of non-irradiated controls was subtracted from FDR of irradiated samples. In order to compare results of different cell lines and different repair kinetic experiments, a dose response curve was generated by plotting FDR of samples that have been irradiated with different doses against the applied radiation dose. Dose response curves were used to calculate dose equivalents (DEQ) from each FDR value of the repair kinetics (Figure 8 B, dotted lines). DEQ was plotted against time and repair kinetic curves were fitted using non-linear regression analysis of SigmaPlot software (Version 13, Systat Software Inc).

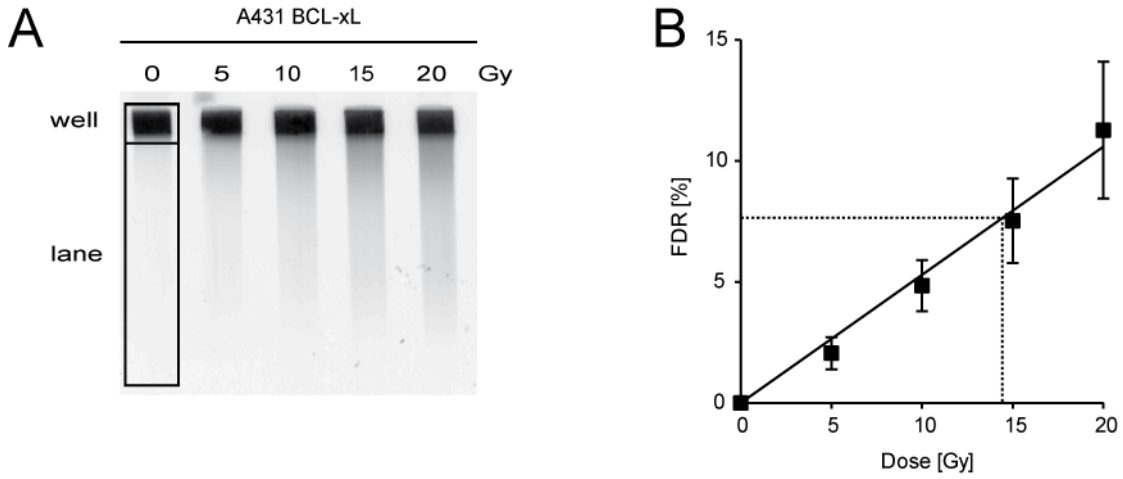

Figure 8: Representative dose response curve of PFGE. (A) Image of ethidium bromide stained gel. Fraction of DNA released (FDR) from the well into the lane (regions as indicated) was analyzed to plot a dose response curve **(B)**. Dotted lines indicate the approach that was used to calculate DEQ from FDR for repair kinetics.

4.10.2 RAD51 foci formation and dissolution

RAD51 is an important component of HRR (see 2.2.2.1) and can be detected with a confocal microscope as foci upon immunofluorescent staining. Thus, RAD51 foci do not only give information about the presence of DSBs, but also indicates the used repair pathway. Formation and dissolution of RAD51 foci upon irradiation was analyzed by immunofluorescence stainings followed by fluorescence microscopy.

Cells were grown on glass coverslips (20 mm diameter, VWR) for two days and irradiated with 4 Gy of X-rays. At different time points after irradiation, cells were fixed with 2 % paraformaldehyde/PBS (Roth) for 15 min at RT. After washing with PBS, permeabilization was performed by incubating coverslips in P-solution (see 8.2.14) at RT for 7 min. Coverslips were washed with PBS and blocked with PBG (see 8.2.14) either at RT for 1.5 h or at 4 °C overnight. For immunostaining, primary antibodies (see list 8.2.4.3) were diluted in PBG and incubated at RT for 1 h. After washing thrice with PBS at RT for 5 min, coverslips were incubated with fluorophore-coupled secondary antibodies (see list 8.2.4.4) diluted in PBG at RT in the dark for 1 h. After washing thrice with PBS for 5 min (in the dark), cells were stained with 50 ng/ml DAPI for 10 min and mounted with PromoFluor Antifade reagent (PromoKine) in the dark at RT overnight. Microscopy was performed on a Leica DMR fluorescence microscope. Pictures were taken with a QuantiFire XI camera (Intas) using LAS AF software (Leica Microsystems) and analyzed with Imaris 8.0.2 (Bitplane).

4.10.3 Analysis of metaphases

Molecular DNA lesions, particularly DSBs, may lead to chromosomal changes (e.g. chromatid breaks, translocations). Visualizing chromosomes in metaphase facilitates analysis of chromosomal aberrations upon irradiation.

Metaphase preparation was performed as described previously (Bryant et al. 2008). Exponentially growing cells were irradiated with 1 Gy of X-rays and were allowed to repair for 8 – 20 h at 37 °C. To accumulate cells at metaphase, 0.1 µg/ml colcemid (L-6221, Biochrom) was added 1 h before collecting the cells. At each time point, cells were collected and treated with hypotonic solution

(see 8.2.15) at RT for 10 min. After centrifugation with 1,000 rpm at 4 °C for 7 min, supernatant was discarded and cells were fixed with Carnoy's fixative (see 8.2.15) at 4 °C overnight. Before dropping cells on clean glass slides (Roth), fixed cells were washed 4 times with Carnoy's fixative. Chromosomes were stained with 3 % Giemsa (Roth) in Sorenson's buffer (Gibco, life technologies) and mounted with coverslips (Roth) using Entellan® (Merck). Images of metaphases were taken using an Olympus Vanix-T bright field microscope with an AVT Vimba Marlin F046B camera. For each experimental point, 50 – 100 metaphases were analyzed in terms of chromatid breaks, dicentrics, sister unions, chromosomal translocations, and acentric fragments (see Figure 24 A).

4.11 Mouse xenografts

In order to validate modulators of the radiotherapy response *in vivo*, tumor xenografts were established in non-obese diabetic severe combined immunodeficiency (NOD/SCID) mice, followed by local tumor irradiation and analysis of tumor growth. Mice were sacrificed, when tumors reached 1.5 mm diameter or when general conditions declined. All animal studies were conducted in compliance with institutional guidelines and German Animal Protection Law, and were approved by the responsible regulatory authority (Landesamt für Natur, Umwelt und Ver-braucherschutz Nordrhein-Westfalen, Az. G1399/13).

4.11.1 Injection of tumor cells

$1x10^6$ exponentially growing cells were suspended in 50 µl matrigel (growth factor reduced, Corning) and injected subcutaneously into the right hind limb of NOD/SCID mice (Charles River Laboratories).

4.11.2 Induction of transgenes

In order to induce transgene activation in xenografts of A431 [AKT-ER^{tam}] or A431 [ΔRAF1-ER^{tam}], feeding of mice with Tamoxifen Diet (400 mg/kg, irradiated, Harlan) started four days after injection of cells.

4.11.3 Local tumor irradiation

When tumors reached about 0.3 to 0.6 mm in diameter, tumor-bearing limbs were irradiated with a local, single dose of 4 Gy using a Co-60 γ-ray machine (Philips) while the total body was shielded.

4.11.4 Measurement of tumor growth

Tumor size was measured with an Electronic Digital Caliper (VWRI819-0013, Control Company) in two diameters thrice a week and calculated by multiplying width and length. As tumors differed in size at the time of irradiation, relative size was calculated for each time point using the day before irradiation as reference. The relative impact of irradiation on tumor growth was calculated as follows:

$$\text{mean of relative size}_{\text{non-irradiated}} - \text{mean relative size}_{\text{irradiated}}$$

4.11.5 Protein extracts from tumor tissues

To validate expression and activation of transgenes within tumor tissue, subcutaneous tumors were carefully dissected from skin and surrounding tissue, placed in a tube with NP40 lysis buffer supplemented with inhibitors (see 8.2.11), and cut with a scissors. After vortexing and incubating for at least 15 min on ice, tumor tissue was homogenized using the MagNA Lyser Instrument (Roche) at 7,000 min^{-1} for 5 s. Homogenates were further incubated on ice for 10 min and centrifuged at 14,000 rpm and 4 °C for 10 min. Protein-containing supernatants were stored at -80 °C. Before measuring protein concentration (compare 4.5.2), lysates were centrifuged again at 14,000 rpm and 4 °C for 30 min.

4.12 Data evaluation

Cell culture experiments were repeated up to three times, if not other stated. Analysis and graphing was done using GraphPad Prism (Version 6). For statistical analysis, unpaired t-test or Two-Way ANOVA were applied.

5 Results

The central aim of this project was to identify and characterize modulators of the radiotherapy response of NSCLC *in vitro* and *in vivo*. To this end, the functional impact of selected regulators of apoptosis, oncogenes, and signal transduction mediators on irradiation-induced cell death, clonogenic survival, cell cycle regulation as well as DNA repair was evaluated. Starting with a small-scale *in vitro* screen (see 5.1) to identify potential modulators, two paradigms were further characterized: members of the BCL-2 family (see 5.2) and the signal transduction mediator RAF-1 (see 5.3).

5.1 Identification of potential modulators of the radiotherapy response *in vitro*

In order to identify potential modulators of the radiotherapy response, a small-scale screen of selected modulator candidates was performed *in vitro*. For candidate selection, a literature study of candidates mediating resistance against other treatment modalities was conducted. Several groups discovered that resistance to DNA-damaging drugs and targeted therapies is often caused by functional defects in the apoptotic machinery (Wesarg et al. 2007; Meiler et al. 2012; Kasper, Breitenbuecher, Heidel, et al. 2012; Kutuk & Letai 2008). The same mechanism also influenced the outcome of antibody-based therapies and immunotherapies (Stolz et al. 2008; Huber et al. 2005; Ravi et al. 2006). Besides this, oncogenes and deregulation of growth factor signaling impeded with the success of cancer therapy *in vitro* (Kasper, Breitenbuecher, Reis, et al. 2012; Hähnel et al. 2008; Mok et al. 2009; Pogorzelski et al. 2014). Based on this, the following clinically relevant candidates were selected to determine their effect on radiation modulation:

- regulator of cell death: BCL-xL
- mediators of growth factor signaling: AKT, K-RAS^{wt}, RAF-1
- oncogenes: K-RAS^{G12V}, E6, E7

The small-scale screen was performed using A431 cells, which originate from an epidermoid carcinoma (Giard et al. 1973) and are often used as a model for lung

cancer due to their high expression of the epidermal growth factor receptor (EGFR). A431 cells stably expressing BCL-xL, K-RAS^{wt}, K-RAS^{G12V}, E6 or E7 were established by retroviral transduction, which allowed constitutive overexpression of these transgenes. Additionally, A431 cells were transduced with AKT-ER^{tam} or ΔRAF-1-ER^{tam} expression vectors to induce AKT or RAF-1 activity pharmacologically in those cells.

AKT-ER^{tam} is a fusion product of a constitutively active variant of AKT and a mutant hormone-binding domain of the murine estrogen receptor (ER) (Kohn et al. 1998; Hähnel et al. 2008) (Figure 9 A, left). The constitutively active variant of AKT lacks its PH domain, which mediates protein-lipid or protein-protein interactions (Haslam et al. 1993; Mayer et al. 1993), but contains a *src* myristoylation signal that targets AKT to membranes and causes AKT activation by an increase in phosphorylation (Kohn et al. 1996). The mutant hormone-binding domain of the murine ER is transcriptionally inactive and unable to bind estrogen (17β-estradiol), but retains normal affinity for the synthetic ligand 4-hydroxytamoxifen (4OHT) (Littlewood et al. 1995). In this fusion construct, kinase activity depends on the addition of exogenous 4OHT. In the absence of 4OHT, the fusion protein is kept in an inactive state due to a conformation that masks the myristoylation signal. In the presence of 4OHT, the fusion protein undergoes a conformational change, which unmasks the myristoylation signal, and therefore, allows integration of AKT into a membrane compartment that leads to its activation by phosphorylation (Figure 9 B, left).

RAF-1 consists of an N-terminal regulatory domain including region CR1, which is necessary for RAS-binding (Nassar et al. 1995), and region CR2, which contains several regulatory sites (Morrison et al. 1993). This regulatory domain functions to suppress the catalytic activity of the kinase, which is located at the C-terminus in region CR3 (Figure 9 A, right). In the ΔRAF-1-ER^{tam} fusion protein, RAF-1 lacks the regulatory domain, which leads to a constitutively active kinase (Balmanno et al. 2003; Stanton Jr. et al. 1989). For inducible control of the kinase, ΔRAF-1 is fused to the mutant hormone-binding domain of the murine ER mentioned above (Littlewood et al. 1995). In the absence of 4OHT, ER mimics the regulatory domain of RAF-1 and keeps the kinase inactive by conformational features. In the presence of 4OHT, the fusion protein undergoes a conformational change, which promotes kinase activation by phosphorylation, which is possibly maintained by

either interaction with other proteins or by homodimerization-induced auto- or trans-phosphorylation (Figure 9 B, right).

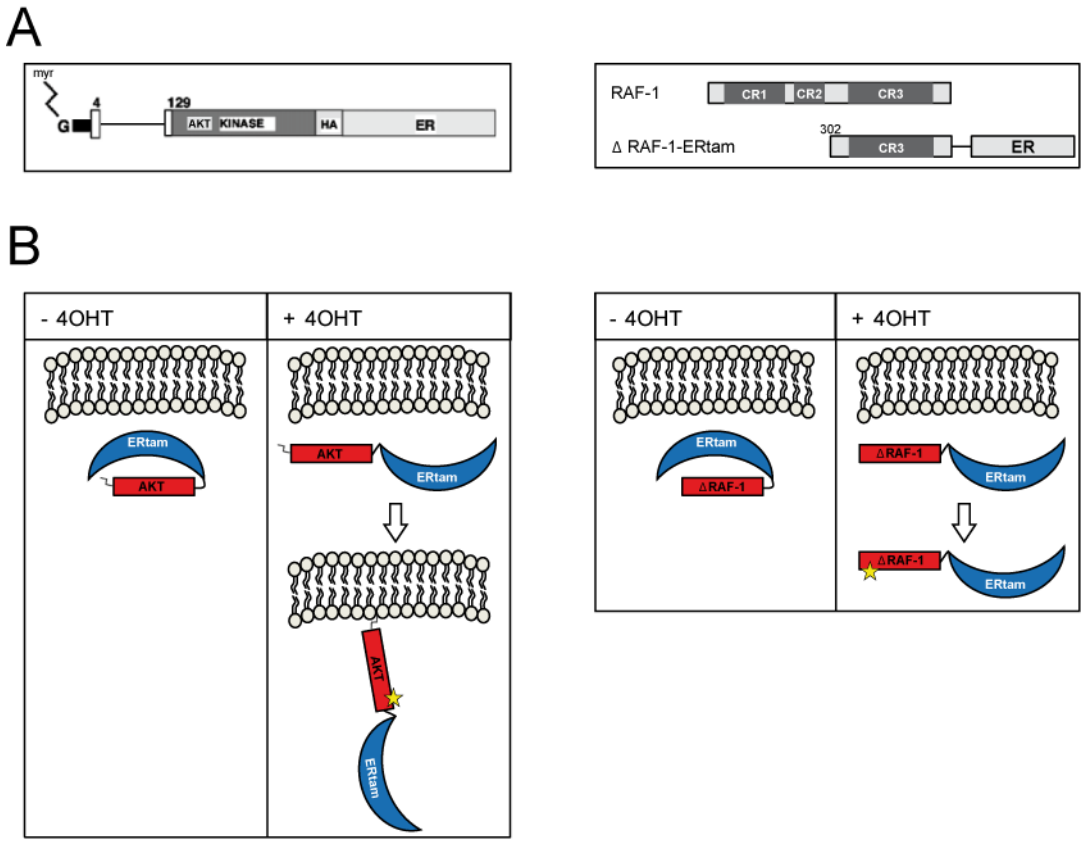

Figure 9: Activation mechanism of conditionally activatable transgenes. (A) Schematic drawing of AKT-ER^{tam} construct modified from Kohn et al. 1998 (left) and ΔRAF1-ER^{tam} (right). **(B)** Mechanism of activation of AKT-ERtam (left) and ΔRAF1-ER^{tam} (right) upon treatment with 4-hydroxytamoxifen (4OHT). The asterisk indicates active kinases.

Expressions of K-RAS^{wt}, K-RAS^{G12V}, and BCL-xL as well as conditional activation of AKT-ER^{tam} and ΔRAF-1-ER^{tam} in A431 cells stably transduced with the corresponding vectors were validated by immunoblotting (Figure 10). Activation of AKT and RAF-1 in the presence of 4OHT was stable for at least 68 h (Figure 10 C, D). E6 and E7 expression in stably transduced A431 cells was confirmed by qPCR, as antibodies for those proteins were not available (Figure 10 E).

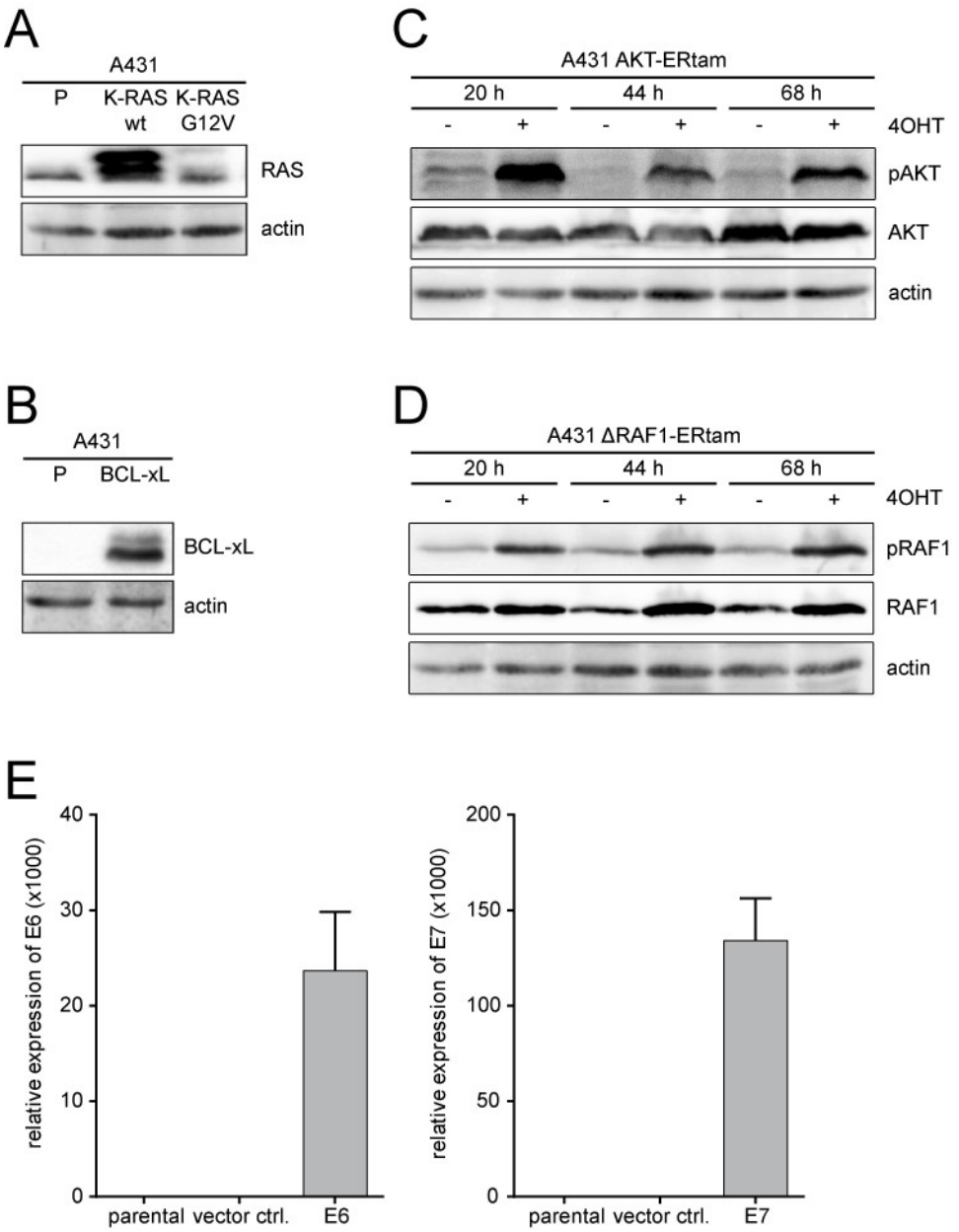

Figure 10: Validation of transgene expression and activation. (A, B) Expression of K-RAS^{wt}, K-RAS^{G12V} (A) and BCL-xL (B) in A431 cells stably transduced with the corresponding pBabe-Puro expression vectors compared to parental cells (P). Protein levels were evaluated by immunoblotting, actin served as a loading control. **(C, D)** Kinetics of AKT-ER^{tam} (C) or ΔRAF-1-ER^{tam} (D) activation in A431 cells stably transduced with the corresponding expression vectors and treated with 100 nM 4OHT for indicated time intervals. Protein levels of phosphorylated AKT (Ser473) and total AKT or RAF1 (Ser338) or total RAF1 were evaluated by immunoblotting. Actin served as a loading control. **(E)** Relative expression of HPV E6 and E7 mRNA in A431 cells stably transduced with the corresponding expression vectors. mRNA levels were measured by qPCR after transcription into cDNA.

In the small-scale screen, all transgenes were initially tested for their impact on radiation-induced cell death. To this end, cells were treated with different doses of γ-irradiation (0, 2, 6, 10 Gy) at 20 h after seeding and inducing kinase activity. Cell death was determined by PI exclusion assay at different time points after irradiation (48 and 72 h). The induction of cell death upon irradiation was dose

dependent and increased from 48 to 72 h (Figure S 1, Figure 11). All selected transgenes, except for AKT, mediated a significant decrease of irradiation-induced cell death compared to control cells, either parental A431 cells or A431 cells stably transduced with an empty vector control (Figure 11). BCL-xL and RAF-1 showed the strongest effects. As BCL-xL was already known to confer resistance to other treatment modalities and has strong clinical relevance (compare 2.3.5), the following studies were focused on this protein and its other family members (see 5.2). Furthermore, some initial experiments were also performed to further characterize the impact of RAF-1 (see 5.3) on the radiotherapy response.

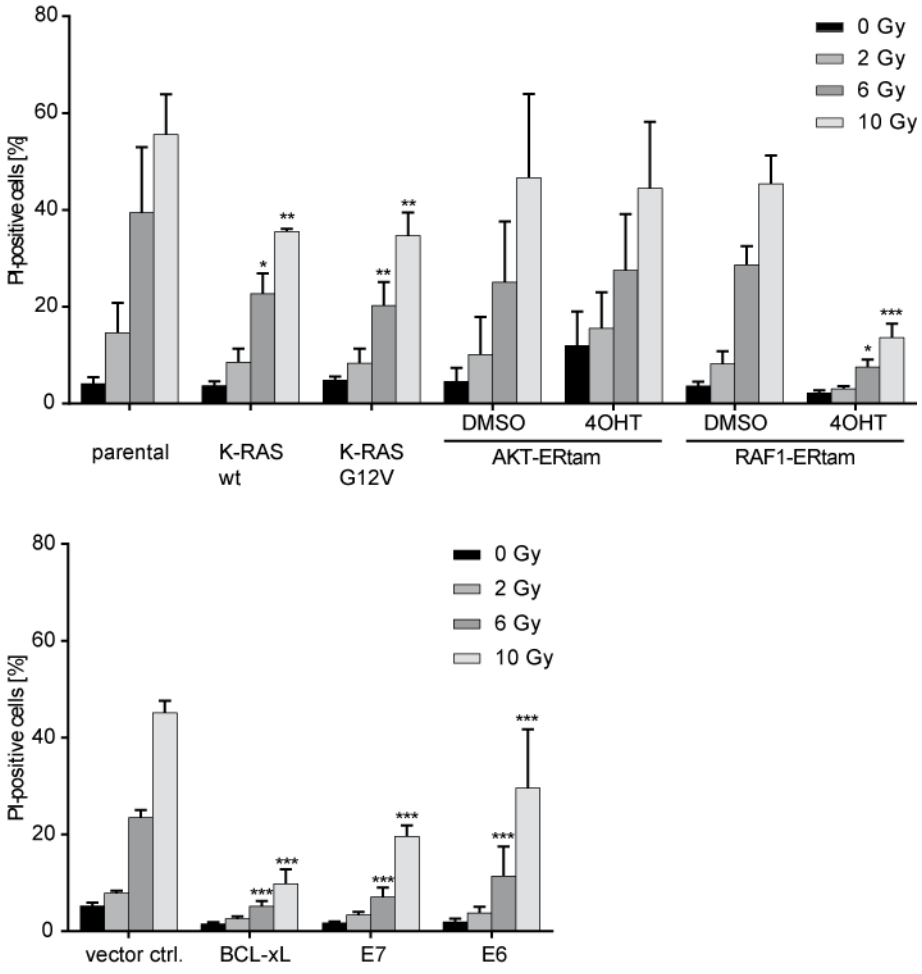

Figure 11: Impact of different transgenes on irradiation-induced cell death. A431 cells stably expressing indicated transgenes were stained with PI 72 h after irradiation with indicated doses (0 – 10 Gy) and the fraction of PI-positive cells was determined by flow cytometry (mean + SD, n=3). * p ≤0.05, ** p ≤0.01, *** p ≤0.001 (compared to parental or vector control cells).

5.2 Characterization of BCL-2 family members as modulators of radiotherapy response

As shown above, BCL-xL mediated the strongest resistance effect against irradiation evaluated by determining cell death in short-term experiments. Therefore, the impact of the BCL-2 family, which BCL-xL is a member of, on the radiotherapy response of NSCLC models was further characterized.

5.2.1 Long-term survival after irradiation in the presence of BCL-xL overexpression

Two different approaches were followed to examine whether BCL-xL also has an impact on long-term survival after irradiation. In the first approach, equal numbers of A431 cells, either parental or with constitutive BCL-xL overexpression, were seeded, irradiated with increasing doses of γ-irradiation (0 – 10 Gy), and grown for 6 – 9 d until colonies were visible (Figure 12 A). By this, it was visualized that the clonogenic survival of BCL-xL cells after irradiation was higher compared to parental cells. Non-irradiated parental and BCL-xL cells showed similar numbers and sizes of colonies, whereas in irradiated samples BCL-xL cells always presented more and bigger colonies.

In the second approach, different numbers of cells were plated allowing accurate counting of resulting colonies to calculate survival fractions. Colonies from all samples were fixed and stained on the same day. Survival fractions were normalized to the plating efficiency of corresponding non-irradiated cells. Plotting survival fractions against the applied dose confirmed a survival benefit of BCL-xL overexpressing cells compared to parental and empty vector control cells (Figure 12 B).

In summary, this shows that enforced expression of BCL-xL not only mediates resistance against irradiation-induced cell death but also promotes long-term survival.

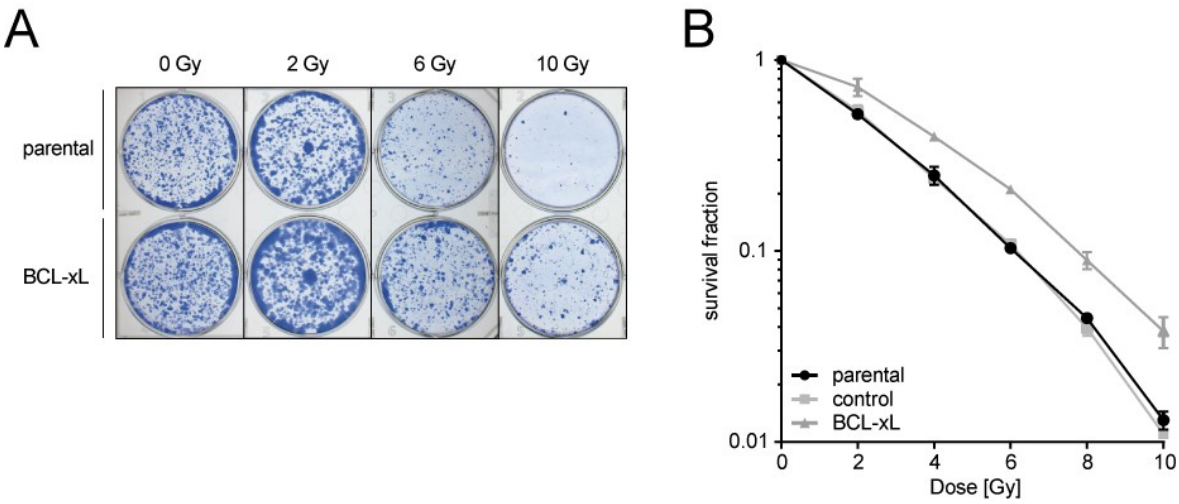

Figure 12: Long-term survival of A431 cells with enforced BCL-xL expression. (A) Representative images of colony formation of A431 cells stably transduced with BCL-xL expression vector compared to parental A431 cells. Equal numbers of cells were plated and irradiated with indicated doses (0 – 10 Gy). Images of stained colonies were taken after 6 – 9 d. **(B)** Clonogenic survival of A431 cells stably expressing BCL-xL and control cells (parental, vector control). Different numbers of cells were plated and irradiated with 0 – 10 Gy. Colonies were stained and counted after 11 d (mean + SD, n=2).

To validate the impact of BCL-xL on the radiation response in an organismal context *in vivo*, subcutaneous tumors were established by injection of A431 cells, expressing either BCL-xL or empty vector control, in the right hind limb of NOD/SCID mice. Comparing tumors with BCL-xL expression and control tumors, equal initial outgrowth and growth rates were observed. On day 11 after injection, outgrowing tumors were irradiated with a single fraction of 4 Gy local dose while the total body was shielded. At this time point, tumors had reached 0.3 to 0.6 cm in diameter. Due to this diversity in tumor size at the time of irradiation, relative tumor growth was calculated and compared between BCL-xL overexpressing tumors and control tumors. Interestingly, the impact of irradiation on relative tumor growth was higher in control xenografts compared to BCL-xL expressing xenografts (Figure 13).

This shows, that expression of BCL-xL also confers radioresistance *in vivo*.

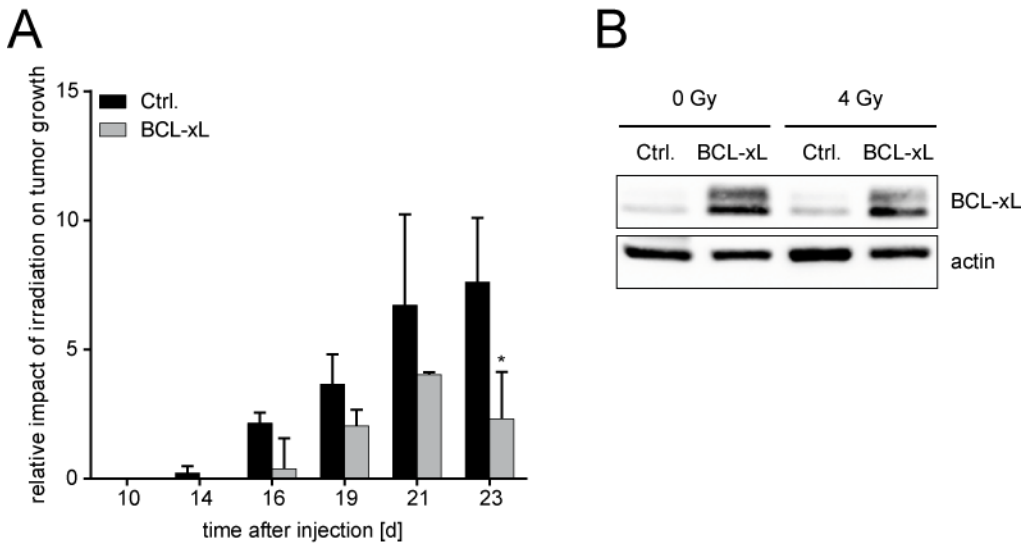

Figure 13: Relative impact of irradiation on tumor growth of BCL-xL overexpressing xenografts compared to control. (A) NOD/SCID mice received subcutaneous injections of A431 cells stably transduced with a BCL-xL expression vector (BCL-xL) or an empty vector control (Ctrl.). After 11 days, established tumors were irradiated with 4 Gy. Tumor growth was measured using a caliper and the impact of irradiation on relative tumor growth was calculated. **(B)** BCL-xL expression in tumors was controlled by immunoblotting, actin served as a loading control. * p ≤0.05 (compared to control cells at the same time point).

5.2.2 MCL-1-mediated radioresistance

Next, it was asked whether other anti-apoptotic BCL-2 family members also mediate resistance against irradiation or whether it is a BCL-xL-specific effect. To rule this out, MCL-1 was analyzed. This anti-apoptotic BCL-2 family member is one of the most frequently amplified genes in human cancer (Beroukhim et al. 2010; Wei et al. 2012) and is therefore of specific clinical interest. A431 cells stably expressing MCL-1 (Figure 14 A) were applied to short-term cell death and long-term clonogenic survival experiments. PI exclusion measured at 72 h post irradiation with 10 Gy revealed a significant decrease of PI-positive dead cells upon enforced expression of MCL-1 (Figure 14 B). However, compared to BCL-xL the effect was less pronounced. Nevertheless, MCL-1 also gave a competitive edge in clonogenic survival compared to control cells (Figure 14 C).

In summary, mediation of resistance against irradiation is no specific feature of BCL-xL, but also other anti-apoptotic BCL-2 family members like MCL-1 show similar effects concerning short-term as well as long-term survival *in vitro*.

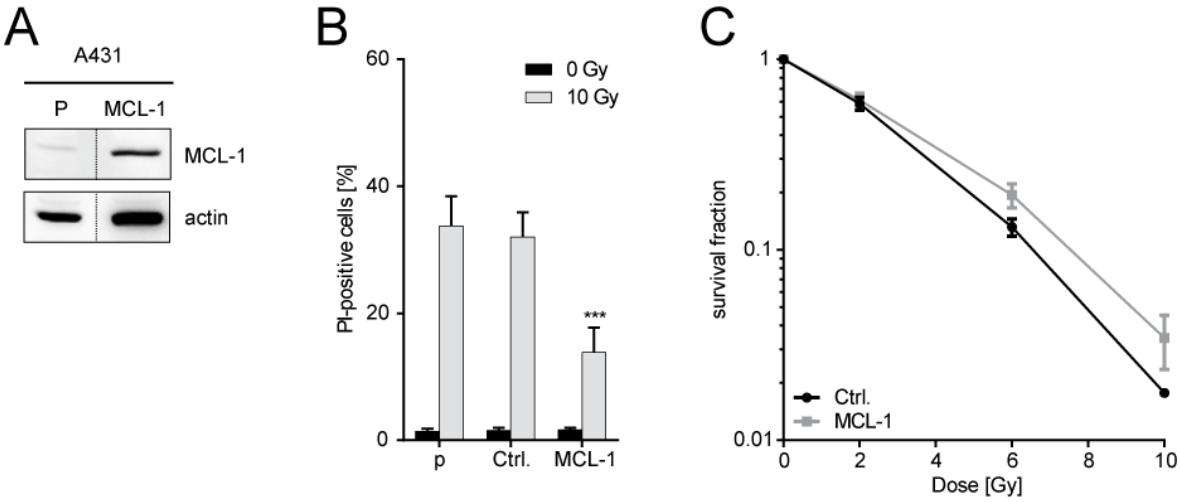

Figure 14: MCL-1-mediated resistance against irradiation. (A) Expression of MCL-1 in A431 cells stably transduced with a MCL-1 expression vector compared to parental cells (P). Protein levels were evaluated by immunoblotting, actin served as a loading control. **(B)** Irradiation-induced cell death of parental A431 cells, A431 cells stably transduced with an empty vector control (Ctrl.) and A431 cell stably transduced with a MCL-1 expression vector. Cells were stained with PI 72 h after irradiation with 10 Gy or sham-irradiation. The fraction of PI-positive cells was determined by flow cytometry (mean + SD, n = 3). **(C)** Long-term survival of MCL-1 overexpressing and control cells measured by colony formation after irradiation with different doses (mean + SD, n = 3). *** $p \leq 0.001$ (compared to parental and vector control cells).

5.2.3 Interference with endogenous anti-apoptotic BCL-2 family members to radiosensitize NSCLC cells

The above-mentioned results demonstrate that two different anti-apoptotic BCL-2 family members mediate resistance against irradiation in A431 cells. In the next step, the data should be verified in different NSCLC cell lines to exclude cell line specific functions of BCL-xL and MCL-1. However, several NSCLC cell lines showed higher intrinsic radioresistance than A431 cells (compare Figure 15), which rendered these cells unsuitable to validate resistance-mediating modulators. Thus, the data was validated by targeting endogenous anti-apoptotic BCL-2 family members in those cells, which should result in sensitization towards irradiation. Two different approaches were used to test this hypothesis: (1) short hairpin RNA (shRNA)-mediated knockdown of BCL-xL and MCL-1, and (2) conditional expression of pro-apoptotic BAK.

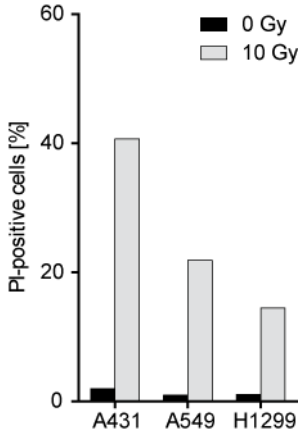

Figure 15: Resistance of NSCLC cells against irradiation. Irradiation-induced cell death of different NSCLC cells measured by PI staining 72 h after irradiation with 10 Gy or sham irradiation. The fraction of PI-positive cells was determined by flow cytometry (n=1).

For the first approach, stable knockdown of BCL-xL or MCL-1 was established by lentiviral transduction with vectors encoding shRNA from the MISSION TRC Mm 1.0 library (BCL-xL: TRCN 0000033499 – 503, MCL-1: TRCN 0000005514 – 518; Sigma-Aldrich) in A549 and H1299 lung cancer cell lines as well as in A431 cells. Immunoblotting confirmed knockdown efficiency of five different shRNAs for each target (Figure 16). Regarding BCL-xL knockdown, A549 and H1299 showed comparable patterns, whereas A431 cells differed slightly (Figure 16 A, C, E). In all three cell lines clone 499 induced a very efficient knockdown and was therefore used for all following experiments. Knockdown of MCL-1 was in general less effective and differed among the three cell lines (Figure 16 B, D, F). In A549 cells, clone 518 showed the highest knockdown efficiency. In H1299 cells, only three shRNAs allowed survival of transduced cells, but compared to parental H1299 cells none of those was really efficient in knocking MCL-1 down. Knockdown efficiency of clone 516 and 517 was best in A431 cells.

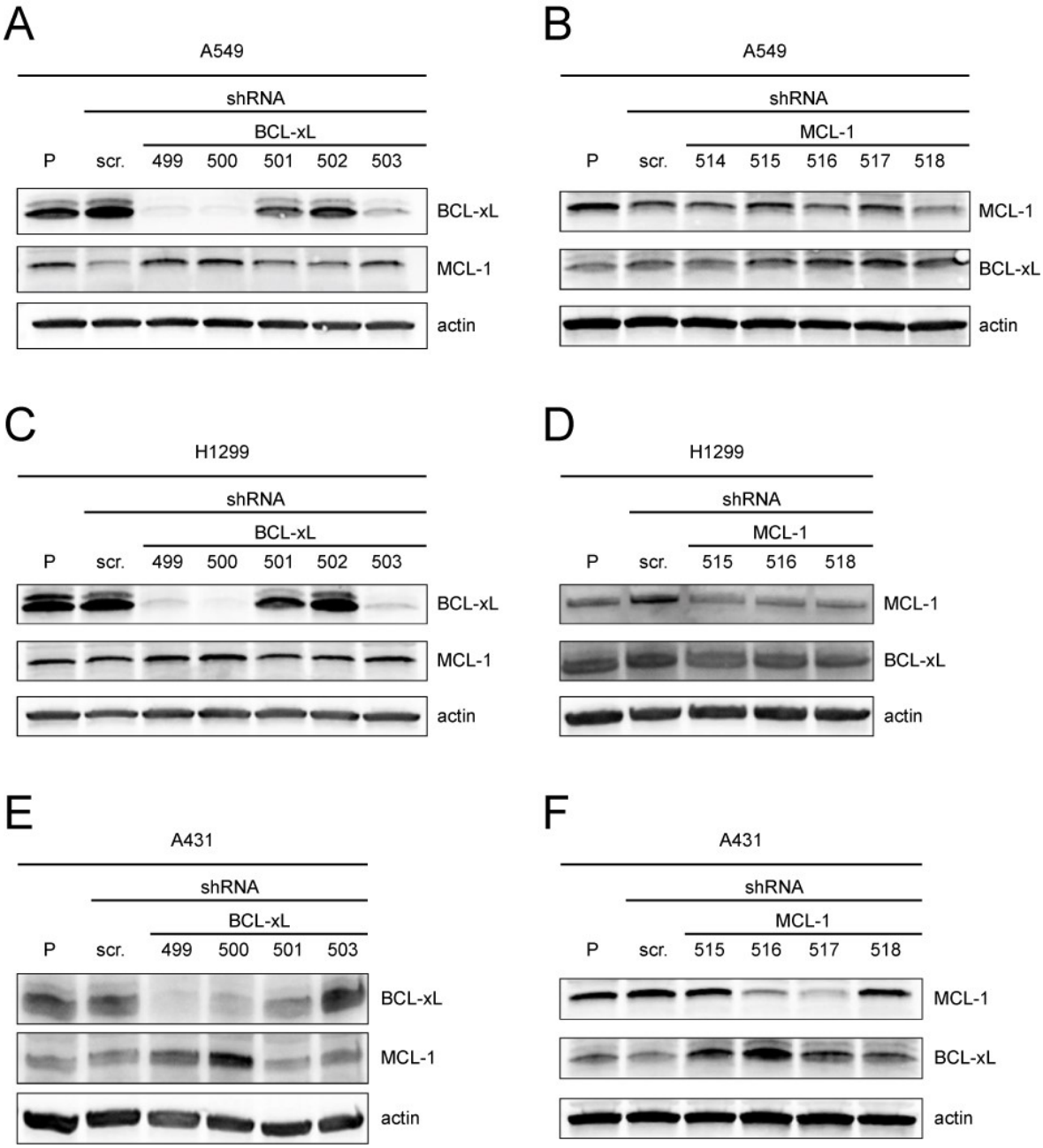

Figure 16: Expression of BCL-xL and MCL-1 in cells with knockdown. Expression of BCL-xL and MCL-1 was evaluated by immunoblotting in indicated cells stably expressing different lentiviral shRNA expression vectors targeting BCL-xL or MCL-1. Protein levels were compared to parental cells (P) and cells stably expressing a control shRNA vector (shRNA scr.). Actin served as a loading control. **(A)** A549 with BCL-xL knockdown, **(B)** A549 with MCL-1 knockdown, **(C)** H1299 with BCL-xL knockdown, **(D)** H1299 with MCL-1 knockdown, **(E)** A431 with BCL-xL knockdown, **(F)** A431 with MCL-1 knockdown.

The impact of BCL-xL and MCL-1 knockdown on the radiotherapy response was elucidated in short-term and long-term survival assays. As expected, knockdown of both modulators revealed radiosensitizing effects in A549 and A431 cells: knockdown cells showed significantly increased radiation-induced cell death (Figure 17 A – D) and decreased clonogenic survival (Figure 17 E – H).

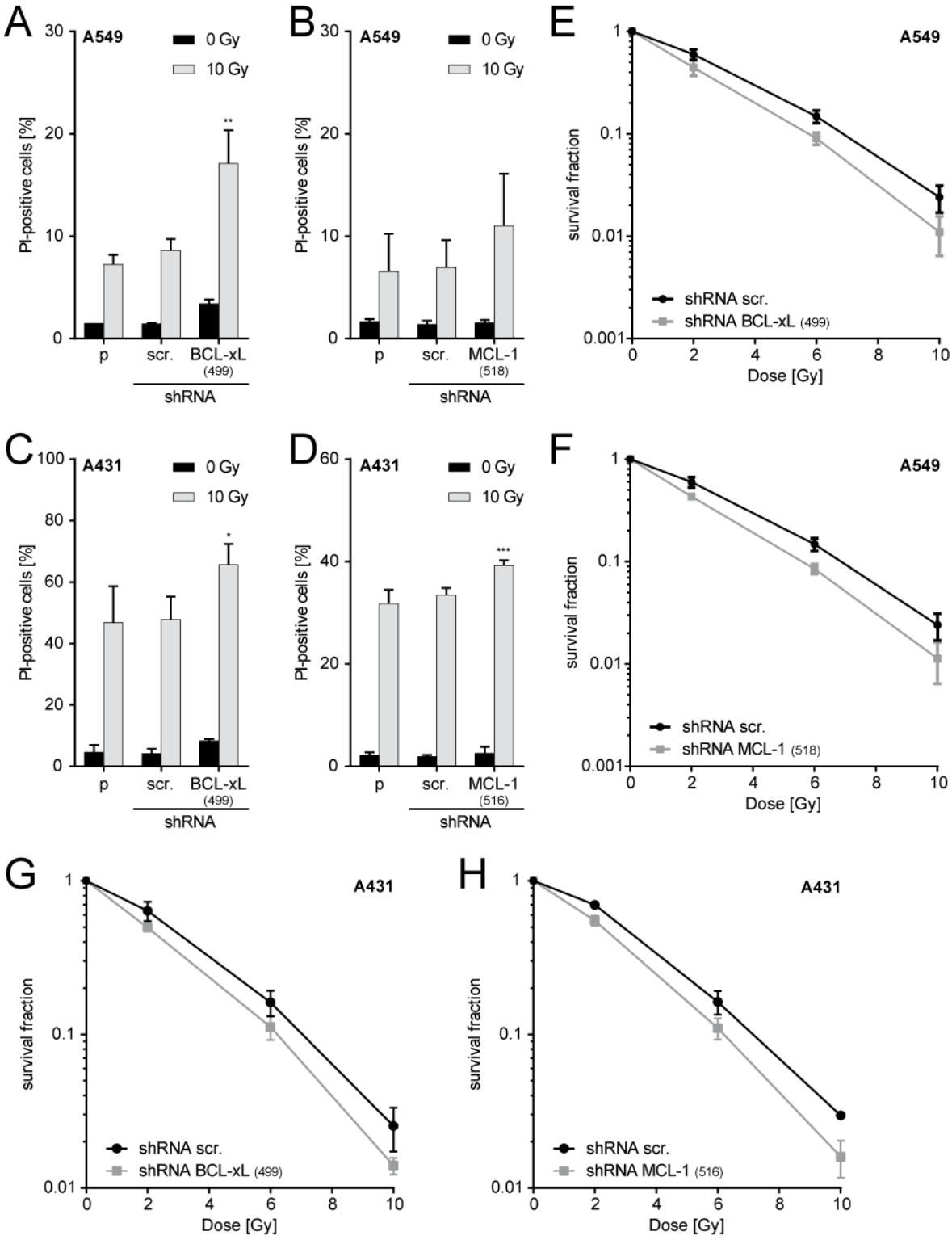

Figure 17: Sensitization of A549 and A431 cells to IR by knockdown of BCL-xL and MCL-1. (A, B) Irradiation-induced cell death of control A549 cells (parental, shRNA scr.) and BCL-xL (A) or MCL-1 (B) knockdown A549 cells (shRNA BCL-xL, shRNA MCL-1) 72 h after irradiation with 10 Gy or sham irradiation. The portion of dead cells was determined by staining with PI followed by flow cytometry (mean + SD, n = 2). **(C, D)** Irradiation-induced cell death of control A431 cells (parental, shRNA scr.) and BCL-xL (C) or MCL-1 (D) knockdown A431 cells (shRNA BCL-xL, shRNA MCL-1) 72 h after irradiation with 10 Gy or sham irradiation. Cell death was measured as in A. **(E, F)** Long-term survival of BCL-xL (E) or MCL-1 (F) knockdown A549 cells compared to control cells (shRNA scr.) measured by colony formation after irradiation with different doses (mean + SD, n = 3). **(G, H)** Long-term survival of BCL-xL (G) or MCL-1 (H) knockdown A431 cells compared to control cells (shRNA scr.) measured by colony formation after irradiation with different doses (mean + SD, n = 3). * $p \leq 0.05$, ** $p \leq 0.01$, *** $p \leq 0.001$.

In H1299 cells, the radiosensitizing effect of BCL-xL knockdown was also confirmed, while MCL-1 knockdown was not efficient in those cells and therefore had no impact on short- or long-term survival (Figure 18).

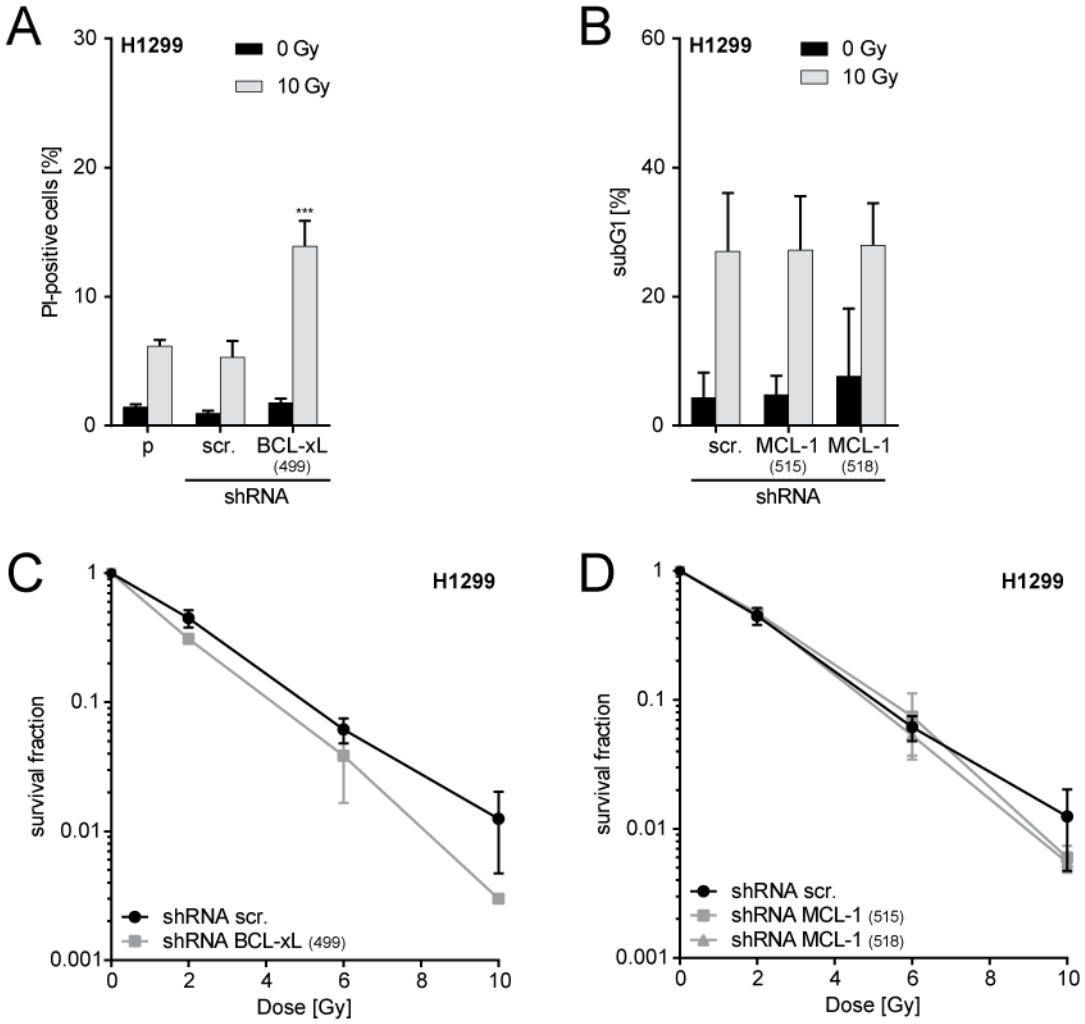

Figure 18: Sensitization of H1299 cells to IR by knockdown of BCL-xL. (A, B) Irradiation-induced cell death of control cells (parental, shRNA scr.) and BCL-xL (A) or MCL-1 (B) knockdown cells (shRNA BCL-xL, shRNA MCL-1) 72 h after irradiation with 10 Gy or sham irradiation. Cell death was determined by staining with PI followed by flow cytometry or determination of subgenomic DNA content (mean + SD, n = 2). **(C, D)** Long-term survival of BCL-xL (C) or MCL-1 (D) knockdown cells compared to control cells (shRNA scr.) measured by colony formation after irradiation with different doses (mean + SD, n = 3). *** $p \leq 0.001$.

The second approach of targeting endogenous anti-apoptotic BCL-2 family members was conditional expression of pro-apoptotic BAK in primarily radioresistant A549 cells. BAK belongs to the Bax-like death factors of the BCL-2 family and is a functional antagonist of BCL-xL and MCL-1 (Chittenden et al. 1995; Willis et al. 2005). Conditional overexpression of BAK changes the balance between pro-survival proteins (like BCL-xL and MCL-1) and pro-apoptotic proteins (like BAK and BAX), which primes cells for dying upon death signals (Danial &

Korsmeyer 2004). In this system, which was established before (Wesarg et al. 2007), addition of doxycycline (Dox) induced transcription of *BAK*, which led to increased BAK protein levels (Figure 19 A). The impact of conditional BAK expression on the radiotherapy response was again analyzed in short- and long-term assays. Induction of BAK in itself was slightly toxic, however the combination with irradiation (10 Gy) augmented the number of PI-positive, dead cells (Figure 19 B). More importantly, accelerated BAK expression also reduced long-term clonogenic survival of radioresistant A549 cells (Figure 19 C).

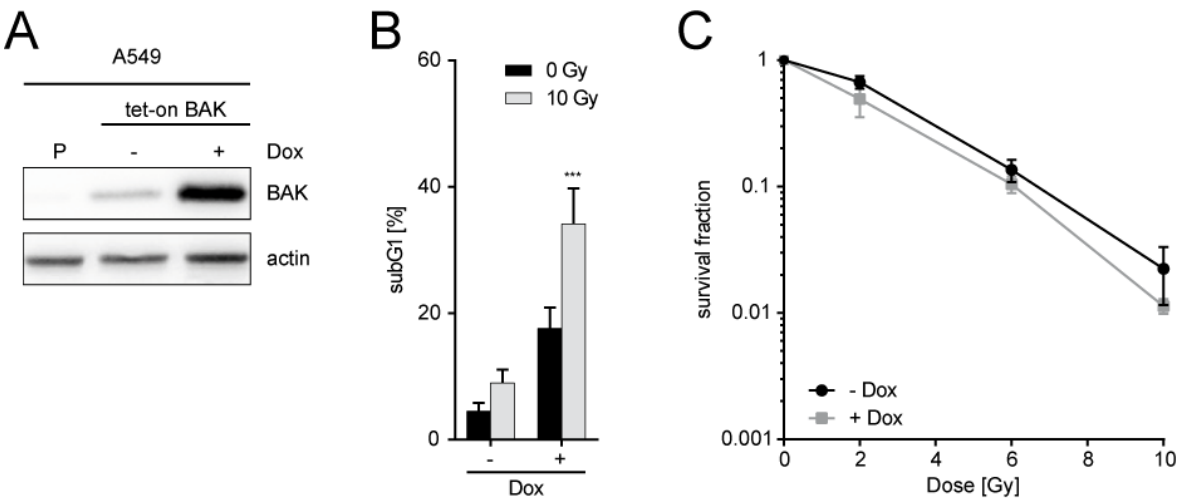

Figure 19: Functional block of BCL-xL by conditional overexpression of pro-apoptotic BAK. (A) Validation of conditional BAK expression in A549 cells stably transduced with a tet-on BAK expression system. BAK expression was induced by adding 100 ng/ml doxycycline for 24 h. Expression was evaluated by immunoblotting and compared to non-treated tet-on BAK cells and parental cells. Actin served as a loading control. **(B)** Irradiation-induced cell death of tet-on BAK cells in the presence or absence of doxycycline. 24 h before irradiation with 10 Gy or sham irradiation, BAK expression was induced as in A. Cell death was measured 72 h after irradiation by determining the cell fraction with subgenomic DNA content using flow cytometry (mean + SD, n = 4). **(C)** Long-term survival of tet-on BAK cells in the presence or absence of 100 ng/ml doxycycline and irradiation with indicated doses (mean + SD, n = 3). *** p ≤0.001.

5.2.4 Mechanistic dissection of radioresistance mediated by BCL-2 family proteins

Thinking about underlying mechanisms leading to resistance against irradiation mediated by BCL-xL and MCL-1, the obvious assumption was the inhibition of apoptosis, as this is the main known function of both modulators. Interestingly, only a minor fraction of irradiated A431 cells exhibited features of early apoptosis such as membrane externalization of phosphatidylserine (Figure 20). This was analyzed by AnnexinV-PI double stainings followed by flow cytometry at several time points post irradiation (4, 6.5, 24, and 48 h). Thus, those results suggested

that BCL-xL and MCL-1 also interfere with non-apoptotic radiation-induced death pathways.

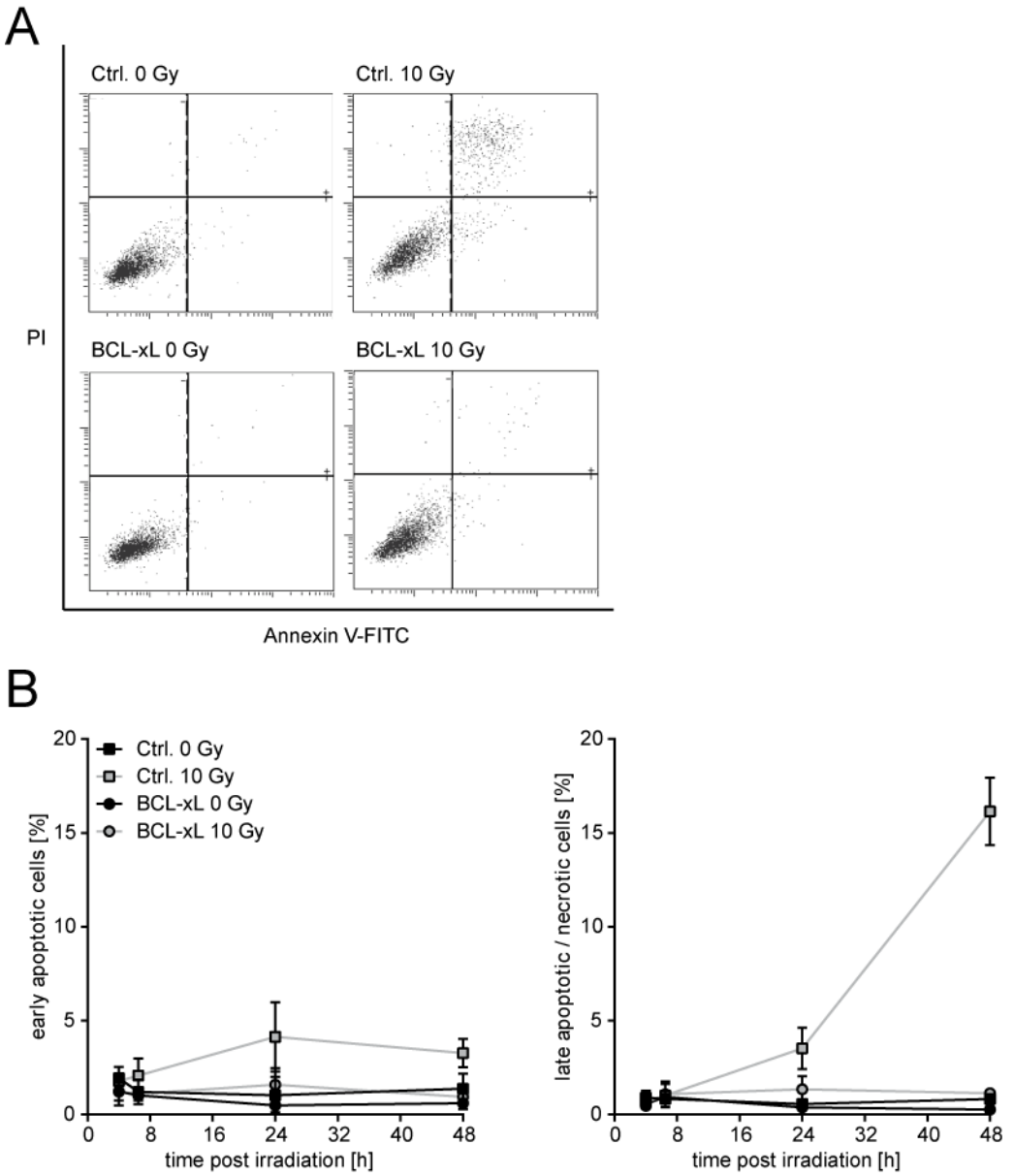

Figure 20: Analysis of apoptosis induced by irradiation. A431 cells stably expressing either vector control or BCL-xL vector were treated with 10 Gy or sham irradiation and stained with AnnexinV-FITC and PI at different time points (4, 6.5, 24 and 48 h). Early apoptotic cells (AnnexinV-positive, PI-negative) and late apoptotic / necrotic cells (AnnexinV-positive, PI-positive) were determined by flow cytometry. **(A)** Representative images of flow cytometry plots. X-axis: AnnexinV-FITC, y-axis: PI. **(B)** Quantification of early apoptotic (left) and late apoptotic / necrotic cells (right) plotted against time (mean + SD, n = 3).

To further explore the mechanistic basis of radioresistance, cell cycle checkpoints and DNA repair pathways were studied in relation to expression of anti-apoptotic BCL-xL, as these are the major cellular responses to ionizing radiation (Ross 1999). Irradiation induced a transient G2-arrest in A431 vector control cells and A431 cells with BCL-xL overexpression (Figure 21). The G2-arrest reached its

plateau at 8 h and was maintained until 24 h post irradiation. Cells with BCL-xL overexpression seemed to recover slightly faster, but this was no significant effect. Consequently, it was hypothesized that BCL-xL might interfere with DNA repair pathways.

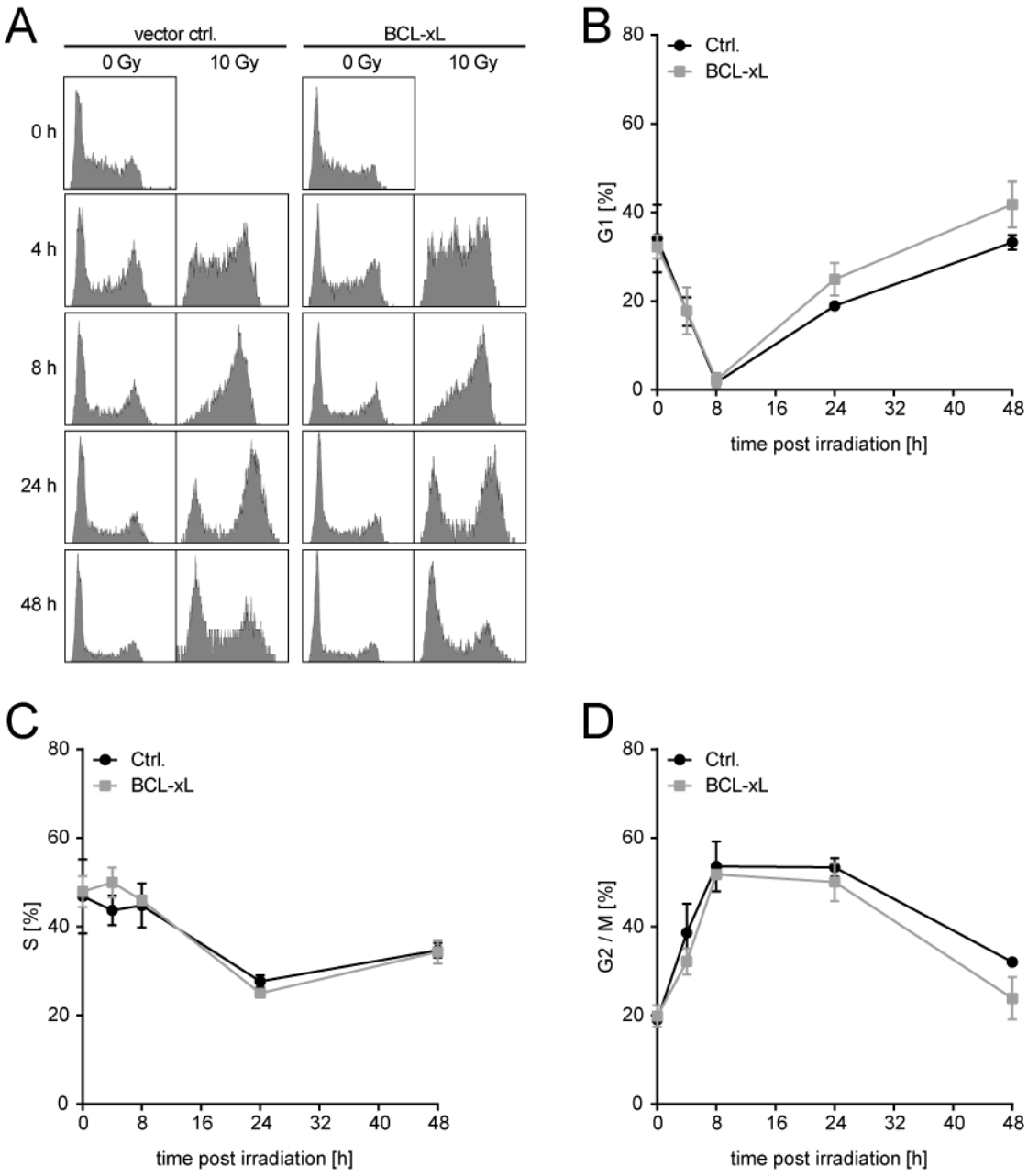

Figure 21: Analysis of cell cycle distribution upon irradiation. A431 cells stably expressing either vector control or BCL-xL vector were treated with 10 Gy or sham irradiation and cell cycle distribution was analyzed by flow cytometry at indicated time points (0, 4, 8, 24, and 48 h). **(A)** Representative images of histograms. **(B-D)** Quantification of cells in G1 phase (B), S phase (C), and G2/M phase (D after irradiation with 10 Gy (mean + SD, n = 3).

Ionizing radiation induces several DNA damages whereupon DNA DSBs are the principle cytotoxic lesions (Iliakis 1991). Hence, kinetics of DSB repair were evaluated in the presence or absence of enforced BCL-xL expression. DSBs accumulate upon ionizing radiation, which leads to DNA fragmentation in a dose-dependent manner and can be visualized by pulsed-field gel electrophoreses (PFGE). DNA fragments migrate size-dependently in an agarose gel under the influence of a pulsed electric field. The higher the dose, the higher the number of fragments and the more DNA migrates from the well into the lane (compare Figure 8 A). The fraction of DNA released (FDR) was quantified and plotted as a function of the applied radiation dose to generate dose-response curves (see Figure 22 A). In both cell lines, control A431 cells and BCL-xL overexpressing A431 cells, the increase of FDR was linear to the applied dose and equaled in both cell lines. This confirmed that BCL-xL has no impact on the induction of DSBs per unit of absorbed radiation dose.

For DSB repair kinetics, control A431 cells and BCL-xL overexpressing cells were irradiated with 20 Gy and repair was measured in the time interval of 0.5 to 8 h. Dose equivalents (DEQ) were calculated from the FDR at each time point based on dose-response curves to allow a higher comparability between different experiments (compare Methods section 4.10.1). DEQ reflects the equivalent dose for remaining DSBs at each time point. In both cell lines, about 90 % of induced DSBs were processed with fast kinetics within 1 h. Remaining DSBs were repaired within 4 to 8 h (Figure 22 B). Under these conditions, c-NHEJ is the dominant repair pathway and only marginal differences were observed in cells expressing BCL-xL.

To explore whether BCL-xL impacts on other DSB repair pathways, repair kinetic experiments were conducted in the presence or absence of NU7441. This small molecule is a highly potent and selective inhibitor of DNA-dependent protein kinase (DNA-PK), which is a key enzyme of c-NHEJ (compare 2.2.2.2). Under conditions of inhibited c-NHEJ, alt-EJ functions as backup and operates with slow kinetics, while HRR is not found to be involved in repair of DSBs under those conditions (Wang et al. 2001; Wu, Wang, Mussfeldt, et al. 2008; Wu, Wang, Wu, et al. 2008). As expected, inhibition of DNA-PK resulted in a slowdown of DSB repair compared to non-treated cells (Figure 22 C). Whereas all DSBs were repaired within 8 h in non-treated cells, in NU7441-treated cells about 25 % of

DSBs were still remaining after 8 h. Strikingly, in BCL-xL overexpressing cells approximately 50 % of DSBs were processed within 0.5 to 1 h, while control cells showed 50 % repair after 4 h. Thus, A431-BCL-xL cells tended to repair faster than A431-control cells, when c-NHEJ was blocked. This indicated that BCL-xL reduces the delay of alt-EJ repair.

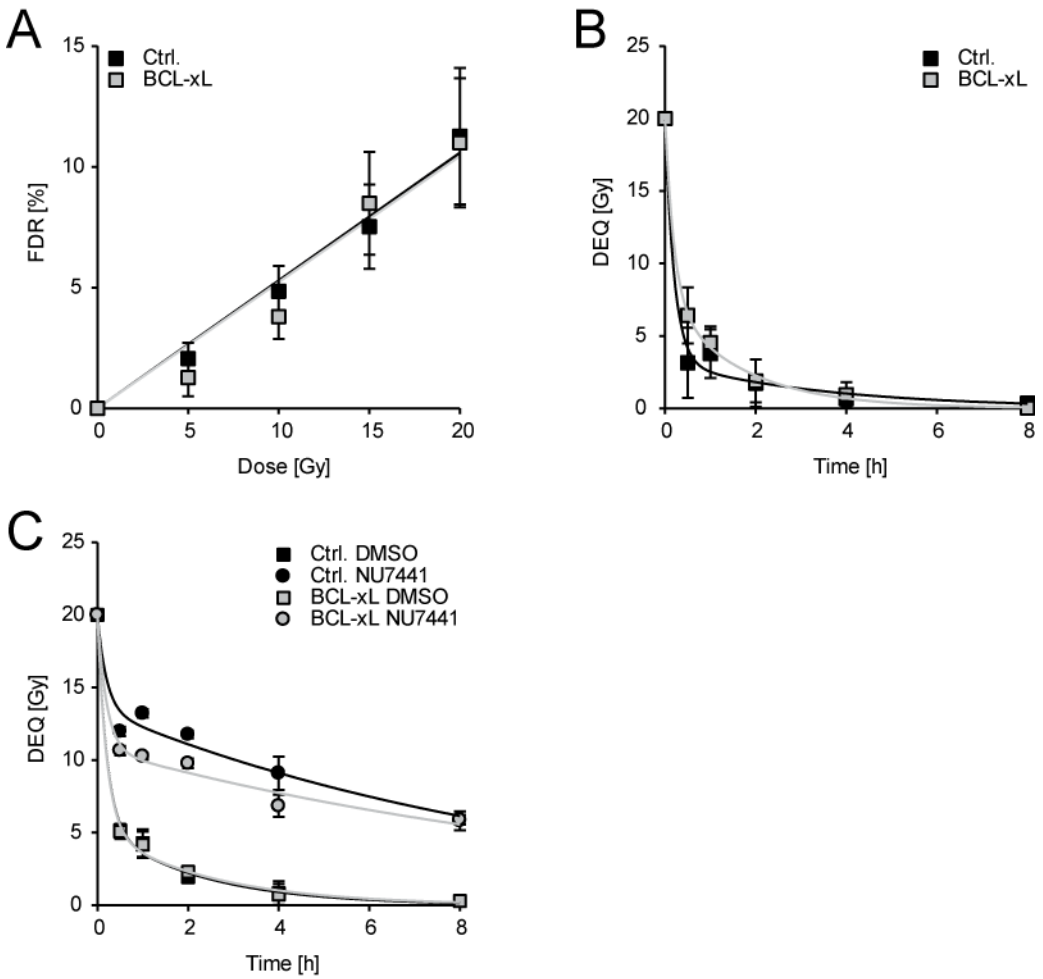

Figure 22: Analysis of DSB repair kinetics as a function of BCL-xL expression. **(A)** Dose response curves for the induction of DSBs in control A431 cells and BCL-xL overexpressing A431 cells exposed to different doses of IR (0 – 20 Gy) and measured by PFGE. **(B)** Repair kinetics of IR-induced DSBs after irradiation with 20 Gy. FDR at each time point after irradiation was converted to dose equivalents (DEQ) with the help of dose response curves, as described in the methods section (mean + SD). **(C)** Repair kinetics of IR-induced DSBs in A431 control and BCL-xL overexpressing cells measured in the presence or absence of the DNA-PK inhibitor NU7441. Cells were pretreated with 10 µM NU7441 for 1 h prior to irradiation with 20 Gy. FDR of each time point was converted in DEQ using dose response curves (mean + standard error, n = 2 with 4 samples each).

To further specify whether those effects have also an impact on cellular outcome after irradiation, colony formation assays were performed in the presence of NU7441. Interestingly, inhibition of c-NHEJ indeed reduced clonogenic survival

after irradiation, but BCL-xL overexpressing cells still showed higher survival compared to control cells (Figure 23 A).

The third repair pathway of DSBs, namely HRR, was inhibited by B02, a RAD51-specific inhibitor. B02 markedly reduced radiation-induced RAD51 foci formation (Figure S 3), but colony formation assays revealed only minor contribution of HRR to DSB repair in this context, as clonogenic survival in the presence of B02 was only marginally reduced compared to non-treated cells. Interestingly, the BCL-xL-mediated increase of clonogenic survival was abolished by treatment with B02 and there was no difference observable between BCL-xL overexpressing cells and control cells upon impaired HRR (Figure 23 B). This indicates that BCL-xL-mediated resistance depends on HRR, at least under these experimental conditions. However, kinetic studies for the formation and dissolution of RAD51 foci upon irradiation with 4 Gy revealed no significant differences (Figure S 4).

In summary, BCL-xL specifically impacts on radiation-induced DSB repair via HRR and alt-EJ. Whereas HRR seems to be fundamental for BCL-xL-mediated radioresistance, activity of alt-EJ is additionally enhanced in BCL-xL overexpressing cells.

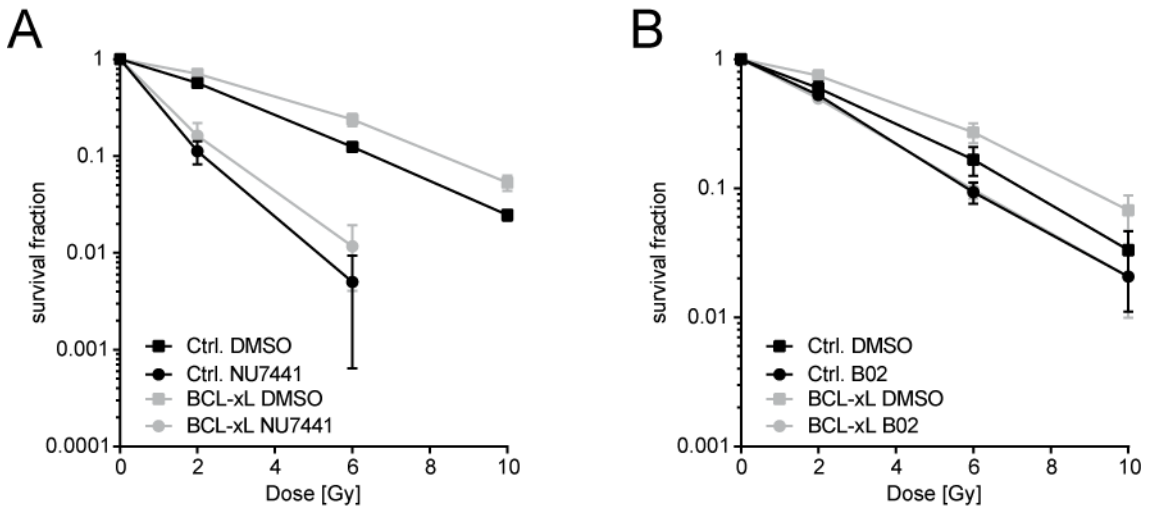

Figure 23: Long-term survival of A431 cells after combined treatment with irradiation and repair inhibitors. (A) A431 cells stably expressing either vector control (Ctrl.) or BCL-xL expression vector were pre-treated with 2 µM NU7441 or DMSO for 1 h before irradiation with different doses (0 – 10 Gy). After incubation for 24 h, medium was changed to inhibitor-free medium and colonies were grown for 11 days. **(B)** BCL-xL overexpressing A431 cells and control cells were pre-treated with 50 µM B02 or DMSO for 1 h before irradiation with different doses (0 – 10 Gy). Medium was changed to inhibitor-free medium after 6 h and colonies were grown for 11 day.

C-NHEJ repair is known to be error-prone, while alt-EJ even amplifies gross genomic aberrations (Dueva & Iliakis 2013). Enhanced alt-EJ in irradiated cancer cells expressing high levels of BCL-xL could thus result in the propagation of cancer cells with more damaged genomes, which could give rise to resistant and more aggressive subclones. To examine whether BCL-xL overexpression accumulates chromosomal aberrations, metaphase analyses of cells irradiated with 1 Gy were conducted in the presence or absence of NU7441 to favor c-NHEJ or alt-EJ. Cells were arrested in metaphase by colcemid treatment at 8 and 20 h after irradiation and chromosomes were analyzed microscopically. Figure 24 shows the mean of all aberrations per metaphase, including chromatid breaks, dicentrics, sister unions, chromosomal translocations, and acentric fragments (see Figure 24 A for representative images). These data confirm that preferential activity of alt-EJ amplifies irradiation-induced formation of chromosomal aberrations, as NU7441-treated cells have about twice as much aberrations as DMSO control cells. A difference between BCL-xL overexpressing cells and control cells was not observed under c-NHEJ conditions (absence of NU7441, Figure 24 B, left). On the contrary, the number of radiation-induced chromosomal aberrations was significantly increased in A431 cells with BCL-xL overexpression in the presence of NU7441 at 8 h after irradiation. However, at the later time point (20 h), this difference between BCL-xL and control cells was diminished which indicates an involvement of cells in S / G2 phase of the cell cycle and events of HRR abrogation that are backed up by alt-EJ.

In summary, these results suggest that BCL-xL overexpresssion mediates HRR-dependent resistance against irradiation and fosters the highly error-prone alt-EJ pathway, potentially resulting in the accumulation of genomic alterations.

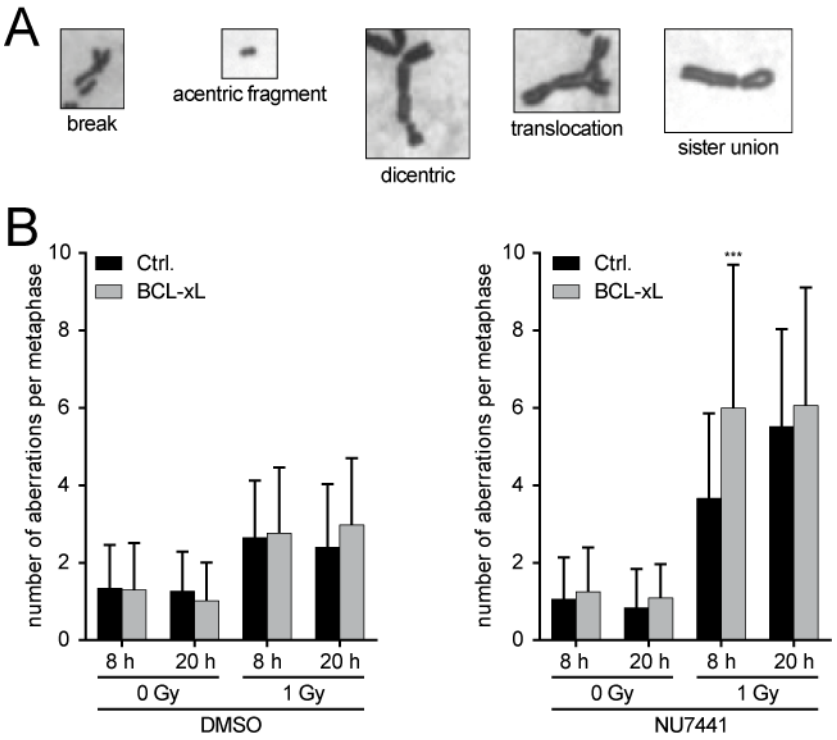

Figure 24: Chromosomal aberrations in the presence or absence of NU7441. A431 cells stably expressing either vector control (Ctrl.) or BCL-xL vector (BCL-xL) were pre-treated with 5 µM NU7441 for 1 h before irradiation with 1 Gy or sham irradiation. Cells were fixed after 8 and 20 h and metaphases were prepared. At least 50 metaphases of each sample were analyzed for chromosomal aberrations. **(A)** Representative images of different chromosomal aberrations. **(B)** Quantification of all chromosomal aberrations after different treatments. *** p ≤0.001.

5.2.5 Pharmacologic targeting of BCL-2 family members in combination with radiotherapy

Targeting anti-apoptotic BCL-2 family members by genetic or functional approaches sensitized lung cancer cells towards irradiation (compare 5.2.3). As those approaches are not feasible in the clinics, pharmacological interference with those proteins was tested to validate them as therapeutic targets. To this end, cells were treated with different BH3-mimetics. BH3-only proteins are a group of pro-apoptotic BCL-2 family members, which act upstream of BAX and BAK by neutralizing BCL-2-like survival factors (like BCL-xL and MCL-1) (Kirkin et al. 2004). Several peptides and small molecules have been developed to mimic BH3-only proteins in order to inhibit anti-apoptotic BCL-2 family members. ABT-737 is a small-molecule inhibitor of BCL-2, BCL-xL, and BCL-w, which enhances the effects of death signals (Oltersdorf et al. 2005). Although it has been reported that ABT-737 itself does not directly initiate the apoptotic process, an increase of dead

cells was observed in non-irradiated A549 cells upon ABT-737 treatment (Figure 25 A). However, additional irradiation of the cells amplified ABT-737-induced cell death significantly. Long-term survival after irradiation was marginally decreased by ABT-737 treatment (Figure 25 B).

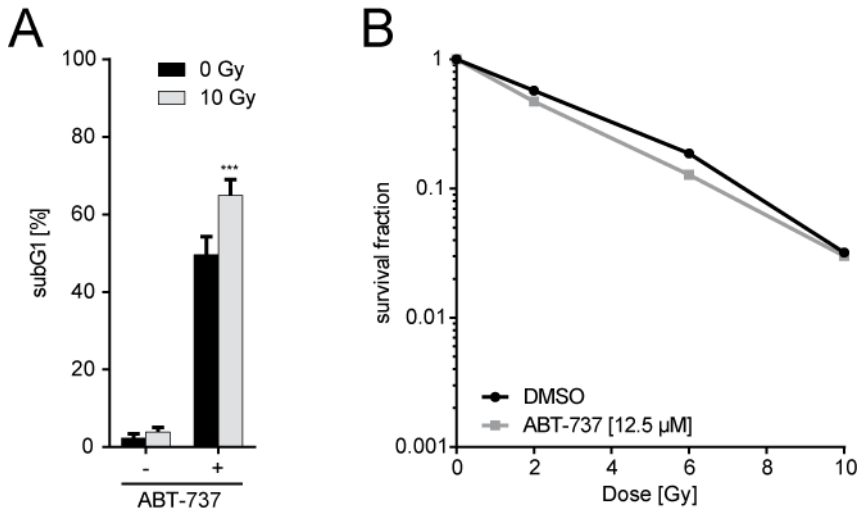

Figure 25: Functional block of BCL-2 family members by the BH3-mimetic ABT-737. (A) Irradiation-induced cell death of A549 cells treated with the BH3-mimetic ABT-737. A549 cells were pretreated with 12.5 µM ABT-737 for 1 h prior to irradiation with 10 Gy or sham irradiation. Cell death was quantified 72 h after irradiation by measuring the cell fraction with subgenomic DNA content using flow cytometry (mean + SD, n = 3). **(B)** Long-term survival of A549 cells treated with 12.5 µM ABT-737 and different doses of irradiation. A549 cells were pretreated with ABT-737 for 1 h prior to irradiation and ABT-737 was washed out 24 h after irradiation. Colonies were grown for 11 d (n=1).

As ABT-737 cannot be used as a therapeutic agent due to its low aqueous solubility and poor oral bioavailability, the second-generation BH3-mimetics ABT-263 (Navitoclax) and GX15-070 (Obatoclax) were included in this study. ABT-263 is orally bioavailable (Tse et al. 2008) and currently under clinical development in several cancer entities. Dose response curves for Navitoclax in A549 and H1299 cells, achieved from MTT assays, revealed 1 to 2.5 µM to be effective but not toxic (Figure S 2). Interestingly, even 0.5 to 1 µM Navitoclax were enough to highly sensitize A549 cells to irradiation-induced cell death (Figure 26 A). Moreover, 1 µM Navitoclax also enhanced the suppression of long-term clonogenic survival by radiation therapy of A549 cells (Figure 26 B). In H1299 cells, higher doses of Navitoclax (5 µM) were necessary to sensitize cells towards irradiation in short-term and long-term survival (Figure 26 C, D).

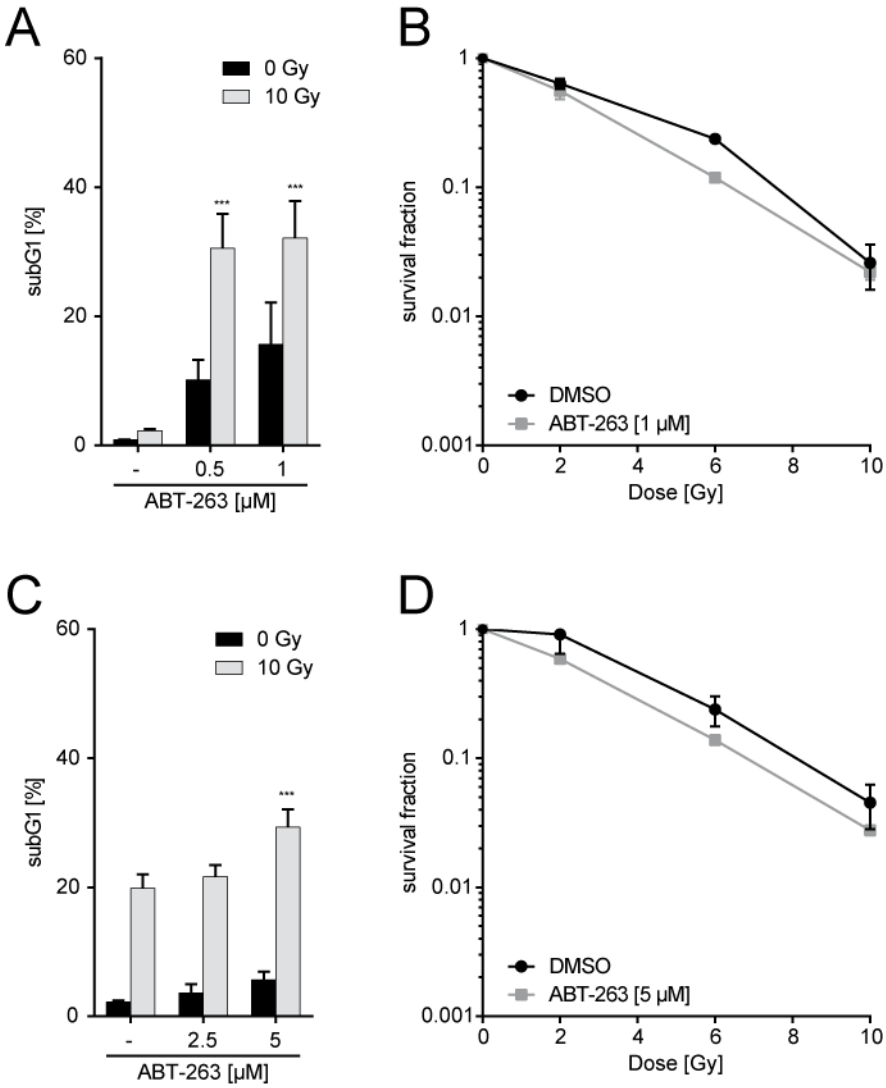

Figure 26: Functional block of BCL-2 family members by the bioavailable BH3-mimetic ABT-263. (A, C) Irradiation-induced cell death of A549 (A) and H1299 (C) cells in the presence or absence of the BH3-mimetic ABT-263. Cells were pretreated with indicated doses of ABT-263 for 1 h prior to irradiation with 10 Gy or sham irradiation. Cell death was quantified 72 h after irradiation by measuring the cell fraction with subgenomic DNA content using flow cytometry (mean + SD, n = 3). **(B, D)** Long-term survival of A549 (B) and H1299 (D) treated with indicated doses of ABT-263 and different doses of irradiation. ABT-263 was added 1 h before irradiation and cells were re-seeded for clonogenic survival in medium without ABT-263 24 h after irradiation (mean + SD, n = 3).

The third tested BH3-mimetic was Obatoclax. This small molecule is predicted to be a pan-BCL-2 inhibitor targeting all six anti-apoptotic BCL-2 family members (Zhai et al. 2006). Dose response curves showed that Obatoclax already inhibited proliferation in nanomolar concentrations (50 – 100 nM; Figure S 2). However, in contrast to Navitoclax, Obatoclax had rather no radiosensitizing effect in A549 and H1299 cells. Low concentrations (25 – 50 nM) did not increase irradiation-induced cell death significantly. Therefore, higher concentrations (0.5 – 1 µM) were also

tested, but the same results were observed in H1299 cells, while the dose was already highly toxic in A549 cells (Figure 27).

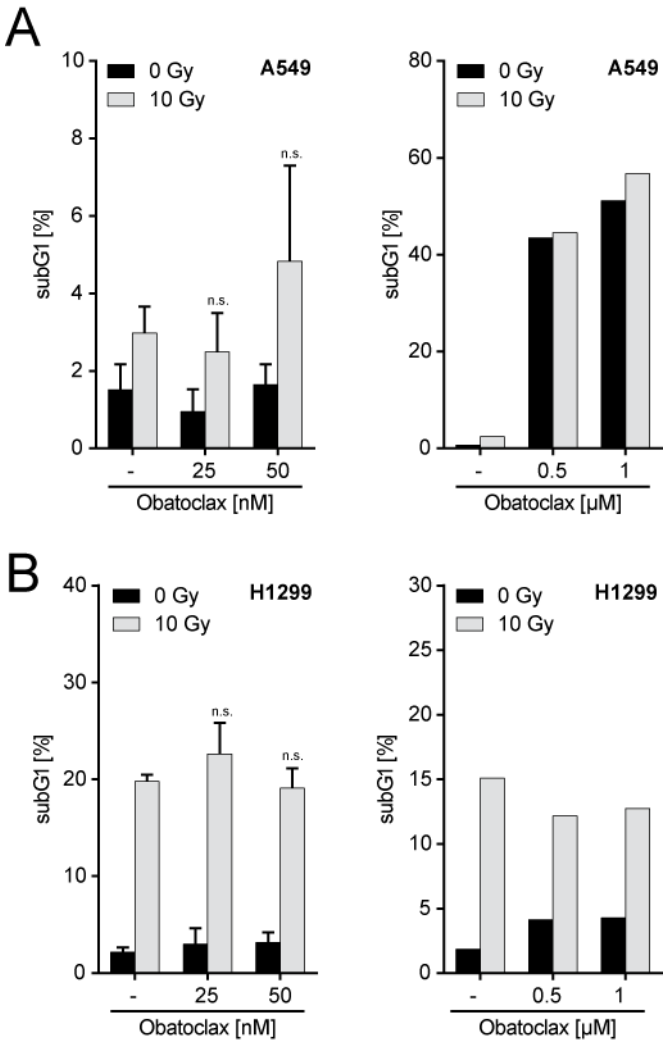

Figure 27: Treatment of A549 and H1299 cells with the pan BH3-mimetic Obatoclax. (A) Irradiation-induced cell death of A549 cells pre-treated with indicated concentrations of Obatoclax for 1 h before irradiation with 10 Gy or sham irradiation. Cell death was measured by determination of cell with subgenomic DNA content. **(B)** Irradiation-induced cell death of H1299 cells analyzed as in A. n.s. $p > 0.05$.

In summary, different approaches revealed that targeting either BCL-xL or MCL-1 sensitizes NSCLC cells towards irradiation. However, many cells still survived after combining irradiation with BH3-mimetics. Due to this, it was aimed to further sensitize cells towards irradiation. As both effective BH3-mimetics ABT-737 and Navitoclax do not interfere with MCL-1, which also mediated resistance against irradiation (Figure 14), it was hypothesized that simultaneous targeting of BCL-xL and MCL-1 should further increase irradiation-induced cell death. To test this, two different approaches were followed. In the first setup, BCL-xL knockdown and control A549 cells were treated with the synthetic compound flavopiridol, which

decreases MCL-1 levels (Ma et al. 2003, Figure 28 A / B left). Co-treatment with flavopiridol enhanced the sensitization of A549 and H1299 cells to irradiation-induced cell death by shRNA-mediated suppression of endogenous BCL-xL significantly (Figure 28 A / B right).

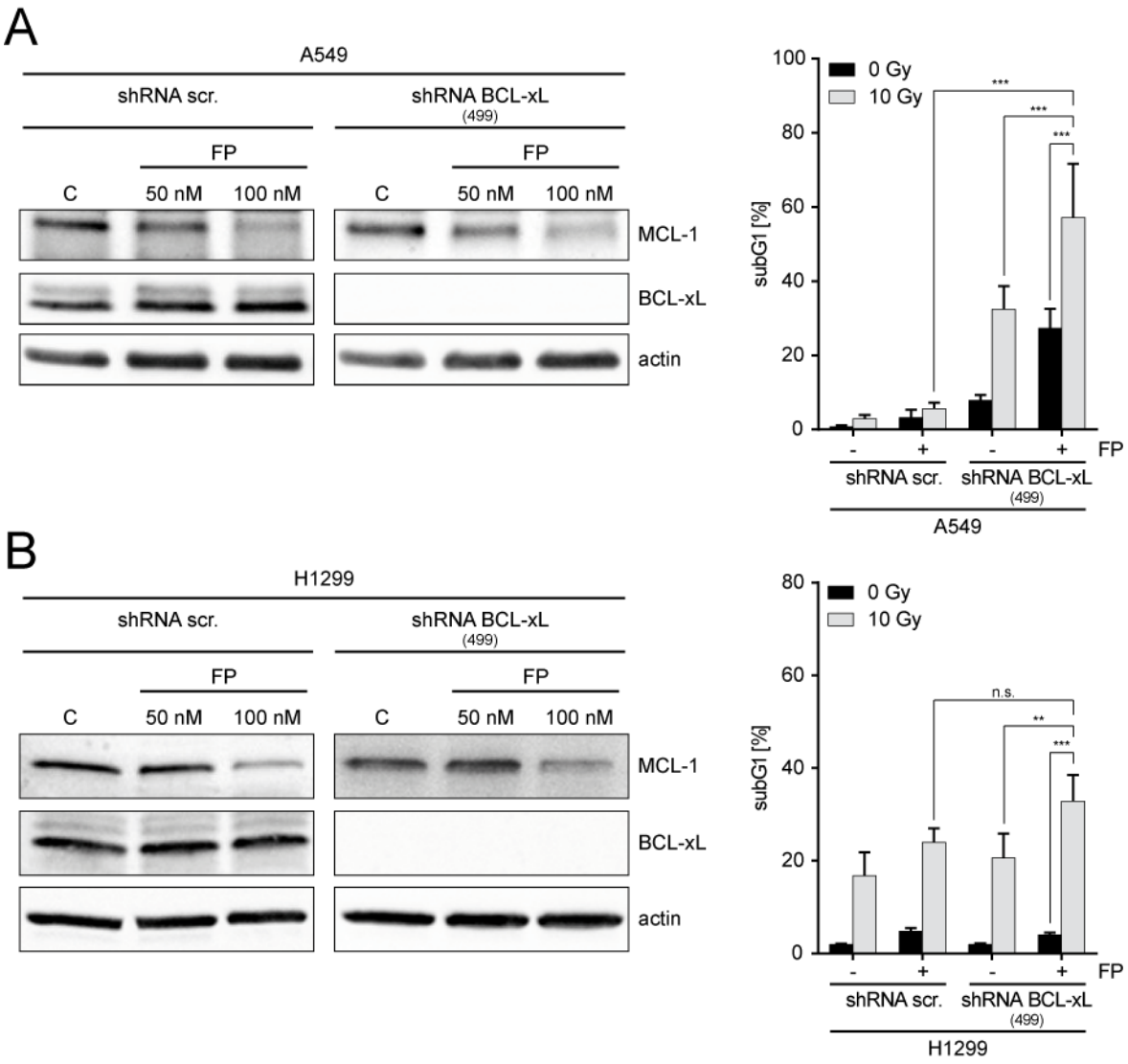

Figure 28: Combined treatment of BCL-xL and MCL-1 with shRNA knockdown and flavopiridol. (A) A549 cells stably expressing a lentiviral shRNA expression vector targeting BCL-xL (shRNA BCL-xL) or a control shRNA vector (shRNA scr.) were treated with flavopiridol (FP) to decrease MCL-1 protein levels. Left: Validation of MCL-1 decrease upon treatment with 50 and 100 nM FP compared to DMSO-treated cells (C). Protein levels were determined by immunoblotting 3 h after treatment. Actin served as a loading control. Right: Irradiation-induced cell death of indicated A549 cells, pre-treated with 100 nM FP for 3 h before irradiation with 10 Gy or sham irradiation. Cell death was measured 72 h after irradiation by determining the cell fraction with subgenomic DNA content using flow cytometry (mean + SD, n = 3). **(B)** H1299 cells stably expressing a lentiviral shRNA expression vector targeting BCL-xL (shRNA BCL-xL) or a control shRNA vector (shRNA scr.) were treated with FP to decrease MCL-1 protein levels. H1299 cells were treated and analyzed as A549 cells in A. n.s. $p>0.05$, ** $p \leq 0.01$, *** $p \leq 0.001$.

To confirm this observation, MCL-1 knockdown and control A549 cells were treated with ABT-737. The mimetic alone had again toxic effects as observed before and this was more pronounced in cells with MCL-1 knockdown. As mentioned above, the combination of ABT-737 and irradiation increased cell death and as expected, this was significantly higher in cells with stable MCL-1 knockdown (Figure 29 A). Interestingly, shRNA-mediated suppression of endogenous MCL-1 also further increased radiosensitization of the BH3-mimetic ABT-737 in H1299 (Figure 29 B), although MCL-1 knockdown was inefficient in those cells (compare Figure 16 D). In general, the combination of BCL-xL knockdown and flavopiridol treatment was more effective than MCL-1 knockdown and ABT-737 treatment. As shRNA-mediated gene suppression was more effective for BCL-xL than for MCL-1 (Figure 16), the observed differences have to be interpreted with caution.

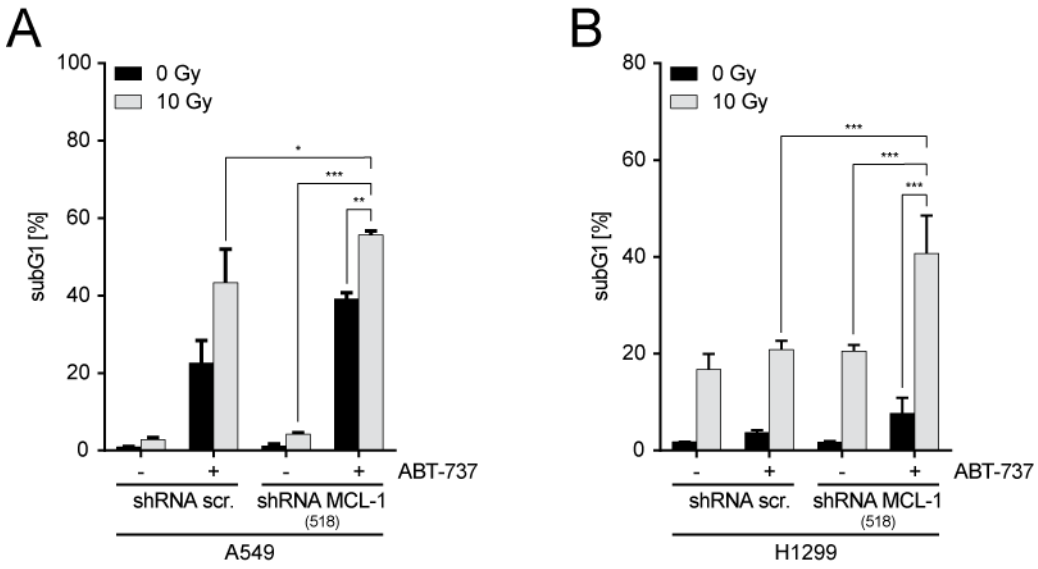

Figure 29: Combined treatment of BCL-xL and MCL-1 with ABT-737 and shRNA knockdown. A549 **(A)** and H1299 **(B)** cells stably expressing a lentiviral shRNA expression vector targeting MCL-1 (shRNA MCL-1) or a control shRNA vector (shRNA scr.) were pretreated with 5 µM ABT-737 for 1 h followed by irradiation with 10 Gy or sham irradiation. Cell death was determined by quantifying the cell fraction with subgenomic DNA content using flow cytometry (mean + SD, n = 3) * p ≤0.05, ** p ≤0.01, *** p ≤0.001.

5.3 Characterization of RAF-1 as a modulator of radiotherapy response

Besides BCL-xL, the signal transduction mediator RAF-1 was identified as a strong modulator of the radiotherapy response in the initial screen in A431 cells (see 5.1). The following section will further characterize the impact of RAF-1 on radiotherapy modulation.

5.3.1 Long-term survival after irradiation in the presence of active RAF-1

To determine radiosensitivity of cells, the most common method is the clonogenic survival assay. To analyze the impact of RAF-1 activation on clonogenic survival, equal numbers of A431 cells stably transduced with a vector containing ΔRAF-1-ER^{tam} were seeded in the presence or absence of 4OHT and irradiated with different doses of γ-irradiation (0 – 10 Gy). Colony formation was analyzed after 6 d of growing. Figure 30 shows that permanent activation of RAF-1 by 4OHT led to inhibition of clonogenic survival. A lower number of colonies were grown in non-irradiated controls treated with 4OHT compared to cells without 4OHT treatment. Thus, it is questionable whether cells irradiated in the presence or absence of activated RAF-1 are comparable.

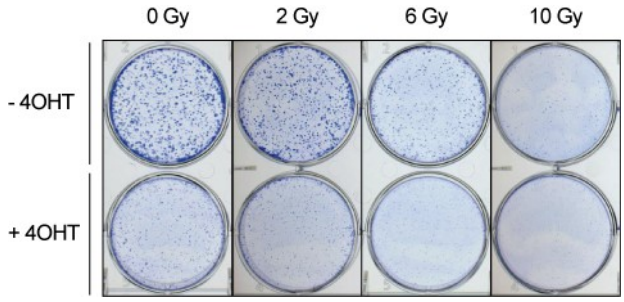

Figure 30: Long-term survival of A431 cells with conditionally active RAF-1. Representative images of colony formation of A431 cells stably transduced with ΔRAF-1-ER^{tam} expression vector in the presence or absence of 4OHT. Equal numbers of cells were plated and RAF-1 was induced by addition of 100 nM 4OHT. After irradiation with indicated doses (0 – 10 Gy), colonies were grown for 6 d.

5.3.2 Cell cycle changes upon RAF-1 activation

To further characterize the modulation of the radiotherapy response by RAF-1, irradiation-induced changes in cell cycle distribution of A431 cells transduced with conditionally active RAF-1 were analyzed in the presence or absence of 4OHT. Upon irradiation, A431 cells with conditionally activatable RAF-1 underwent a transient G2-arrest, which was stable from 8 to 24 h post irradiation (Figure 31). The induction of RAF-1 activity by 4OHT did not influence this effect.

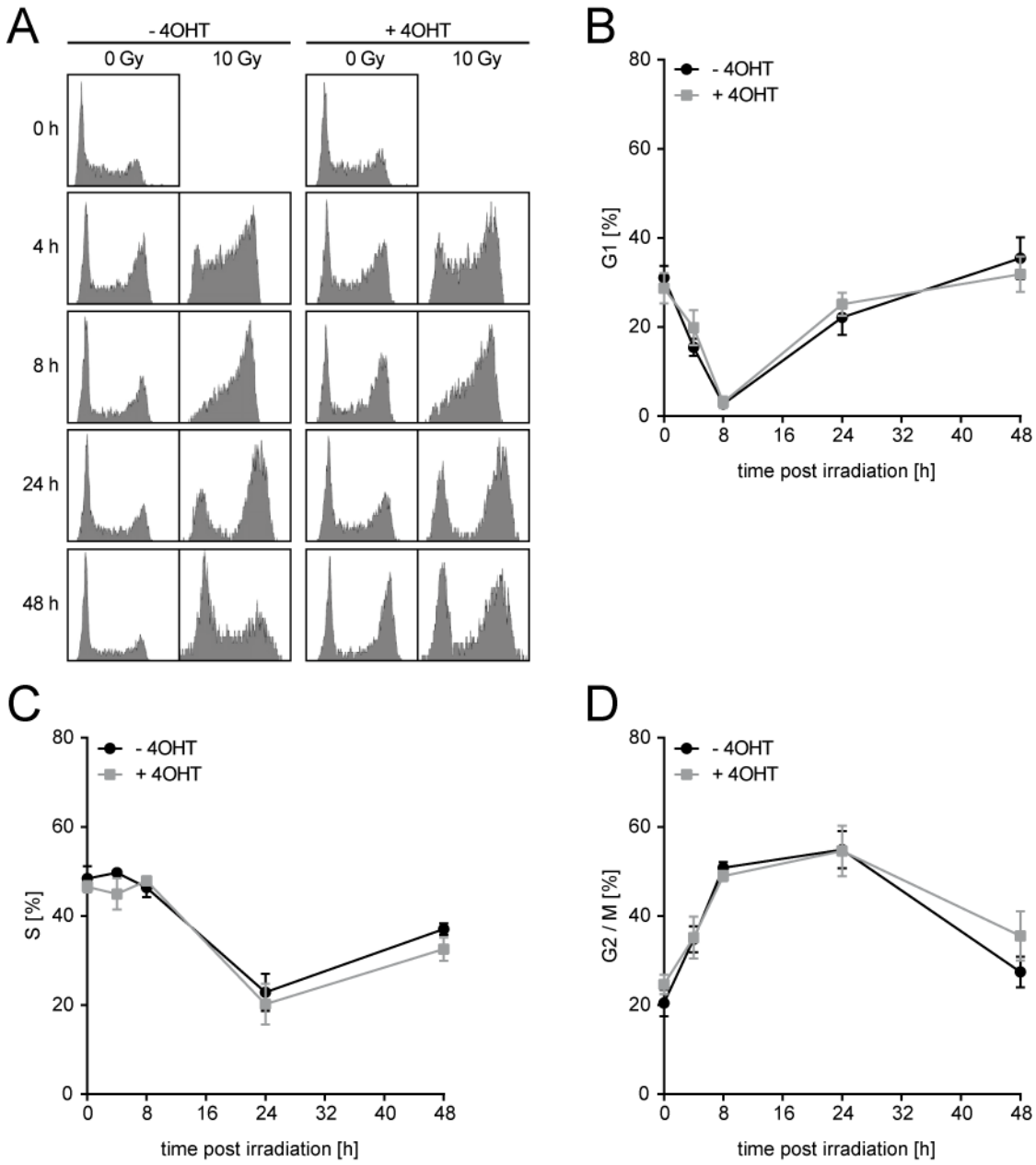

Figure 31: Analysis of cell cycle distribution upon irradiation of A431 cells with conditionally active RAF-1. A431 cells stably transduced with ΔRAF-1-ER^{tam} expression vector were treated with 10 Gy or sham irradiation in the presence (+ 4OHT) or absence (- 4OHT) of 100 nM 4OHT. Cell cycle distribution was analyzed by flow cytometry at indicated time points (0, 4, 8, 24, and 48 h). **(A)** Representative images of histograms. **(B-D)** Quantification of cells in G1 phase (B), S phase (C), and G2 / M phase (D) after irradiation with 10 Gy. (mean + SD, n = 3).

Interestingly, it was observed that permanent activation of RAF-1 in non-irradiated cells induced cell cycle changes. While cells with inactive RAF-1 (- 4OHT) arrested in G1 phase of the cell cycle after 24 h post sham irradiation, possibly due to contact inhibition, cells with activated RAF-1 (+ 4OHT) accumulated in G2 phase after 24 h post sham irradiation (Figure 32).

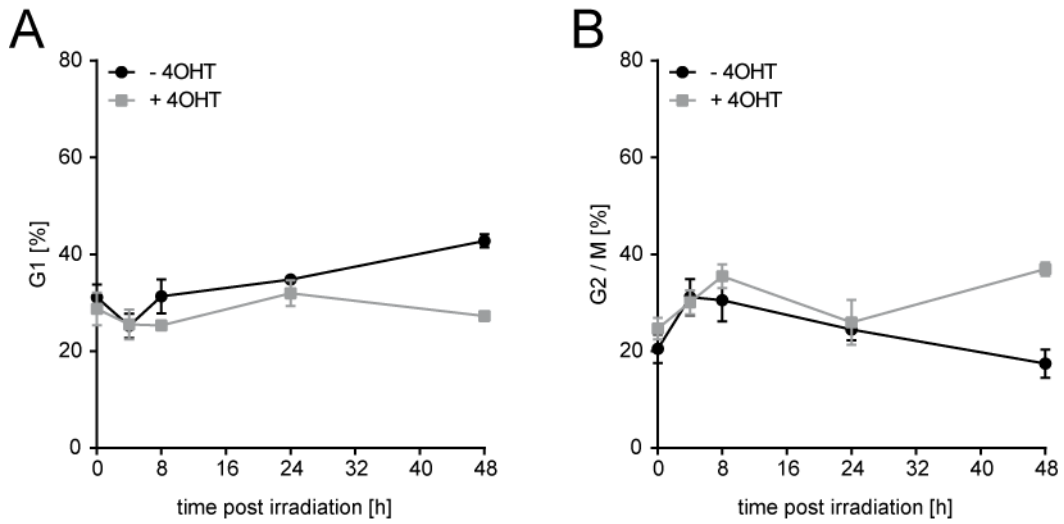

Figure 32: Analysis of cell cycle distribution in non-irradiated A431 cells with conditionally active RAF-1. A431 cells stably transduced with ΔRAF-1-ER^{tam} expression vector were treated with sham irradiation in the presence (+ 4OHT) or absence (- 4OHT) of 100 nM 4OHT. Cell cycle distribution was analyzed by flow cytometry at indicated time points (0, 4, 8, 24, and 48 h). Quantification of cells in G1 phase **(A)** and G2 / M phase **(B)** (mean + SD, n = 3).

5.3.3 Characterization of cell death mechanisms

The initial screening experiment using PI exclusion assay revealed that irradiation of cells with activated RAF-1 induced less cell death. However, the underlying cell death mechanism was not characterized at that point. Therefore, AnnexinV – PI double stainings were performed in the presence or absence of 4OHT in irradiated A431 cells stably transduced with conditionally activatable RAF-1. Cells were stained at multiple time points post irradiation (4, 6.5, 24, and 48 h) to follow kinetics of apoptosis. As described above, only a minor fraction of irradiated A431 cells exhibited externalization of phosphatidylserine, which is a known feature of early apoptosis (Figure 33 A / B). The activation of RAF-1 had no impact on this. Surprisingly, it was observed that activation of RAF-1 in A431 cells induced morphological changes under these experimental settings. While A431 cells with inactive RAF-1 (- 4OHT) shared epithelial-like morphologies as parental cells and

grew quite dense, A431 cells with active RAF-1 (+ 4OHT) seemed to grow bigger in size, had a more spindle-like cell shape with some filopodia, and most impressively had a lot of vacuole-like structures in the cell body (Figure 33 C).

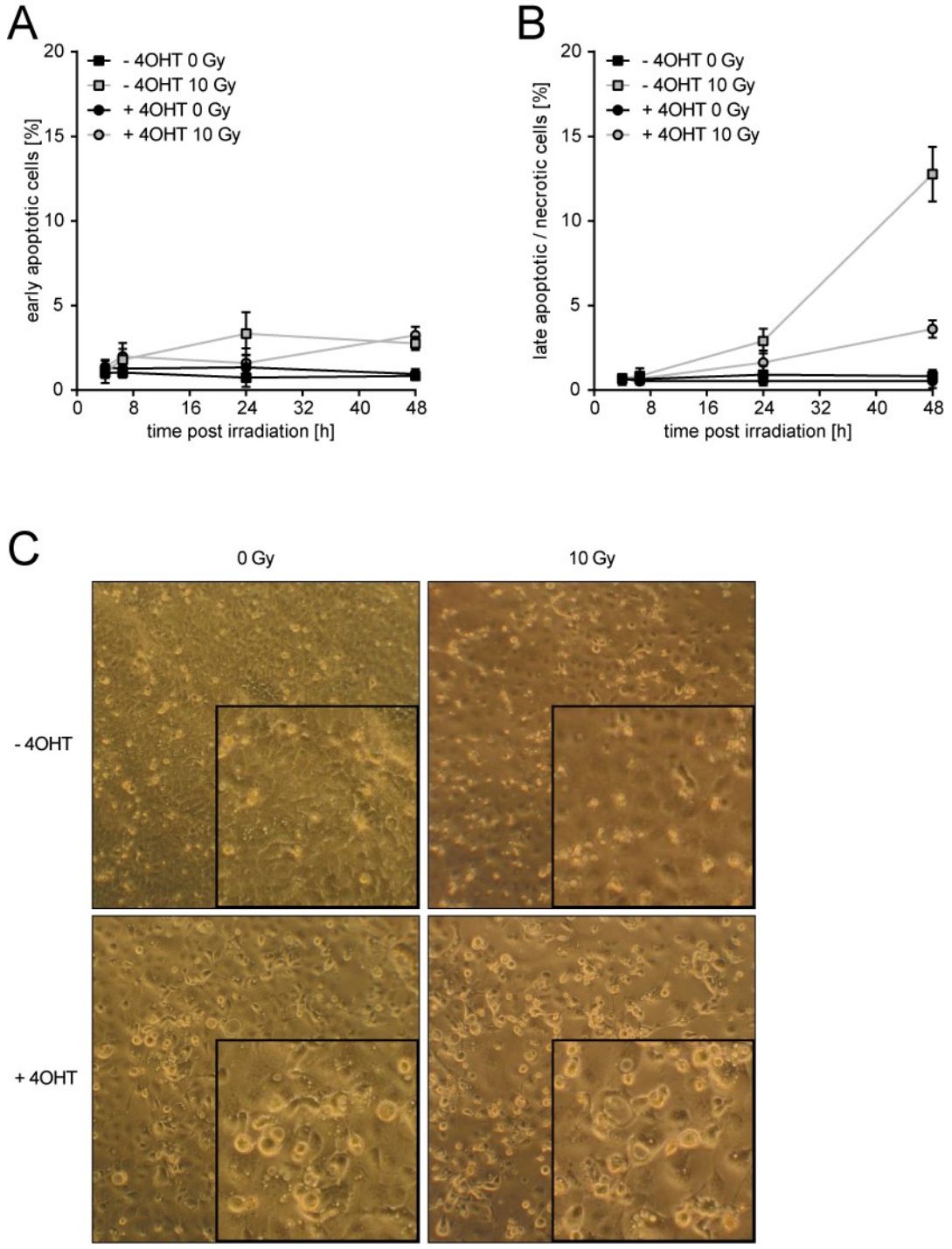

Figure 33: Analysis of apoptosis induced by irradiation in A431 cells with conditionally active RAF-1. A431 cells stably transduced with ΔRAF-1-ER^{tam} expression vector were irradiated with 10 Gy or sham irradiation in the presence (+ 4OHT) or absence (- 4OHT) of 100 nM 4OHT. Cell were stained with AnnexinV-FITC and PI at different time points (4, 6.5, 24 and 48 h) and measured by flow cytometry. **(A)** Quantification of early apoptotic cells (AnnexinV-positive, PI-negative; mean + SD, n = 3). **(B)** Quantification of late apoptotic / necrotic cells (AnnexinV-positive, PI-positive; mean + SD, n = 3). **(C)** Representative images of A431 [ΔRAF-1-ER^{tam}] cells in the presence or absence of 4OHT taken at 72 h post irradiation.

5.3.4 Impact of different timing of RAF-1 activation on radiotherapy response

To further rule out the impact of RAF-1 on the radiotherapy response, it was taken advantage of the conditional activation system. It was investigated whether different timings of RAF-1 activation and de-activation by addition and removal of 4OHT, respectively, leads to different responses upon irradiation. Immunoblotting showed that RAF-1 is activated in the cells, at least, after 1 h of incubation with 4OHT (Figure 34 A). Removal of 4OHT did not directly result in RAF-1 deactivation as shown by immunoblotting. Even 98 h after removal of 4OHT, RAF-1 was still activated in those cells (Figure 34 B).

In the first setup, four different timing strategies were tested:

- presence of 4OHT from seeding till read-out
- presence of 4OHT from seeding till 1 h post irradiation
- presence of 4OHT from 1 h before irradiation till 1 h post irradiation
- presence of 4OHT from 1 h after irradiation till read-out.

The impact of timing of RAF-1 activation on radiosensitivity was analyzed by PI exclusion assay at 72 h after irradiation. Interestingly, there was no significant difference between the different timing strategies (Figure 34 C). Cell death was always significantly reduced when RAF-1 was activated. Surprisingly, even activation after irradiation was enough to protect cells from irradiation-induced cell death.

In the next step, it was further analyzed when RAF-1 has to be activated after irradiation to mediate resistance against irradiation. To this end, the effect of 8 different activation time points was examined:

- at seeding (20 h before irradiation)
- directly before irradiation
- 5 min after irradiation
- 15 min after irradiation
- 30 min after irradiation
- 1 h after irradiation
- 2 h after irradiation
- 6 h after irradiation

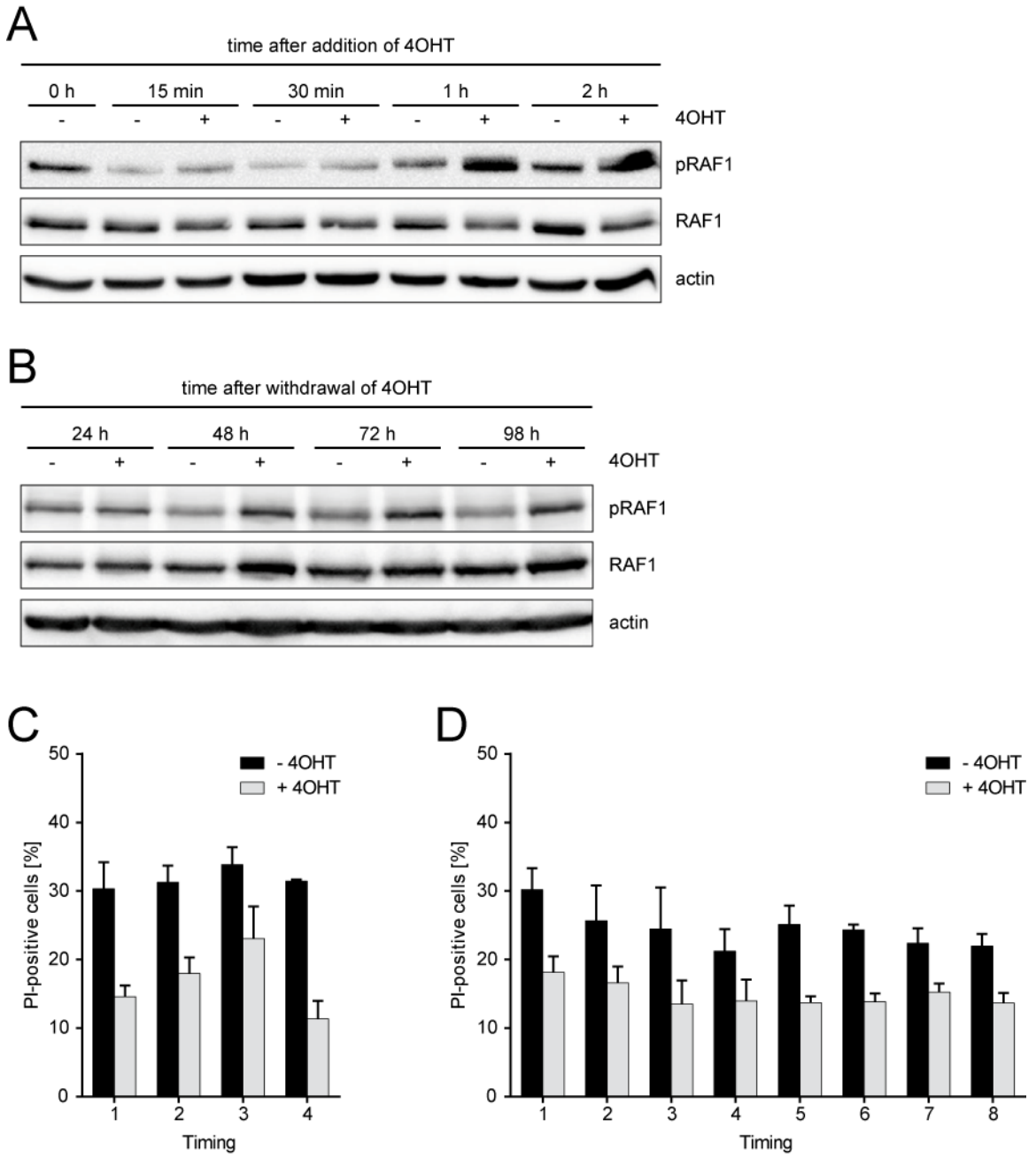

Figure 34: Analysis of different timing of RAF1 activation. (A) Kinetic of RAF-1 activation after addition of 4OHT. A431 cells stably expressing ΔRAF-1-ER^{tam} were seeded in medium with 0.5 % FBS and treated with 100 nM 4OHT for indicated time intervals. Protein expression was measured by immunoblotting, actin served as a loading control. **(B)** Kinetic of RAF-1 deactivation after withdrawal of 4OHT. A431 cells stably expressing ΔRAF-1-ER^{tam} were treated with 100 nM 4OHT. After 20 h, medium was changed to 4OHT-free medium and cells were lysed at indicated time points. Protein expression was measured by immunoblotting, actin served as a loading control. **(C)** Radiation-induced cell death of A431 cells stably transduced with ΔRAF-1-ER^{tam} expression vector treated with different timings of 4OHT addition and removal. Cell death was measured at 72 h after irradiation with 10 Gy. Percentage of PI-positive cells in irradiated cells was normalized to non-irradiated cells. 1) 100 nM 4OHT was added at seeding, no withdrawal of 4OHT; 2) 100 nM 4OHT was added at seeding, withdrawal of 4OHT 1 h after irradiation; 3) 100 nM 4OHT was added 1 h before irradiation, withdrawal of 4OHT 1 h after irradiation; 4) 100 nM 4OHT was added 1 h after irradiation, no withdrawal of 4OHT (mean + SD, n = 3). **(D)** Radiation-induced cell death of A431 cells stably transduced with ΔRAF-1-ER^{tam} expression vector treated with 100 nM 4OHT at different time points after irradiation. Cell death was measured as in A. 1) 4OHT was added at seeding; 2) 4OHT was added directly before irradiation; 3) 4OHT was added 5 min after irradiation; 4) 4OHT was added 15 min after irradiation; 5) 4OHT was added 30 min after irradiation; 6) 4OHT was added 1 h after irradiation; 7) 4OHT was added 2 h after irradiation; 8) 4OHT was added 6 h after irradiation (mean + SD, n = 3).

As observed before, activation of RAF-1 always reduced radiation-induced cell death significantly (Figure 34 D) and only minor differences between the samples of diverse activation time points were observed.
In summary, this shows that timing of RAF-1 activation does not play a role for its radioprotective effects, even at 6 h after irradiation activation leads to protection against irradiation-induced cell death. However, the results for RAF-1 deactivation have to be considered with caution as removal of 4OHT did not directly lead to RAF-1 deactivation.

5.3.5 Analysis of RAF-1 *in vivo*

Another aim of this study was the *in vivo* validation of potential modulators of the radiotherapy response that have been identified *in vitro*. Therefore, a preliminary experiment was performed to test whether conditional activation of RAF-1 is still functional *in vivo*. Tumors were established in the hind limbs of NOD / SCID mice by subcutaneous injection of A431 cells stably expressing ΔRAF-1-ER^{tam}. When tumors were palpable after 4 days, one group of mice received tamoxifen-supplemented diet to induce RAF-1 activation in those xenografts. Outgrowth and growth rates did not change upon tamoxifen treatment. However, immunoblotting of extracts from tumors revealed no induction of RAF-1 by feeding with tamoxifen diet (Figure 35). Functionality of the antibody was confirmed by whole cell extracts of 4OHT-treated A431 ΔRAF-1-ER^{tam} cells. Furthermore, xenografts with AKT-ER^{tam} were established in parallel. Each mouse was injected with A431 ΔRAF-1-ER^{tam} cells in one limb and A431 AKT-ER^{tam} in the other limb. Interestingly, immunoblotting validated functional AKT activation by tamoxifen (Figure S 5). Therefore, poor tamoxifen feeding has to be excluded as a reason for non-functional RAF-1 activation. Thus, the system has to be optimized before investigating the impact of RAF-1 *in vivo*.

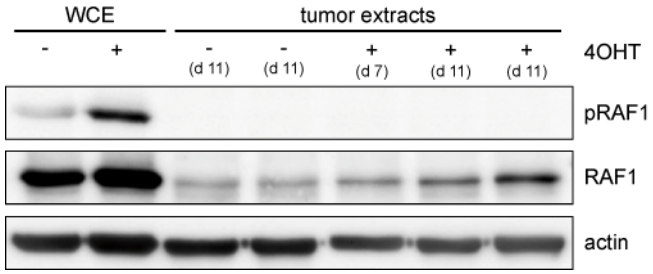

Figure 35: RAF-1 activation in tumor xenografts. NOD/SCID mice received subcutaneous injections of A431 cells stably transduced with ΔRAF-1-ER^{tam} expression vector. At day 4 after injection, one group was fed with tamoxifen diet to induce RAF-1 activation for 7 to 11 d. Expression of proteins in extracts from tumors was measured by immunoblotting and compared to whole cell extracts (WCE), actin served as a loading control.

6 Discussion

The ultimate goal of all anti-cancer therapies is long-term eradication of tumor cells. However to date, this goal is only achievable in patients with early-stage tumors and small subgroups of some entities. Despite initial tumor control, localized and systemic relapse is frequently observed and has been linked to primary and secondary resistance against treatment strategies. To minimize the probability that the tumor escapes by developing resistance, dose escalation strategies are broadly provided in the clinics. These also comprise advanced planning and delivery strategies in photon therapy, and application of alternative beam sources like particle therapy (Christodoulou et al. 2014). The limitation factor of current radiotherapy protocols is still normal tissue toxicity and standard protocols are already administered at the maximum-tolerated doses (Morgan et al. 2014).

Another strategy to prevent early resistance is combined treatment of radiation with pharmacological agents, so far mostly standard chemotherapeutics like cisplatin (Begg et al. 2011; Eberhardt et al. 2015; Albain et al. 2009; Turrisi et al. 1999). Those protocols are particularly effective in locally advanced cancers like NSCLC stage III, and can even achieve cure in some patients. Nevertheless, the majority of patients still relapses and dies from the disease (Pignon et al. 2008). As there is currently no predictive biomarker for the radiotherapy response available, radiosensitization protocols have been developed empirically. All clinically active agents that are used for treatment of stage IV disease and show an acceptable safety profile when combined with radiation are potentially administered. As only a subgroup of patients benefits from those protocols, there is an urgent need to develop new treatment strategies. It was hypothesized that an improved understanding of the molecular mechanisms leading to radioresistance will provide a reasonable basis for patient stratification and the development effective treatments.

Against this background, a systematic study of the functional impact of deregulated signal transduction pathways on the radiation sensitivity of cancer cells was conducted. By this, two potential modulators of the radiotherapy response, namely BCL-2 family members and the RAF-1 kinase, were identified.

The results and the suitability of those modulators as drug targets for combined treatment strategies will be discussed in the next sections.

6.1 Contribution of BCL-2 family members to radiosensitivity

Current treatment modalities, like chemotherapy, radiotherapy, and targeted therapies, operate by either directly blocking cell viability or by indirectly inducing tumor cells to kill themselves (Kaufmann & Vaux 2003). According to this, treatment efficacy depends fundamentally on intact cell death mechanisms of tumor cells. On the contrary, evasion of programmed cell death (apoptosis) is one of the hallmarks of cancer (Hanahan & Weinberg 2000) and tumor cells evolve a variety of strategies to circumvent cell death (Hanahan & Weinberg 2011) including deregulation of BCL-2 family members (Strasser et al. 1997). This protein family is described as being involved in tumor initiation, progression, and development of resistance against several treatment modalities (e.g. cytotoxic drugs, antibodies, T-cells) (Wesarg et al. 2007; Meiler et al. 2012; Stolz et al. 2008; Kasper, Breitenbuecher, Heidel, et al. 2012; Kasper, Breitenbuecher, Reis, et al. 2012; Huber et al. 2005; Ravi et al. 2006; Hähnel et al. 2008; Kutuk & Letai 2008).

Fully in line with this, the initial small-scale screen in A431 cells demonstrated a significant impact of BCL-xL, an anti-apoptotic member of the BCL-2 family, on reduction of irradiation-induced cell death (see 5.1). Concerning their potential importance in development of resistance, the radiotherapy modulation by BCL-2 family members was further characterized.

BCL-xL-mediated radioresistance was validated by colony formation assays and also in tumor-bearing mice *in vivo*, which proofs its relevance in an organismal context (see 5.2.1). Interestingly, this effect was not restricted to BCL-xL, but also MCL-1 showed similar results although the regulation of this protein is completely different from BCL-xL. MCL-1 presents low protein stability (Maurer et al. 2006; Brunelle et al. 2009) and has opposing functions in terms of binding different BH3-only proteins compared to BCL-xL (L. Chen et al. 2005). Nevertheless, in the presence of enforced MCL-1 expression, irradiation-induced cell death was significantly reduced and clonogenic survival was enhanced, both demonstrating

that MCL-1 also mediates resistance against irradiation (see 5.2.2). This is in line with a previous study, which observed MCL-1 stabilization upon overexpression of the deubiquitinase ubiquitin-specific protease 9x (USP9x) being responsible for radioresistance (Trivigno et al. 2012).

The results indicate that it is a general feature of anti-apoptotic BCL-2 family members to inhibit the efficacy of radiotherapy. However, compared to BCL-xL the effect of MCL-1 was less pronounced, possibly due to its consecutive proteasomal degradation, which might inherently sustain lower expression levels compared to BCL-xL.

As the NSCLC cell lines A549 and H1299 were endogenously more radioresistant than A431 cells, the mediation of resistance could not be validated in those cell lines to exclude cell line specific effects. However, this was taken as an advantage for studies of radiosensitization by targeting BCL-xL and MCL-1 to exclude off-target effects from enforced expression of transgenes. Knockdown of BCL-xL and MCL-1 in all three cell lines allowed determining the impact of different genetic backgrounds on the effect of radiosensitization. It has been shown before that downregulation of MCL-1 or BCL-xL via RNAi increases the sensitivity of tumor cells to chemotherapy (Peddaboina et al. 2012; Song et al. 2005). Interestingly, A431 and A549 cells showed quite similar results in terms of radiosensitization after BCL-xL or MCL-1 knockdown (5.2.3). In contrast, MCL-1 knockdown was inefficient in H1299 cells, which might indicate that this cell line is more dependent on functional MCL-1 than A431 or A549 cells. Surprisingly, knockdown of one anti-apoptotic family member was frequently accompanied with upregulation of the other (compare Figure 16). This is especially true for upregulated MCL-1 in A549 cells with stable BCL-xL knockdown and could indicate a reciprocal regulation of those two modulators, but additional studies are required to confirm this hypothesis. However, these results clearly demonstrate that targeting endogenous BCL-xL and/or MCL-1 is a promising strategy to compete radioresistance.

To further validate this, anti-apoptotic BCL-2 family members were additionally targeted on a functional level by conditional overexpression of pro-apoptotic BAK. This changes the balance between pro-survival and pro-apoptotic proteins and primes the cells for death (Danial & Korsmeyer 2004). As expected, conditional BAK expression opposed the BCL-xL- and MCL-1-mediated radioresistance in

A549 cells (5.2.3). This was also demonstrated for other treatment modalities before (Wesarg et al. 2007).

In summary, there is strong evidence that the group of anti-apoptotic BCL-2 family members confers radioresistance in lung cancer cells. However, the underlying mechanisms had to be analyzed and the suitability of those proteins as pharmacological targets remained to be elucidated. These aspects will be discussed in the following sections.

6.1.1 Potential mechanisms of radioresistance mediated by BCL-2 family members

The finding that BCL-xL and MCL-1 reduce irradiation-induced cell death in lung cancer cells was expected due to their anti-apoptotic function. Surprisingly, there was only a little increase in apoptosis in response to irradiation at doses that induced significant cell death and reduced clonogenic survival (Figure 20). Thus, the anti-apoptotic function of those proteins could not explain the radioresistant effects and additional roles of anti-apoptotic BCL-2 family members in the radiation response were considered.

Since the major cellular responses to ionizing radiation are the activation of cell cycle checkpoints and DNA repair pathways (Ross 1999), the influence of BCL-xL on these response pathways was exemplarily investigated. As BCL-xL did not change radiation-induced transient G2-arrest (Figure 21), it was hypothesized that BCL-xL might interfere with DNA repair pathways.

As described in 2.3.6, there have been some studies published linking BCL-2 family members to DNA repair pathways (reviewed in Hardwick & Soane 2013; Laulier & Lopez 2012). However, most of them focus on BCL-2 itself and the data are highly contradictory.

Repair kinetics assessed by PFGE demonstrated that enforced expression of BCL-xL educed a repair benefit under conditions of blocked c-NHEJ. Inhibition of c-NHEJ by treatment with NU7441 in PFGE experiments provided conditions where alt-EJ is more strongly involved in DSB repair than HRR. It was shown before that cells with defective c-NHEJ repair DSBs with slower kinetics which are not affected by additional mutations in HRR components (Wang et al. 2001; Iliakis

et al. 2004). Under those conditions, BCL-xL cells tended to repair faster, which indicated an enhanced activity of alt-EJ in those cells (Figure 22 C). In contrast, there was no difference between BCL-xL and control cells under conditions with predominating c-NHEJ (Figure 22 B). Analyses of the cellular outcome after irradiation, as shown by clonogenic survival assays, revealed that BCL-xL mediated resistance was not influenced by inhibition of c-NHEJ. Treatment with NU7441 reduced clonogenic survival in BCL-xL and control cells, while the survival benefit of BCL-xL cells was still maintained (Figure 23 A). Interestingly, conditions that inhibited HRR using B02, a RAD51-specific inhibitor, eliminated survival benefits of cells with BCL-xL overexpression in clonogenic survival assays, although B02 treatment compromised clonogenic survival less compared to NU7441 treatment (Figure 23 B). This could be explained by the observation that the majority of DSBs in eukaryotic cells is repaired by c-NHEJ and probably only a small subset of DSBs is repaired by HRR (Shrivastav et al. 2008; Rothkamm et al. 2003; Mao et al. 2008). Thus, eukaryotic cells seem to be more dependent on c-NHEJ than on HRR, which explains stronger survival deficits in cells with abrogated c-NHEJ. However, the results show that BCL-xL-mediated radioresistance depends on functional HRR.

End-joining pathways are considered error-prone with alt-EJ even amplifying complex genomic alterations (Dueva & Iliakis 2013). As BCL-xL promoted enhanced function of alt-EJ in the used cell system, the induction of chromosomal aberrations by irradiation in the presence or absence of NU7441 was examined by metaphase analyses. As expected, the mean number of chromosomal aberrations per cell was increased after irradiation. In line with the enhanced activity of alt-EJ in cells with BCL-xL overexpression, the number of radiation-induced gross chromosomal aberrations was significantly increased in the presence of NU7441 in those cells at 8 h, but faded after 20 h (Figure 24). This indicates that cells irradiated in S / G2 phase of the cell cycle are the major contributors to those effects. Accordingly, it was shown before that alt-EJ function is enhanced in G2 in cells with c-NHEJ defects with minor contribution of HRR (Wu, Wang, Wu, et al. 2008; Wu, Wang, Mussfeldt, et al. 2008).

In summary, the results of DNA repair experiments suggest a model according to which BCL-xL affects both HRR and alt-EJ. BCL-xL-mediated radioresistance depends on HRR, but potentially, DSB repair by HRR is not always productive

leading to shunting of DSBs to error-prone alt-EJ and therewith accumulation of genomic alterations after irradiation. In line with this, there are some hints that alt-EJ gains functional relevance when the 'standard' repair processes fail on a global or local level (Dueva & Iliakis 2013). As the majority of DSBs was shown to be repaired by c-NHEJ and accordingly, PFGE revealed no difference between BCL-xL and control cells under standard conditions, the quantitative effect of BCL-xL-mediated enhancement of alt-EJ activity in a large irradiated tumor bulk might be subtle. However, a few surviving cells with gross chromosomal aberrations may be enough to give rise to more resistant and aggressive subclones leading to relapse.

The exact mechanism how BCL-xL interferes with different DNA repair pathways remains to be elucidated. It seems likely that BCL-xL interacts with DNA repair proteins as it was shown before that, for example, BCL-2 binds to KU70, thereby disrupting the KU/DNA-PKcs complex (Kumar et al. 2010; Wang et al. 2008). Also interaction of BCL-2 with BRCA1 and PARP-1 was shown before, which links it with HRR and alt-EJ, respectively.

6.1.2 Clinical relevance of BCL-2 family members for radiotherapy

Several types of cancer are known to have deregulated BCL-2 family members, which contributes to tumor initiation, progression, and resistance to different treatment strategies (Kirkin et al. 2004; Amundson et al. 2000). Especially *MCL-1* and *BCL-xL* belong to the most frequently amplified genes in all human cancers (Beroukhim et al. 2010), and high expression of both is very common in lung cancer (Wesarg et al. 2007; Borner et al. 1999; Berrieman et al. 2005). This emphasizes the significance of those proteins for NSCLC.

This study provided further evidence that BCL-xL and MCL-1 contribute to radioresistance in NSCLC. Furthermore, it was shown that targeting of endogenously expressed anti-apoptotic BCL-2 proteins by genetic knockdown or by conditional expression of BAK sensitized lung cancer cells to irradiation. This strongly indicates that BCL-xL and MCL-1 are potential targets for pharmacological radiosensitization of lung cancer models. To validate this, different BH3-mimetics, which are frequently used to antagonize BCL-xL, were

tested. Indeed, ABT-737 and Navitoclax were effective in radiosensitizing A549 and H1299 cells, although the effects were partly only marginal (5.2.5). This could be explained by the non-functional targeting of MCL-1 of those BH3-mimetics (Oltersdorf et al. 2005; Tse et al. 2008). It has been shown before that ABT-737 treatment is ineffective in cells with high MCL-1 protein levels (Wesarg et al. 2007) and that acquired resistance to ABT-737 is, at least in part, mediated by upregulation of MCL-1 (Yecies et al. 2010). In line with this, upregulation of MCL-1 was observed in cells with stable BCL-xL knockdown.

Radiosensitivity was promoted by combining knockdown of MCL-1 with ABT-737 treatment or by combining knockdown of BCL-xL with flavopiridol-treatment to reduce MCL-1 levels. Accordingly, another study demonstrated that concomitant targeting of MCL-1 and treatment with BH3-mimetics potentiates cell lethality (van Delft et al. 2006; Chen et al. 2007). Thus, combined treatment of BCL-xL and MCL-1 might be feasible to achieve the maximal radiosensitization. Here, the major limitation is the lack of specific clinically applicable MCL-1 inhibitors. Several potential inhibitors operating in an indirect manner (like flavopiridol) lack selectivity and might therefore be highly toxic. Recently, new potent and selective small-molecule MCL-1 inhibitors have been identified (Leverson et al. 2015), but their potential as therapeutics remains to be elucidated.

In conclusion, the results of this study suggest that monotherapeutic irradiation of tumors harboring high levels of BCL-xL or MCL-1 may result in generation of resistant and more aggressive tumor subclones rather than eradicating the tumor due to accumulation of aberrant chromosomes. To circumvent this, molecules such as BCL-xL and MCL-1 may serve as rational targets for novel therapy strategies combining targeted pharmacotherapy with radiotherapy aiming at long-term eradication of cancer cells. Translation of this approach into clinical proof-of-principle is feasible and the clinically developed BH3-mimetic Navitoclax might be an applicable compound for this aim (Gandhi et al. 2011; Tan et al. 2011; Rudin et al. 2012; Vlahovic et al. 2014). To kill tumor cells, the particular expression profile of pro-survival and BH3-only proteins should be examined as it determines the required drug target for individual tumors (L. Chen et al. 2005; Certo et al. 2006).

6.2 Contribution of RAF-1 to radiosensitivity

Approximately 30 % of human cancers show an upregulation of the MAPK pathway due to either deregulated growth factor receptors or oncogenic RAS mutations (Rushworth et al. 2006; Downward 2003). In contrast to this, direct mutations of RAF-1 are rather rare (Gollob et al. 2006).

In NSCLC, overexpression of the epidermal growth factor receptor (EGFR) is found in 40 to 80 % (Lynch et al. 2004). Additionally, depending on the epidemiological background, 10 to 40 % of NSCLC patients present with activating *EGFR* mutations (Lovly et al. 2015a; Lynch et al. 2004; Paez et al. 2004; Pao et al. 2004; Kosaka et al. 2004; Shigematsu et al. 2005), which are also frequently amplified (Soh et al. 2009). Oncogenic *KRAS* mutations, which result in constitutive activation of the downstream cascade, are found in 15 to 25 % of patients with lung adenocarcinoma (Lovly et al. 2015b). Both frequent cancer-associated aberrations promote RAF-1 phosphorylation as well as activation and make RAF-1 an interesting target for future treatment strategies.

The contribution of RAF-1 to radioresistance has been differentially discussed in the literature. Some studies predicted radiosensitizing effects of RAF-1 (Warenius et al. 1994; Warenius et al. 1996; Warenius et al. 1998), while others showed RAF-1 to mediate radioresistance (Kasid et al. 1987; Kasid et al. 1989; Kasid et al. 1996; Riva et al. 1995; Grana et al. 2002). However, the underlying mechanisms remained to be elucidated.

Conditionally activatable RAF-1 was included as a model for several mechanisms of aberrant activation of the MAPK pathway into the initial small-scale screen for identifying potential modulators of the radiotherapy response of NSCLC. Interestingly, RAF-1 activation showed one of the strongest death-reducing effects upon irradiation (Figure 11) and was therefore investigated in more detail. However, the first limitation of this study was that A431 cells stably transduced with the conditionally activatable RAF-1-ER^{tam} construct were not able to form proper colonies, especially when RAF-1 was activated in the presence of 4OHT (5.3.1). This could, at least in part, be explained by cell cycle effects of activated RAF-1 (5.3.2). Permanent RAF-1 activation (in the presence of 4OHT) promoted accumulation of cells in G2 and therewith might have prevented unlimited cell divisions to form proper colonies. It has been shown before that strong induction of

ERK signaling due to RAF manipulation results in transcriptional increase of cell cycle inhibitors like p21Cip1 and subsequently cell cycle arrest (Woods et al. 1997; Kerkhoff & Rapp 1998). In contrast to this, other studies suggested RAF-1 dependent cell cycle progression (Mielgo et al. 2011). It has been claimed that signal intensity of inducible RAF systems triggers either proliferation or cell cycle arrest (Wellbrock et al. 2004).

To test these hypotheses, the impact of different RAF-1 timings was investigated. In cell death assays, differential RAF-1 activation and deactivation did not result in significant differences in the cellular outcome upon irradiation. RAF-1 activation before, during or after irradiation always decreased the number of dead cells compared to cells that were not treated with 4OHT (5.3.4). However, the results for RAF-1 deactivation have to be considered with caution, as removal of 4OHT did not directly lead to RAF-1 deactivation (Figure 34 A, B). For this reason, the question whether signal intensity or timing plays a role for RAF-1 function could not be answered and colony formation could not be improved. Potentially, deactivation was hampered by serum-containing medium. Thus, it is suggested to repeat the experiments under serum deprivation.

The second limitation of the RAF-1 project was the inability to propagate cancer cells with conditionally active RAF-1 *in vivo*. This hampered the validation of RAF-1 as a potential radiotherapy modulator in tumor-bearing mice *in vivo*. As AKT induction upon tamoxifen treatment was effective *in vivo* (Figure S 5), there was no explanation for this RAF-1-specific effect and further research is required to enlighten this observation.

Concerning the underlying mechanisms leading to RAF-1-mediated resistance, it is only possible to speculate (compare 6.2.1).

6.2.1 Potential mechanisms leading to RAF-1-mediated radioresistance

Recent studies have provided growing evidence that RAF-1 has several kinase-independent functions, which interfere with different cellular processes like apoptosis, cell motility, and cell cycle progression (compare 2.4.1).

Very recently, Advani et al. demonstrated that RAF-1 also interferes with DNA repair in a kinase-independent but phosphorylation-dependent manner. They

showed that RAF-1 phosphorylation at Serine 338 (Ser338) mediates radioresistance, at least in part, by interacting with the cell cycle checkpoint kinase CHK2, promoting its activation and enhancing the DNA damage response, in which CHK2 is involved (Advani et al. 2015). Additionally, it has been shown before that activation of CHK2 contributes to radioresistance (e.g. Bao et al. 2006; Jobson et al. 2009). In the present study, Ser338 was also phosphorylated upon addition of 4OHT (Figure 10). Therefore, the described mechanism of CHK2 activation might be relevant for RAF-1-mediated radioresistance in the model of this study. However, the observation that addition of 4OHT 6 h after irradiation confers decreased cell death as well as addition before irradiation (see 5.3.4) contradicts this hypothesis, as the DNA damage response should be activated within a few minutes up to few hours.

The second hypothesis is that RAF-1 might mediate radioresistance by inhibiting cell death, especially apoptosis. It has been shown that RAF-1 inhibits apoptosis by specific inactivation of pro-apoptotic kinases ASK (Alavi et al. 2007) and MST2 (O'Neill et al. 2004). The results of RAF-1 timing experiments could favor this hypothesis, as apoptosis is a later effect of irradiation than DNA damage response. On the contrary, it was also analyzed whether apoptosis plays a role in this radiation context, but only marginal apoptosis-related changes, like externalization of phosphatidylserine, were observed upon irradiation (5.3.3). Additionally, RAF-1 has been shown to mediate inactivation of pro-apoptotic BAD, activation of BCL-2, and stabilization of MCL-1 (Jin et al. 2005; Salomoni et al. 1998; Yoon et al. 2002). Thus, hypothetically RAF-1 mediates resistance via deregulation of BCL-2 family members leading to the effects discussed above (6.1.1)

Surprisingly, RAF-1 activation induced morphological changes (Figure 33 C), which might allow another hypothesis of mechanism. Especially, the observation of vacuole-like structures was striking and might be a hind for autophagy-related effects.

In summary, further research is needed to clarify the underlying mechanisms leading to RAF-1-mediated resistance in the model of this study. It is of special interest whether the mechanism depends on kinase activity or phosphorylation processes, as this would have a high impact on the development of treatment strategies (see 6.2.2).

6.2.2 Clinical relevance of RAF-1 for radiotherapy

Taking into account that the MAPK pathway is aberrantly activated in approximately 30 % of human cancers (Rushworth et al. 2006), the clinical relevance of its essential mediator RAF-1 in general is not questionable. The findings that ionizing radiation promotes phosphorylation of RAF-1 and that anti-sense strategies for RAF-1 increase radiosensitivity *in vitro* as well as in some patients (Pirollo et al. 1997; Kasid & Dritschilo 2003; Dritschilo et al. 2006) additionally supports its impact on the radiotherapy response. However, targeting RAF-1 or its downstream targets with kinase inhibitors often fail to radiosensitize (Advani et al. 2015; Grana et al. 2002). This highly suggests kinase-independent functions of RAF-1 to be responsible for its radioresistant effects. Indeed, allosteric RAF-1 inhibitors (e.g. KG5) that block dimerization with BRAF and phosphorylation at Ser338 sensitized cells to IR (Advani et al. 2015). The same inhibitor was also shown to induce cell cycle arrest by PLK1 (Mielgo et al. 2011). Thus allosteric RAF-1 inhibitors would prevent tumor progression and sensitize to therapy. Therefore, they are considered being quite promising. Further research is needed to develop clinically applicable RAF-1 inhibitors that primarily function in an allosteric fashion to inhibit kinase-independent functions of RAF-1.

6.3 Conclusion and Outlook

This study demonstrates that anti-apoptotic BCL-2 family members and RAF-1 mediate resistance against irradiation and therewith, provides new concepts for treatment using biomarker-driven targets in combination with irradiation instead of empirically driven protocols of chemoradiotherapy.

The underlying mechanism for BCL-2 family members is, at least in part, the enhancement of repair kinetics for radiation-induced DSBs via the error-prone alt-EJ pathway. Thus, irradiation of tumors with BCL-2 family deregulation could promote tumor progression, which emphasizes the importance of rational biomarker profiling of each individual tumor before treatment. Tumors with overexpression of anti-apoptotic BCL-2 family members should be irradiated in combination with concomitant targeting of BCL-xL and MCL-1, if clinically feasible.

The underlying mechanisms for RAF-1-mediated radioresistance still remain to be elucidated. In order to develop new treatment protocols combining radiotherapy with targeted therapies against RAF-1, it is of special interest to work out whether RAF-1-mediated resistance is a kinase-dependent or kinase-independent phenomenon.

7 References

Adams, J.M. & Cory, S., 2007. The Bcl-2 apoptotic switch in cancer development and therapy. *Oncogene*, 26, pp.1324–1337.

Advani, S.J. et al., 2015. Kinase-independent role for CRAF-driving tumour radioresistance via CHK2. *Nature Communications*, 6(8154), pp.1–8.

Ahnesorg, P., Smith, P. & Jackson, S.P., 2006. XLF Interacts with the XRCC4-DNA Ligase IV Complex to Promote DNA Nonhomologous End-Joining. *Cell*, 124, pp.301–313.

Alavi, A.S. et al., 2007. Chemoresistance of Endothelial Cells Induced by Basic Fibroblast Growth Factor Depends on Raf-1-Mediated Inhibition of the Proapoptotic Kinase, ASK1. *Cancer Research*, 67(6), pp.2766–2772.

Albain, K.S. et al., 2009. Radiotherapy plus chemotherapy with or without surgical resection for stage III non-small-cell lung cancer: a phase III randomised controlled trial. *The Lancet*, 374, pp.379–386.

Allen, C. et al., 2002. DNA-dependent protein kinase suppresses double-strand break-induced and spontaneous homologous recombination. *PNAS*, 99(6), pp.3758–3763.

Allen, C., Halbrook, J. & Nickoloff, J.A., 2003. Interactive Competition Between Homologous Recombination and Non-Homologous End Joining. *Molecular Cancer Research*, 1, pp.913–920.

American Cancer Society, 2015. Cancer Facts & Figures 2015. Available at: http://www.cancer.org/research/cancerfactsstatistics/ [Accessed September 16, 2015].

Amundson, S.A. et al., 2000. An Informatics Approach Identifying Markers of Chemosensitivity in Human Cancer Cell Lines. *Cancer Research*, 60, pp.6101–6110.

Audebert, M. et al., 2006. Involvement of Polynucleotide Kinase in a Poly(ADP-ribose) Polymerase-1-dependent DNA Double-strand Breaks Rejoining Pathway. *Journal of Molecular Biology*, 356, pp.257–265.

Audebert, M., Salles, B. & Calsou, P., 2008. Effect of double-strand break DNA sequence on the PARP-1 NHEJ pathway. *Biochemical and Biophysical Research Communications*, 369, pp.982–988.

Audebert, M., Salles, B. & Calsou, P., 2004. Involvement of Poly(ADP-ribose) Polymerase-1 and XRCC1/DNA Ligase III in an Alternative Route for DNA Double-strand Breaks Rejoining. *The Journal of Biological Chemistry*, 279(53), pp.55117–55126.

Ausborn, N.L. et al., 2012. Molecular Profiling to Optimize Treatment in Non-Small Cell Lung Cancer: A Review of Potential Molecular Targets for Radiation Therapy by the Translational Research Program of the Radiation Therapy Oncology Group. *International Journal of Radiation Oncology Biology Physics*, 83(4), pp.e453–e464.

Balmanno, K. et al., 2003. DeltaRaf-1:ER* Bypasses the Cyclic AMP Block of Extracellular Signal-Regulated Kinase 1 and 2 Activation but Not CDK2 Activation or Cell Cycle Reentry. *Molecular and Cellular Biology*, 23(24), pp.9303–9317.

Bao, S. et al., 2006. Glioma stem cells promote radioresistance by preferential activation of the DNA damage response. *Nature*, 444, pp.756–760.

Begg, A.C., Stewart, F.A. & Vens, C., 2011. Strategies to improve radiotherapy with targeted drugs. *Nature reviews. Cancer*, 11, pp.239–253.

Beroukhim, R. et al., 2010. The landscape of somatic copy-number alteration across human cancers. *Nature*, 463, pp.899–905.

Berrieman, H.K. et al., 2005. The Expression of Bcl-2 Family Proteins Differs between Nonsmall Cell Lung Carcinoma Subtypes. *Cancer*, 103(7), pp.1415–1419.

Bianco, C. et al., 2002. Enhancement of Antitumor Activity of Ionizing Radiation by Combined Treatment with the Selective Epidermal Growth Factor Receptor-Tyrosine Kinase Inhibitor ZD1839 (Iressa). *Clinical Cancer Research*, 8, pp.3250–3258.

Boise, L.H. et al., 1993. bcl-X, a bcl-2-Related Gene That Functions as a Dominant Regulator of Apoptotic Cell Death. *Cell*, 74, pp.597–608.

Borner, M.M. et al., 1999. Expression of apoptosis regulatory proteins of the Bcl-2 family and p53 in primary resected non-small-cell lung cancer. *British Journal of Cancer*, 79(5/6), pp.952–958.

Boyd, J.M. et al., 1995. Bik, a novel death-inducing protein shares a distinct sequence motif with Bcl-2 family proteins and interacts with viral and cellular survival-promoting proteins. *Oncogene*, 11(9), pp.1921–1928.

Bradford, M.M., 1976. A Rapid and Sensitive Method for the Quantitation of Microgram Quantities of Protein Utilizing the Principle of Protein-Dye Binding. *Analytical biochemistry*, 72, pp.248–254.

Brunelle, J.K. et al., 2009. MCL-1-dependent leukemia cells are more sensitive to chemotherapy than BCL-2-dependent counterparts. *Journal of Cell Biology*, 187(3), pp.429–442.

Bryant, P.E., Mozdarani, H. & Marr, C., 2008. G2-phase chromatid break kinetics in irradiated DNA repair mutant hamster cell lines using calyculin-induced PCC and colcemid-block. *Mutation Research/Genetic Toxicology and Environmental Mutagenesis*, 657, pp.8–12.

Certo, M. et al., 2006. Mitochondria primed by death signals determine cellular addiction to antiapoptotic BCL-2 family members. *Cancer Cell*, 9, pp.351–365.

Chen, B.P.C. et al., 2005. Cell Cycle Dependence of DNA-dependent Protein Kinase Phosphorylation in Response to DNA Double Strand Breaks. *The Journal of Biological Chemistry*, 280(15), pp.14709–14715.

Chen, J. et al., 2001. Raf-1 promotes cell survival by antagonizing apoptosis signal-regulating kinase 1 through a MEK-ERK independent mechanism. *PNAS*, 98(14), pp.7783–7788.

Chen, L. et al., 2005. Differential Targeting of Prosurvival Bcl-2 Proteins by Their BH3-Only Ligands Allows Complementary Apoptotic Function. *Molecular Cell*, 17, pp.393–403.

Chen, S. et al., 2007. Mcl-1 Down-regulation Potentiates ABT-737 Lethality by Cooperatively Inducing Bak Activation and Bax Translocation. *Cancer Research*, 67(2), pp.782–791.

Cheng, E.H.-Y.A. et al., 2001. BCL-2, BCL-XL sequester BH3 Domain-Only Molecules Preventing BAX- and BAK-Mediated Mitochondrial Apoptosis. *Molecular Cell*, 8, pp.705–711.

Chinnaiyan, P. et al., 2005. Mechanisms of Enhanced Radiation Response following Epidermal Growth Factor Receptor Signaling Inhibition by Erlotinib (Tarceva). *Cancer Research*, 65(8), pp.3328–3335.

Chipuk, J.E. et al., 2010. The BCL-2 Family Reunion. *Molecular Cell*, 37, pp.299–310.

Chittenden, T. et al., 1995. Induction of apoptosis by the Bcl-2 homologue Bak. *Nature*, 374, pp.733–736.

Christodoulou, M. et al., 2014. New radiotherapy approaches in locally advanced non-small cell lung cancer. *European Journal of Cancer*, 50, pp.525–534.

Cimprich, K.A. & Cortez, D., 2008. ATR: an essential regulator of genome integrity. *Nature reviews. Molecular Cell Biology*, 9, pp.616–627.

Condon, L.T. et al., 2002. Overexpression of Bcl-2 in squamous cell carcinoma of the larynx: a marker of radioresistance. *International Journal of Cancer*, 100, pp.472–475.

Cory, S., Huang, D.C.S. & Adams, J.M., 2003. The Bcl-2 family: roles in cell survival and oncogenesis. *Oncogene*, 22, pp.8590–8607.

Czabotar, P.E. et al., 2014. Control of apoptosis by the BCL-2 protein family: implications for physiology and therapy. *Nature reviews. Molecular cell biology*, 15, pp.49–63.

Danial, N.N. & Korsmeyer, S.J., 2004. Cell Death: Critical Control Points. *Cell*, 116, pp.205–219.

Das, A.K. et al., 2010. Radiogenomics Predicting Tumor Responses to Radiotherapy in Lung Cancer. *Seminars in Radiation Oncology*, 20, pp.149–155.

Delacôte, F. et al., 2002. An xrcc4 defect or Wortmannin stimulates homologous recombination specifically induced by double-strand breaks in mammalian cells. *Nucleic Acids Research*, 30(15), pp.3454–3463.

van Delft, M.F. et al., 2006. The BH3 mimetic ABT-737 targets selective Bcl-2 proteins and efficiently induces apoptosis via Bak/Bax if Mcl-1 is neutralized. *Cancer Cell*, 10, pp.389–399.

Della-Maria, J. et al., 2011. Human Mre11/Human Rad50/Nbs1 and DNA ligase IIIalpha/XRCC1 Protein Complexes Act Together in an Alternative Nonhomologous End Joining Pathway. *The Journal of Biological Chemistry*, 286(39), pp.33845–33853.

Dewson, G. et al., 2008. To Trigger Apoptosis, Bak Exposes Its BH3 Domain and Homodimerizes via BH3:Groove Interactions. *Molecular Cell*, 30, pp.369–380.

Dibiase, S.J. et al., 2000. DNA-dependent Protein Kinase Stimulates an Independently Active, Nonhomologous, End-Joining Apparatus. *Cancer Research*, 60, pp.1245–1253.

Ding, L. et al., 2008. Somatic mutations affect key pathways in lung adenocarcinoma. *Nature*, 455, pp.1069–1075.

Dinkelmann, M. et al., 2009. Multiple functions of MRN in end-joining pathways during isotype class switching. *Nature Structural & Molecular Biology*, 16(8), pp.808–813.

Downward, J., 2003. Targeting RAS signalling pathways in cancer therapy. *Nature reviews. Cancer*, 3, pp.11–22.

Dritschilo, A. et al., 2006. Phase I Study of Liposome-Encapsulated c-raf Antisense Oligodeoxyribonucleotide Infusion in Combination with Radiation Therapy in Patients with Advanced Malignancies. *Clinical Cancer Research*, 12(4), pp.1251–1259.

Dueva, R. & Iliakis, G., 2013. Alternative pathways of non-homologous end joining (NHEJ) in genomic instability and cancer. *Translational Cancer Research*, 2(3), pp.163–177.

Dutta, C. et al., 2012. BCL2 Suppresses PARP1 Function and Nonapoptotic Cell Death. *Cancer Research*, 72(16), pp.4193–4203.

Eberhardt, W.E.E. et al., 2015. Phase III study of surgery versus definitive concurrent chemoradiotherapy boost in patients with resectable stage III A (N2) and selected III B non-small-cell lung cancer following induction chemotherapy and concurrent chemoradiotherapy (ESPATUE). *Journal of Clinical Oncology*, [in press].

Eccles, L.J., O'Neill, P. & Lomax, M.E., 2011. Delayed repair of radiation induced clustered DNA damage: Friend or foe? *Mutation Research/Fundamental and Molecular Mechanisms of Mutagenesis*, 711, pp.134–141.

Ehrenreiter, K. et al., 2005. Raf-1 regulates Rho signaling and cell migration. *The Journal of Cell Biology*, 168(6), pp.955–964.

Esashi, F. et al., 2005. CDK-dependent phosphorylation of BRCA2 as a regulatory mechanism for recombinational repair. *Nature*, 434, pp.598–604.

Fabian, J.R., Daar, I.O. & Morrison, D.K., 1993. Critical Tyrosine Residues Regulate the Enzymatic and Biological Activity of Raf-1 Kinase. *Molecular and Cellular Biology*, 13(11), pp.7170–7179.

Fadok, V.A. et al., 1992. Exposure of phosphatidylserine on the surface of apoptotic lymphocytes triggers specific recognition and removal by macrophages. *The Journal of Immunology*, 148(7), pp.2207–2216.

Fanning, E., Klimovich, V. & Nager, A.R., 2006. A dynamic model for replication protein A (RPA) function in DNA processing pathways. *Nucleic Acids Research*, 34(15), pp.4126–4137.

Ferlay, J. et al., 2013. GLOBOCAN 2012 v1.0, Cancer Incidence and Mortality Worldwide: IARC CancerBase No.11 [Internet]. *Lyon, France: International Agency for Research on Cancer*. Available at: http://globocan.iarc.fr [Accessed September 16, 2015].

Fletcher, J.I. et al., 2008. Apoptosis is triggered when prosurvival Bcl-2 proteins cannot restrain Bax. *PNAS*, 105(47), pp.18081–18087.

Fried, J., Perez, A.G. & Clarkson, B.D., 1978. Rapid hypotonic method for flow cytofluorometry of monolayer cell cultures - Some pitfalls in staining and data analysis. *The Journal of Histochemistry and Cytochemistry*, 26(11), pp.921–933.

Fukuoka, M. et al., 2011. Biomarker Analyses and Final Overall Survival Results From a Phase III, Randomized, Open-Label, First-Line Study of Gefitinib Versus Carboplatin/Paclitaxel in Clinically Selected Patients With Advanced Non-Small-Cell Lung Cancer in Asia (IPASS). *Journal of Clinical Oncology*, 29(21), pp.2866–2874.

Gandhi, L. et al., 2011. Phase I Study of Navitoclax (ABT-263), a Novel Bcl-2 Family Inhibitor, in Patients with Small-Cell Lung Cancer and Other Solid Tumors. *Journal of Clinical Oncology*, 29(7), pp.909–916.

Germain, M. & Duronio, V., 2007. The N Terminus of the Anti-apoptotic BCL-2 Homologue MCL-1 Regulates Its Localization and Function. *The Journal of Biological Chemistry*, 282(44), pp.32233–32242.

Giard, D.J. et al., 1973. In Vitro Cultivation of Human Tumors: Establishment of Cell Lines Derived From a Series of Solid Tumors. *Journal of the National Cancer Institute*, 51(5), pp.1417–1423.

Gilbert, M.S. et al., 1996. Association of BCL-2 With Membrane Hyperpolarization and Radioresistance. *Journal of Cellular Physiology*, 168, pp.114–122.

Goeckejan, G. et al., 2010. Prevention, Diagnosis, Therapy, and Follow-up of Lung Cancer - Interdisciplinary Guideline of the German Respiratory Society and the German Cancer Society. *Pneumologie*, 64, pp.1–164.

Gollob, J.A. et al., 2006. Role of Raf Kinase in Cancer: Therapeutic Potential of Targeting the Raf/MEK/ERK Signal Transduction Pathway. *Seminars in Oncology*, 33, pp.392–406.

Goodhead, D.T. & Nikjoo, H., 1989. Track Structure Analysis of Ultrasoft X-rays Compared to High- and Low-LET Radiations. *International Journal of Radiation Biology*, 55(4), pp.513–529.

Gottlieb, T.M. & Jackson, S.P., 1993. The DNA-Dependent Protein Kinase: Requirement for DNA Ends and Association with Ku Antigen. *Cell*, 72, pp.131–142.

Grana, T.M. et al., 2002. Ras Mediates Radioresistance through Both Phosphatidylinositol 3-Kinase-dependent and Raf-dependent but Mitogen-activated Protein Kinase/Extracellular Signal-regulated Kinase Kinase-independent Signaling Pathways. *Cancer Research*, 62, pp.4142–4150.

Griffiths, G.J. et al., 1999. Cell Damage-induced Conformational Changes of the Pro-Apoptotic Protein Bak In Vivo Precede the Onset of Apoptosis. *The Journal of Cell Biology*, 144(5), pp.903–914.

Gross, A. et al., 1998. Enforced dimerization of BAX results in its translocation, mitochondrial dysfunction and apoptosis. *The EMBO Journal*, 17(14), pp.3878–3885.

Hähnel, P.S. et al., 2008. Targeting AKT Signaling Sensitizes Cancer to Cellular Immunotherapy. *Cancer Research*, 68(10), pp.3899–3906.

Hall, E.J. & Giaccia, A.J., 2006. *Radiobiology for the Radiologist* 6th ed., Lippincott Williams & Wilkins.

Hanahan, D. & Weinberg, R.A., 2011. Hallmarks of Cancer: The Next Generation. *Cell*, 144, pp.646–674.

Hanahan, D. & Weinberg, R.A., 2000. The Hallmarks of Cancer. *Cell*, 100, pp.57–70.

Hanai, R., Yazu, M. & Hieda, K., 1998. On the experimental distinction between ssbs and dsbs in circular DNA. *International Journal of Radiation Biology*, 73(5), pp.475–479.

Hancock, J.F., 2003. Ras proteins: different signals from different locations. *Nature reviews. Molecular Cell Biology*, 4, pp.373–384.

Happo, L., Strasser, A. & Cory, S., 2012. BH3-only proteins in apoptosis at a glance. *Journal of Cell Science*, 125, pp.1081–1087.

Hardwick, J.M. & Soane, L., 2013. Multiple Functions of BCL-2 Family Proteins. *Cold Spring Harbor Perspectives in Biology*, pp.1–22.

Haslam, R.J., Koide, H.B. & Hemmings, B.A., 1993. Pleckstrin domain homology. *Nature*, 363, pp.309–310.

Heyer, W.-D., Ehmsen, K.T. & Liu, J., 2010. Regulation of Homologous Recombination in Eukaryotes. *Annual Review of Genetics*, 44, pp.113–139.

Huber, C. et al., 2005. Inhibitors of apoptosis confer resistance to tumour suppression by adoptively transplanted cytotoxic T-lymphocytes in vitro and in vivo. *Cell Death and Differentiation*, 12, pp.317–325.

Hüser, M. et al., 2001. MEK kinase activity is not necessary for Raf-1 function. *The EMBO Journal*, 20(8), pp.1940–1951.

Ide, H. et al., 2008. Repair of DNA-protein crosslink damage: Coordinated actions of nucleotide excision repair and homologous recombination. *Nucleic Acids Symposium Series*, (52), pp.57–58.

Iliakis, G. et al., 2004. Mechanisms of DNA double strand break repair and chromosome aberration formation. *Cytogenetic and Genome Research*, 104, pp.14–20.

Iliakis, G., 1991. The Role of DNA Double Strand Breaks in Ionizing Radiation-Induced Killing of Eukaryotic Cells. *BioEssays*, 13(12), pp.641–648.

Jackson, S.P., 2002. Sensing and repairing DNA double-strand breaks. *Carcinogenesis*, 23(5), pp.687–696.

Jamil, S. et al., 2008. An Essential Role for MCL-1 in ATR-mediated CHK1 Phosphorylation. *Molecular Biology of the Cell*, 19, pp.3212–3220.

Jamil, S. et al., 2010. MCL-1 localizes to sites of DNA damage and regulates DNA damage response. *Cell Cycle*, 9(14), pp.2843–2855.

Jin, S. et al., 2005. p21-activated Kinase 1 (Pak1)-dependent Phosphorylation of Raf-1 Regulates Its Mitochondrial Localization, Phosphorylation of BAD, and Bcl-2 Association. *The Journal of Biological Chemistry*, 280(26), pp.24698–24705.

Jobson, A.G. et al., 2009. Cellular Inhibition of Checkpoint Kinase 2 (Chk2) and Potentiation of Camptothecins and Radiation by the Novel Chk2 Inhibitor PV1019 [7-Nitro-1H-indole-2-carboxylic acid {4-[1-(guanidinohydrazone)-ethyl]-phenyl}-amide]. *The Journal of Pharmacology and Experimental Therapeutics*, 331(3), pp.816–826.

Kabotyanski, E.B. et al., 1998. Double-strand break repair in Ku86- and XRCC4-deficient cells. *Nucleic Acids Research*, 26(23), pp.5333–5342.

Kadhim, M.A., Hill, M.A. & Moore, S.R., 2006. Genomic instability and the role of radiation quality. *Radiation Protection Dosimetry*, 122(1-4), pp.221–227.

Kasid, U. et al., 1996. Activation of Raf by ionizing radiation. *Nature*, 382, pp.813–816.

Kasid, U. et al., 1989. Effect of Antisense c-raf-1 on Tumorigenicity and Radiation Sensitivity of a Human Squamous Carcinoma. *Science*, 243, pp.1354–1356.

Kasid, U. et al., 1987. The raf Oncogene Is Associated with a Radiation-Resistant Human Laryngeal Cancer. *Science*, 237, pp.1039–1041.

Kasid, U. & Dritschilo, A., 2003. RAF antisense oligonucleotide as a tumor radiosensitizer. *Oncogene*, 22, pp.5876–5884.

Kasper, S., Breitenbuecher, F., Reis, H., et al., 2012. Oncogenic RAS simultaneously protects against anti-EGFR antibody-dependent cellular cytotoxicity and EGFR signaling blockade. *Oncogene*, pp.1–9.

Kasper, S., Breitenbuecher, F., Heidel, F., et al., 2012. Targeting MCL-1 sensitizes FLT3-ITD-positive leukemias to cytotoxic therapies. *Blood Cancer Journal*, 2(e60), pp.1–10.

Kastan, M.B., 2008. DNA Damage Responses: Mechanisms and Roles in Human Disease. *Molecular Cancer Research*, 6(4), pp.517–524.

Kaufmann, S.H. & Vaux, D.L., 2003. Alterations in the apoptotic machinery and their potential role in anticancer drug resistance. *Oncogene*, 22, pp.7414–7430.

Kerkhoff, E. & Rapp, U.R., 1998. High-intensity Raf Signals Convert Mitotic Cell Cycling into Cellular Growth. *Cancer Research*, 58, pp.1636–1640.

King, A.J. et al., 1998. The protein kinase Pak3 positively regulates Raf-1 activity through phosphorylation of serine 338. *Nature*, 396, pp.180–183.

Kirkin, V., Joos, S. & Zörnig, M., 2004. The role of Bcl-2 family members in tumorigenesis. *Biochimica et Biophysica Acta*, 1644, pp.229–249.

Kluck, R.M. et al., 1997. The Release of Cytochrome c from Mitochondria: A Primary Site for Bcl-2 Regulation of Apoptosis. *Science*, 275, pp.1132–1136.

Kohn, A.D. et al., 1998. Construction and Characterization of a Conditionally Active Version of the Serine/Threonine Kinase Akt. *The Journal of Biological Chemistry*, 273(19), pp.11937–11943.

Kohn, A.D., Takeuchi, F. & Roth, R.A., 1996. Akt, a Pleckstrin Homology Domain Containing Kinase, Is Activated Primarily by Phosphorylation. *The Journal of Biological Chemistry*, 271(36), pp.21920–21926.

Kolch, W., 2005. Coordinating ERK/MAPK signalling through scaffolds and inhibitors. *Nature reviews. Molecular Cell Biology*, 6, pp.827–837.

Kosaka, T. et al., 2004. Mutations of the Epidermal Growth Factor Receptor Gene in Lung Cancer: Biological and Clinical Implications. *Cancer Research*, 64, pp.8919–8923.

Kozopas, K.M. et al., 1993. MCL1, a gene expressed in programmed myeloid cell differentiation, has sequence similarity to BCL2. *Proceedings of the National Academy of Sciences of the United States of America*, 90, pp.3516–3520.

Krüger, I., Rothkamm, K. & Löbrich, M., 2004. Enhanced fidelity for rejoining radiation-induced DNA double-strand breaks in the G2 phase of Chinese hamster ovary cells. *Nucleic Acids Research*, 32(9), pp.2677–2684.

Kumar, T.S. et al., 2010. Anti-apoptotic Protein BCL2 Down-regulates DNA End Joining in Cancer Cells. *The Journal of Biological Chemistry*, 285(42), pp.32657–32670.

Kutuk, O. & Letai, A., 2008. Alteration of the Mitochondrial Apoptotic Pathway Is Key to Acquired Paclitaxel Resistance and Can Be Reversed by ABT-737. *Cancer Research*, 68(19), pp.7985–7994.

Kuwana, T. et al., 2005. BH3 Domains of BH3-Only Proteins Differentially Regulate Bax-Mediated Mitochondrial Membrane Permeabilization Both Directly and Indirectly. *Molecular Cell*, 17, pp.525–535.

Kuwana, T. et al., 2002. Bid, Bax, and Lipids Cooperate to Form Supramolecular Openings in the Outer Mitochondrial Membrane. *Cell*, 111, pp.331–342.

Kvols, L.K., 2005. Radiation Sensitizers: A Selective Review of Molecules Targeting DNA and non-DNA Targets. *The Journal of Nuclear Medicine*, 46, p.187S–190S.

Kwak, E.L. et al., 2010. Anaplastic Lymphoma Kinase Inhibition in Non-Small-Cell Lung Cancer. *The New England Journal of Medicine*, 363(18), pp.1693–1703.

Laulier, C. et al., 2011. Bcl-2 Inhibits Nuclear Homologous Recombination by Localizing BRCA1 to the Endomembranes. *Cancer Research*, 71(10), pp.3590–3602.

Laulier, C. & Lopez, B.S., 2012. The secret life of Bcl-2: Apoptosis-independent inhibition of DNA repair by Bcl-2 family members. *Mutation Research/Reviews in Mutation Research*, 751, pp.247–257.

Leber, R. et al., 1998. The XRCC4 Gene Product Is a Target for and Interacts with the DNA-dependent Protein Kinase. *The Journal of Biological Chemistry*, 273(3), pp.1794–1801.

Lee, J.-U. et al., 1999. Role of Bcl-2 Family Proteins (Bax, Bcl-2 and Bcl-X) on Cellular Susceptibility to Radiation in Pancreatic Cancer Cells. *European Journal of Cancer*, 35(9), pp.1374–1380.

Lee, S.E. et al., 1997. Evidence for DNA-PK-Dependent and -Independent DNA Double-Strand Break Repair Pathways in Mammalian Cells as a Function of the Cell Cycle. *Molecular and Cellular Biology*, 17(3), pp.1425–1433.

Lessene, G., Czabotar, P.E. & Colman, P.M., 2008. BCL-2 family antagonists for cancer therapy. *Nature reviews. Drug Discovery*, 7, pp.989–1000.

Letai, A. et al., 2002. Distinct BH3 domains either sensitize or activate mitochondrial apoptosis, serving as prototype cancer therapeutics. *Cancer Cell*, 2, pp.183–192.

Leverson, J.D. et al., 2015. Potent and selective small-molecule MCL-1 inhibitors demonstrate on-target cancer cell killing activity as single agents and in combination with ABT-263 (navitoclax). *Cell Death and Disease*, 6(e1590), pp.1–11.

Li, P. et al., 1997. Cytochrome c and dATP-Dependent Formation of Apaf-1/Caspase-9 Complex Initiates an Apoptotic Protease Cascade. *Cell*, 91, pp.479–489.

Lieber, M.R., 2010. The Mechanism of Double-Strand DNA Break Repair by the Nonhomologous DNA End-Joining Pathway. *Annual Review of Biochemistry*, 79, pp.181–211.

Lieber, M.R. et al., 1997. Tying loose ends: roles of Ku and DNA-dependent protein kinase in the repair of double-strand breaks. *Current Opinion in Genetics and Development*, 7, pp.99–104.

Littlewood, T.D. et al., 1995. A modified oestrogen receptor ligand-binding domain as an improved switch for the regulation of heterologous proteins. *Nucleic Acids Research*, 23(10), pp.1686–1690.

Llambi, F. et al., 2011. A Unified Model of Mammalian BCL-2 Protein Family Interactions at the Mitochondria. *Molecular Cell*, 44, pp.517–531.

Lomax, M.E., Folkes, L.K. & O'Neill, P., 2013. Biological Consequences of Radiation-induced DNA Damage: Relevance to Radiotherapy. *Clinical Oncology*, 25, pp.578–585.

Lovly, C., Horn, L. & Pao, W., 2015a. EGFR in Non-Small Cell Lung Cancer (NSCLC). *My Cancer Genome*. Available at: http://www.mycancergenome.org/content/disease/lung-cancer/egfr/ [Accessed September 22, 2015].

Lovly, C., Horn, L. & Pao, W., 2015b. KRAS in Non-Small Cell Lung Cancer (NSCLC). *My Cancer Genome*. Available at: http://www.mycancergenome.org/content/disease/lung-cancer/kras/ [Accessed September 22, 2015].

Lynch, T.J. et al., 2004. Activating Mutations in the Epidermal Growth Factor Receptor Underlying Responsiveness of Non-Small-Cell Lung Cancer to Gefitinib. *The New England Journal of Medicine*, 350(21), pp.2129–2139.

Ma, Y. et al., 2002. Hairpin Opening and Overhang Processing by an Artemis/DNA-Dependent Protein Kinase Complex in Nonhomologous End Joining and V(D)J Recombination. *Cell*, 108, pp.781–794.

Ma, Y., Cress, W.D. & Haura, E.B., 2003. Flavopiridol-induced Apoptosis Is Mediated through Up-Regulation of E2F1 and Repression of Mcl-1. *Molecular Cancer Therapeutics*, 2, pp.73–81.

Maemondo, M. et al., 2010. Gefitinib or Chemotherapy for Non-Small-Cell Lung Cancer with Mutated EGFR. *The New England Journal of Medicine*, 362(25), pp.2380–2388.

Mao, Z. et al., 2008. Comparison of nonhomologous end joining and homologous recombination in human cells. *DNA Repair*, 7(10), pp.1765–1771.

Marais, R. et al., 1995. Ras recruits Raf-1 to the plasma membrane for activation by tyrosine phosphorylation. *The EMBO journal*, 14(13), pp.3136–3145.

Martin, S.J. et al., 1995. Early Redistribution of Plasma Membrane Phosphatidylserine Is a General Feature of Apoptosis Regardless of the Initiating Stimulus: Inhibition by Overexpression of Bcl-2 and Abl. *The Journal of Experimental Medicine*, 182, pp.1545–1556.

Maurer, U. et al., 2006. Glycogen Synthase Kinase-3 Regulates Mitochondrial Outer Membrane Permeabilization and Apoptosis by Destabilization of MCL-1. *Molecular Cell*, 21, pp.749–760.

Mayer, B.J. et al., 1993. A Putative Modular Domain Present in Diverse Signaling Proteins. *Cell*, 73, pp.629–630.

Mazin, A. V. et al., 2010. Rad54, the motor of homologous recombination. *DNA Repair*, 9, pp.286–302.

Meek, K. et al., 2004. The DNA-dependent protein kinase: the director at the end. *Immunological Reviews*, 200, pp.132–141.

Meiler, J. et al., 2012. Individual dose and scheduling determine the efficacy of combining cytotoxic anticancer agents with a kinase inhibitor in non-small-cell lung cancer. *Journal of Cancer Research and Clinical Oncology*, 138, pp.1385–1394.

Mielgo, A. et al., 2011. A MEK-independent role for CRAF in mitosis and tumor progression. *Nature Medicine*, 17(12), pp.1641–1645.

Mikula, M. et al., 2001. Embryonic lethality and fetal liver apoptosis in mice lacking the c-raf- 1 gene. *The EMBO Journal*, 20(8), pp.1952–1962.

Mimori, T. & Hardin, J.A., 1986. Mechanism of Interaction between Ku Protein and DNA. *The Journal of Biological Chemistry*, 261(22), pp.10375–10379.

Mitsudomi, T. et al., 2010. Gefitinib versus cisplatin plus docetaxel in patients with non-small-cell lung cancer harbouring mutations of the epidermal growth factor receptor (WJTOG3405): an open label, randomised phase 3 trial. *The Lancet Oncology*, 11, pp.121–128.

Mladenov, E. & Iliakis, G., 2011a. Induction and repair of DNA double strand breaks: The increasing spectrum of non-homologous end joining pathways. *Mutation Research/Fundamental and Molecular Mechanisms of Mutagenesis*, 711, pp.61–72.

Mladenov, E. & Iliakis, G., 2011b. The Pathways of Double-Strand Break Repair. In F. Storici, ed. *DNA Repair - On the Pathways to Fixing DNA Damage and Errors*. InTech, pp. 143–168.

Mok, T.S. et al., 2009. Gefitinib or Carboplatin-Paclitaxel in Pulmonary Adenocarcinoma. *The New England Journal of Medicine*, 361(10), pp.947–957.

Moldoveanu, T. et al., 2014. Many players in BCL-2 family affairs. *Trends in Biochemical Sciences*, 39(3), pp.101–111.

Moldoveanu, T. et al., 2006. The X-Ray Structure of a BAK Homodimer Reveals an Inhibitory Zinc Binding Site. *Molecular Cell*, 24, pp.677–688.

Morgan, M.A. et al., 2014. Improving the Efficacy of Chemoradiation with Targeted Agents. *Cancer Discovery*, 4, pp.280–291.

Morrison, D.K. et al., 1993. Identification of the Major Phosphorylation Sites of the Raf-1 Kinase. *The Journal of Biological Chemistry*, 268(23), pp.17309–17316.

Mortensen, U.H., Lisby, M. & Rothstein, R., 2009. Rad52. *Current Biology*, 19(16), pp.R676–R677.

Motoyama, N. et al., 1995. Massive Cell Death of Immature Hematopoietic Cells and Neurons in Bcl-x-Deficient Mice. *Science (New York, N.Y.)*, 267, pp.1506–1510.

Moynahan, M.E. et al., 1999. Brca1 Controls Homology-Directed DNA Repair. *Molecular Cell*, 4, pp.511–518.

Muchmore, S.W. et al., 1996. X-ray and NMR structure of human BCL-xL, an inhibitor of programmed cell death. *Nature*, 381, pp.335–341.

Nakano, K. & Vousden, K.H., 2001. PUMA, a Novel Proapoptotic Gene, Is Induced by p53. *Molecular Cell*, 7, pp.683–694.

Nassar, N. et al., 1995. The 2.2 A crystal structure of the Ras-binding domain of the serine/threonine kinase c-Raf1 in complex with Rap1A and a GTP analogue. *Nature*, 375, pp.554–560.

Nicoletti, I. et al., 1991. A rapid and simple method for measuring thymocyte apoptosis by propidium iodide staining and flow cytometry. *Journal of Immunological Methods*, 139, pp.271–279.

Nikjoo, H., Charlton, D.E. & Goodhead, D.T., 1994. Monte Carlo track structure studies of energy deposition and calculation of initial DSB and RBE. *Advances in Space Research*, 14(10), pp.161–180.

Nikjoo, H. & Goodhead, D.T., 1991. Track structure analysis illustrating the prominent role of low-energy electrons in radiobiological effects of low-LET radiations. *Physics in Medicine and Biology*, 36(2), pp.229–238.

Nimonkar, A. V. et al., 2008. Human exonuclease 1 and BLM helicase interact to resect DNA and initiate DNA repair. *PNAS*, 105(44), pp.16906–16911.

O'Neill, E. et al., 2004. Role of the Kinase MST2 in Suppression of Apoptosis by the Proto-Oncogene Product Raf-1. *Science*, 306, pp.2267–2270.

Oda, E. et al., 2000. Noxa, a BH3-Only Member of the Bcl-2 Family and Candidate Mediator of p53-Induced Apoptosis. *Science*, 288, pp.1053–1058.

Olive, P.L., 1998. The Role of DNA Single- and Double-Strand Breaks in Cell Killing by Ionizing Radiation. *Radiation Research*, 150, pp.S42–S51.

Oltersdorf, T. et al., 2005. An inhibitor of Bcl-2 family proteins induces regression of solid tumours. *Nature*, 435, pp.677–681.

Paez, J.G. et al., 2004. EGFR Mutations in Lung Cancer: Correlation with Clinical Response to Gefitinib Therapy. *Science*, 304, pp.1497–1500.

Pao, W. et al., 2004. EGF receptor gene mutations are common in lung cancers from “never smokers” and are associated with sensitivity of tumors to gefitinib and erlotinib. *PNAS*, 101(36), pp.13306–13311.

Pao, W. & Girard, N., 2011. New driver mutations in non-small-cell lung cancer. *The Lancet Oncology*, 12, pp.175–180.

Paull, T.T. & Gellert, M., 1998. The 3’ to 5' Exonuclease Activity of Mre11 Facilitates Repair of DNA Double-Strand Breaks. *Molecular cell*, 1, pp.969–979.

Peddaboina, C. et al., 2012. The downregulation of Mcl-1 via USP9X inhibition sensitizes solid tumors to Bcl-xl inhibition. *BMC Cancer*, 12(541), pp.1–12.

Perrault, R. et al., 2004. Backup Pathways of NHEJ Are Suppressed by DNA-PK. *Journal of Cellular Biochemistry*, 92, pp.781–794.

Petermann, E. et al., 2010. Hydroxyurea-Stalled Replication Forks Become Progressively Inactivated and Require Two Different RAD51-Mediated Pathways for Restart and Repair. *Molecular Cell*, 37, pp.492–502.

Petros, A.M. et al., 2001. Solution structure of the antiapoptotic protein bcl-2. *PNAS*, 98(6), pp.3012–3017.

Petros, A.M., Olejniczak, E.T. & Fesik, S.W., 2004. Structural biology of the Bcl-2 family of proteins. *Biochimica et Biophysica Acta*, 1644, pp.83–94.

Pierce, A.J. et al., 2001. Ku DNA end-binding protein modulates homologous repair of double-strand breaks in mammalian cells. *Genes and Development*, 15, pp.3237–3242.

Pignon, J.-P. et al., 2008. Lung Adjuvant Cisplatin Evaluation: A Pooled Analysis by the LACE Collaborative Group. *Journal of Clinical Oncology*, 26(21), pp.3552–3559.

Pirollo, K.F. et al., 1997. Evidence Supporting a Signal Transduction Pathway Leading to the Radiation-Resistant Phenotype in Human Tumor Cells. *Biochemical and Biophysical Research Communications*, 230, pp.196–201.

Pogorzelski, M. et al., 2014. Impact of human papilloma virus infection on the response of head and neck cancers to anti-epidermal growth factor receptor antibody therapy. *Cell Death & Disease*, 5(e1091), pp.1–9.

Pritchard, C.A. et al., 1996. Post-natal lethality and neurological and gastrointestinal defects in mice with targeted disruption of the A-Raf protein kinase gene. *Current Biology*, 6(5), pp.614–617.

Ranger, A.M., Malynn, B.A. & Korsmeyer, S.J., 2001. Mouse models of cell death. *Nature Genetics*, 28, pp.113–118.

Rapp, U.R. et al., 1983. Structure and biological activity of v-raf, a unique oncogene transduced by a retrovirus. *PNAS*, 80, pp.4218–4222.

Rass, E. et al., 2009. Role of Mre11 in chromosomal nonhomologous end joining in mammalian cells. *Nature Structural & Molecular Biology*, 16(8), pp.819–824.

Ravi, R. et al., 2006. Resistance of Cancers to Immunologic Cytotoxicity and Adoptive Immunotherapy via X-linked Inhibitor of Apoptosis Protein Expression and Coexisting Defects in Mitochondrial Death Signaling. *Cancer Research*, 66(3), pp.1730–1739.

Rinkenberger, J.L. et al., 2000. Mcl-1 deficiency results in peri-implantation embryonic lethality. *Genes and Development*, 14, pp.23–27.

Riva, C. et al., 1995. Differential c-myc, c-jun, c-raf and p53 Expression in Squamous Cell Carcinoma of the Head and Neck: Implication in Drug and Radioresistance. *Oral Oncology, European Journal of Cancer*, 31B(6), pp.384–391.

Rosell, R. et al., 2012. Erlotinib versus standard chemotherapy as first-line treatment for European patients with advanced EGFR mutation-positive non-small-cell lung cancer (EURTAC): a multicentre, open-label, randomised phase 3 trial. *The Lancet Oncology*, 13, pp.239–246.

Rosidi, B. et al., 2008. Histone H1 functions as a stimulatory factor in backup pathways of NHEJ. *Nucleic Acids Research*, 36(5), pp.1610–1623.

Roskoski Jr., R., 2010. RAF protein-serine/threonine kinases: Structure and regulation. *Biochemical and Biophysical Research Communications*, 399, pp.313–317.

Ross, G.M., 1999. Induction of cell death by radiotherapy. *Endocrine-Related Cancer*, 6, pp.41–44.

Rothkamm, K. et al., 2003. Pathways of DNA Double-Strand Break Repair during the Mammalian Cell Cycle. *Molecular and Cellular Biology*, 23(16), pp.5706–5715.

Rudin, C.M. et al., 2012. Phase II Study of Single-Agent Navitoclax (ABT-263) and Biomarker Correlates in Patients with Relapsed Small Cell Lung Cancer. *Clinical Cancer Research*, 18(11), pp.3163–3169.

Rushworth, L.K. et al., 2006. Regulation and Role of Raf-1/B-Raf Heterodimerization. *Molecular and Cellular Biology*, 26(6), pp.2262–2272.

Saintigny, Y. et al., 2001. A novel role for the Bcl-2 protein family: specific suppression of the RAD51 recombination pathway. *The EMBO Journal*, 20(10), pp.2596–2607.

Sallmyr, A., Tomkinson, A.E. & Rassool, F. V., 2008. Up-regulation of WRN and DNA ligase IIIalpha in chronic myeloid leukemia: consequences for the repair of DNA double-strand breaks. *Blood*, 112(4), pp.1413–1423.

Salomoni, P. et al., 1998. Expression of Constitutively Active Raf-1 in the Mitochondria Restores Antiapoptotic and Leukemogenic Potential of a Transformation-deficient BCR/ABL Mutant. *The Journal of Experimental Medicine*, 187(12), pp.1995–2007.

Sancar, A. et al., 2004. Molecular Mechanisms of Mammalian DNA Repair and the DNA Damage Checkpoints. *Annual Review of Biochemistry*, 73, pp.39–85.

Sartori, A.A. et al., 2007. Human CtIP promotes DNA end resection. *Nature*, 450, pp.509–514.

Sattler, M. et al., 1997. Structure of Bcl-xL-Bak Peptide Complex: Recognition Between Regulators of Apoptosis. *Science*, 275, pp.983–986.

Schlesinger, P.H. et al., 1997. Comparison of the ion channel characteristics of proapoptotic BAX and antiapoptotic BCL-2. *PNAS*, 94, pp.11357–11362.

Seltzer, S.M. et al., 2011. Fundamental Quantities And Units For Ionizing Radiation (Revised). *Journal of the ICRU*, 11(1), pp.1–35.

Sherr, C.J., 2001. The INK4a/ARF network in tumour suppression. *Nature reviews. Molecular Cell Biology*, 2, pp.731–737.

Shigematsu, H. et al., 2005. Clinical and Biological Features Associated With Epidermal Growth Factor Receptor Gene Mutations in Lung Cancers. *Journal of the National Cancer Institute*, 97(5), pp.339–346.

Shrivastav, M., De Haro, L.P. & Nickoloff, J.A., 2008. Regulation of DNA double-strand break repair pathway choice. *Cell Research*, 18, pp.134–147.

Simmons, M.J. et al., 2008. Bfl-1/A1 functions, similar to Mcl-1, as a selective tBid and Bak antagonist. *Oncogene*, 27, pp.1421–1428.

Sirbu, B.M. & Cortez, D., 2013. DNA Damage Response : Three Levels of DNA Repair Regulation. *Cold Spring Harbor Perspectives in Biology*, 5, pp.1–16.

Sleeth, K.M. et al., 2007. RPA Mediates Recombination Repair During Replication Stress and Is Displaced from DNA by Checkpoint Signalling in Human Cells. *Journal of Molecular Biology*, 373, pp.38–47.

Soh, J. et al., 2009. Oncogene Mutations, Copy Number Gains and Mutant Allele Specific Imbalance (MASI) Frequently Occur Together in Tumor Cells. *PLoS ONE*, 4(10), pp.1–13.

Song, L. et al., 2005. Mcl-1 regulates survival and sensitivity to diverse apoptotic stimuli in human non-small cell lung cancer cells. *Cancer Biology & Therapy*, 4(3), pp.267–276.

Sotiropoulou, P.A. et al., 2010. Bcl-2 and accelerated DNA repair mediates resistance of hair follicle bulge stem cells to DNA-damage-induced cell death. *Nature Cell Biology*, 12(6), pp.572–582.

Stamato, T.D. & Denko, N., 1990. Asymmetric Field Inversion Gel Electrophoresis: A New Method for Detecting DNA Double-Strand Breaks in Mammalian Cells. *Radiation Research*, 121, pp.196–205.

Stanton Jr., V.P. et al., 1989. Definition of the Human raf Amino-Terminal Regulatory Region by Deletion Mutagenesis. *Molecular and Cellular Biology*, 9(2), pp.639–647.

Stöhlmacher-Williams, J., 2012. First-Line Therapy of Mutated Non-Small Cell Lung Cancer: An Update. *Onkologie*, 35, pp.293–299.

Stolz, C. et al., 2008. Targeting Bcl-2 family proteins modulates the sensitivity of B-cell lymphoma to rituximab-induced apoptosis. *Blood*, 112(8), pp.3312–3321.

Stracker, T.H. & Petrini, J.H.J., 2011. The MRE11 complex: starting from the ends. *Nature reviews. Molecular Cell Biology*, 12, pp.90–103.

Strasser, A., Huang, D.C.S. & Vaux, D.L., 1997. The role of the bcl-2/ced-9 gene family in cancer and general implications of defects in cell death control for tumourigenesis and resistance to chemotherapy. *Biochimica et Biophysica Acta*, 1333, pp.F151–F178.

Suzuki, M., Youle, R.J. & Tjandra, N., 2000. Structure of Bax: Coregulation of Dimer Formation and Intracellular Localization. *Cell*, 103, pp.645–654.

Swenberg, J.A. et al., 2011. Endogenous versus Exogenous DNA Adducts: Their Role in Carcinogenesis, Epidemiology, and Risk Assessment. *Toxicological Sciences*, 120(S1), pp.S130–S145.

Symington, L.S. & Holloman, W.K., 2008. Resolving Resolvases: The Final Act? *Molecular Cell*, 32, pp.603–604.

Takata, M. et al., 1998. Homologous recombination and non-homologous end-joining pathways of DNA double-strand break repair have overlapping roles in the maintenance of chromosomal integrity in vertebrate cells. *The EMBO Journal*, 17(18), pp.5497–5508.

Tan, N. et al., 2011. Navitoclax Enhances the Efficacy of Taxanes in Non-Small Cell Lung Cancer Models. *Clinical Cancer Research*, 17(6), pp.1394–1404.

Thomas, L.W., Lam, C. & Edwards, S.W., 2010. Mcl-1; the molecular regulation of protein function. *FEBS Letters*, 584, pp.2981–2989.

Thorslund, T. & West, S.C., 2007. BRCA2: a universal recombinase regulator. *Oncogene*, 26, pp.7720–7730.

Trivigno, D. et al., 2012. Deubiquitinase USP9x Confers Radioresistance through Stabilization of Mcl-1. *Neoplasia*, 14(10), pp.893–904.

Tse, C. et al., 2008. ABT-263: A Potent and Orally Bioavailable Bcl-2 Family Inhibitor. *Cancer Research*, 68(9), pp.3421–3428.

Tsujimoto, Y. et al., 1984. Cloning of the Chromosome Breakpoint of Neoplastic B Cells with the t(14;18) Chromosome Translocation. *Science*, 226, pp.1097–1099.

Tsujimoto, Y. & Shimizu, S., 2000. VDAC regulation by the Bcl-2 family of proteins. *Cell Death and Differentiation*, 7, pp.1174–1181.

Turrisi, A.T. et al., 1999. Twice-daily compared with once-daily thoracic radiotherapy in limited small-cell lung cancer treated concurrently with cisplatin and etoposide. *The New England Journal of Medicine*, 340(4), pp.265–271.

Uren, R.T. et al., 2007. Mitochondrial permeabilization relies on BH3 ligands engaging multiple prosurvival Bcl-2 relatives, not Bak. *The Journal of Cell Biology*, 177(2), pp.277–287.

Verkaik, N.S. et al., 2002. Different types of V(D)J recombination and end-joining defects in DNA double-strand break repair mutant mammalian cells. *European Journal of Immunology*, 32, pp.701–709.

Vermes, I. et al., 1995. A novel assay for apoptosis. Flow cytometric detection of phosphatidylserine expression on early apoptotic cells using fluorescein labelled Annexin V. *Journal of Immunological Methods*, 184, pp.39–51.

Virsik-Köpp, P. et al., 2003. Role of DNA-PK in the process of aberration formation as studied in irradiated human glioblastoma cell lines M059K and M059J. *International Journal of Radiation Biology*, 79(1), pp.61–68.

Vlahovic, G. et al., 2014. A phase I safety and pharmacokinetic study of ABT-263 in combination with carboplatin/paclitaxel in the treatment of patients with solid tumors. *Investigational New Drugs*, 32, pp.976–984.

Wagner, T.D. & Yang, G.Y., 2010. The Role of Chemotherapy and Radiation in the Treatment of Locally Advanced Non-Small Cell Lung Cancer (NSCLC). *Current Drug Targets*, 11, pp.67–73.

Wang, H. et al., 2003. Biochemical evidence for Ku-independent backup pathways of NHEJ. *Nucleic Acids Research*, 31(18), pp.5377–5388.

Wang, H. et al., 2001. Efficient rejoining of radiation-induced DNA double-strand breaks in vertebrate cells deficient in genes of the RAD52 epistasis group. *Oncogene*, 20, pp.2212–2224.

Wang, M. et al., 2011. EGF Receptor Inhibition Radiosensitizes NSCLC Cells by Inducing Senescence in Cells Sustaining DNA Double-Strand Breaks. *Cancer Research*, 71(19), pp.6261–6269.

Wang, M. et al., 2006. PARP-1 and Ku compete for repair of DNA double strand breaks by distinct NHEJ pathways. *Nucleic Acids Research*, 34(21), pp.6170–6182.

Wang, Q. et al., 2008. Bcl2 Negatively Regulates DNA Double-Strand-Break Repair through a Nonhomologous End-Joining Pathway. *Molecular Cell*, 29, pp.488–498.

Ward, J.F., 1990. The yield of DNA double-strand breaks produced intracellularly by ionizing radiation: a review. *International Journal of Radiation Biology*, 57(6), pp.1141–1150.

Warenius, H.M. et al., 1994. C-raf-1 Proto-oncogene Expression Relates to Radiosensitivity Rather Than Radioresistance. *European Journal of Cancer*, 30A(3), pp.369–375.

Warenius, H.M. et al., 1998. Late G1 accumulation after 2 Gy of gamma-irradiation is related to endogenous Raf-1 protein expression and intrinsic radiosensitivity in human cells. *British Journal of Cancer*, 77(8), pp.1220–1228.

Warenius, H.M., Jones, M.D. & Thompson, C.C.M., 1996. Exit from G2 Phase after 2 Gy Gamma Irradiation Is Faster in Radiosensitive Human Cells with High Expression of the RAF1 Proto-oncogene. *Radiation research*, 146, pp.485–493.

Wei, G. et al., 2012. Chemical Genomics Identifies Smal-Molecule MCL-1 Repressors and BCL-xL as a Predictor of MCL1 Dependency. *Cancer Cell*, 21(4), pp.547–562.

Wei, M.C. et al., 2000. tBID, a membrane-targeted death ligand, oligomerizes BAK to release cytochrome c. *Genes and Development*, 14, pp.2060–2071.

Weir, B.A. et al., 2007. Characterizing the cancer genome in lung adenocarcinoma. *Nature*, 450, pp.893–898.

Wellbrock, C., Karasarides, M. & Marais, R., 2004. The RAF proteins take centre stage. *Nature reviews. Molecular Cell Biology*, 5, pp.875–885.

Wesarg, E. et al., 2007. Targeting BCL-2 family proteins to overcome drug resistance in non-small cell lung cancer. *International Journal of Cancer*, 121, pp.2387–2394.

West, S.C., 2009. The search for a human Holliday junction resolvase. *Biochemical Society Transactions*, 37, pp.519–526.

Wiese, C. et al., 2002. Gene Conversion Is Strongly Induced in Human Cells by Double-strand Breaks and Is Modulated by the Expression of BCL-xL. *Cancer Research*, 62, pp.1279–1283.

Willis, S.N. et al., 2007. Apoptosis Initiated When BH3 Ligands Engage Multiple Bcl-2 Homologs, Not Bax or Bak. *Science*, 315, pp.856–859.

Willis, S.N. et al., 2005. Proapoptotic Bak is sequestered by Mcl-1 and Bcl-xL, but not Bcl-2, until displaced by BH3-only proteins. *Genes and Development*, 19, pp.1294–1305.

Wittinghofer, A. & Nassar, N., 1996. How Ras-related proteins talk to their effectors. *Trends in Biochemical Sciences*, 21, pp.488–491.

Wojnowski, L. et al., 1997. Endothelial apoptosis in Braf-deficient mice. *Nature genetics*, 16, pp.293–297.

Wold, M.S., 1997. Replication protein A: A Heterotrimeric, Single-Stranded DNA-Binding Protein Required for Eukaryotic DNA Metabolism. *Annual Review of Biochemistry*, 66, pp.61–92.

Woods, D. et al., 1997. Raf-Induced Proliferation or Cell Cycle Arrest Is Determined by the Level of Raf Activity with Arrest Mediated by p21Cip1. *Molecular and Cellular Biology*, 17(9), pp.5598–5611.

Wu, W., Wang, M., Mussfeldt, T., et al., 2008. Enhanced Use of Backup Pathways of NHEJ in G2 in Chinese Hamster Mutant Cells with Defects in the Classical Pathway of NHEJ. *Radiation research*, 170, pp.512–520.

Wu, W., Wang, M., Wu, W., et al., 2008. Repair of radiation induced DNA double strand breaks by backup NHEJ is enhanced in G2. *DNA Repair*, 7, pp.329–338.

Wyllie, A.H., Kerr, J.F.R. & Currie, A.R., 1980. Cell Death: The Significance of Apoptosis. *International Review of Cytology*, 68, pp.251–306.

Yang, T., Kozopas, K.M. & Craig, R.W., 1995. The Intracellular Distribution and Pattern of Expression of Mcl-1 Overlap with, but Are Not Identical to, Those of Bcl-2. *The Journal of Cell Biology*, 128(6), pp.1173–1184.

Yecies, D. et al., 2010. Acquired resistance to ABT-73 in lymphoma cells that upregulate of Mcl1 and BFL-1. *Blood*, 115(16), pp.3304–3313.

Yoon, J.-H. et al., 2002. Bile Acids Inhibit Mcl-1 Protein Turnover via an Epidermal Growth Factor Receptor/Raf-1-dependent Mechanism. *Cancer Research*, 62, pp.6500–6505.

Yu, H. a. et al., 2013. Analysis of Tumor Specimens at the Time of Acquired Resistance to EGFR-TKI Therapy in 155 Patients with EGFR-mutant Lung Cancers. *Clinical Cancer Research*, 19(8), pp.2240–2247.

Zamzami, N. et al., 1998. Subcellular and submitochondrial mode of action of Bcl-2-like oncoproteins. *Oncogene*, 16, pp.2265–2282.

Zamzami, N. & Kroemer, G., 2001. The mitochondrion in apoptosis: how Pandora's box opens. *Nature reviews. Molecular Cell Biology*, 2, pp.67–71.

Zegerman, P. & Diffley, J.F.X., 2009. DNA replication as a target of the DNA damage checkpoint. *DNA Repair*, 8, pp.1077–1088.

Zha, J. et al., 1996. Serine Phosphorylation of Death Agonist BAD in Response to Survival Factor Results in Binding to 14-3-3 not BCL-XL. *Cell*, 87, pp.619–628.

Zhai, D. et al., 2006. Comparison of chemical inhibitors of antiapoptotic Bcl-2-family proteins. *Cell Death and Differentiation*, 13, pp.1419–1421.

Zhang, B., Gojo, I. & Fenton, R.G., 2002. Myeloid cell factor−1 is a critical survival factor for multiple myeloma. *Blood*, 99(6), pp.1885–1893.

Zhang, H. et al., 2011. Mcl-1 is critical for survival in a subgroup of non-small-cell lung cancer cell lines. *Oncogene*, 30, pp.1963–1968.

Zhou, B.-B.S. & Elledge, S.J., 2000. The DNA damage response: putting checkpoints in perspective. *Nature*, 408, pp.433–439.

Zhuang, H. et al., 2014. Progress of clinical research on targeted therapy combined with thoracic radiotherapy for non-small-cell lung cancer. *Drug Design, Development and Therapy*, 8, pp.667–675.

Zong, W.-X. et al., 2001. BH3-only proteins that bind pro-survival Bcl-2 family members fail to induce apoptosis in the absence of Bax and Bak. *Genes and Development*, 15, pp.1481–1486.

Zou, H. et al., 1997. Apaf-1, a Human Protein Homologous to C. elegans CED-4, Participates in Cytochrome c-Dependent Activation of Caspase-3. *Cell*, 90, pp.405–413.

8 Appendix

8.1 Supplementary figures

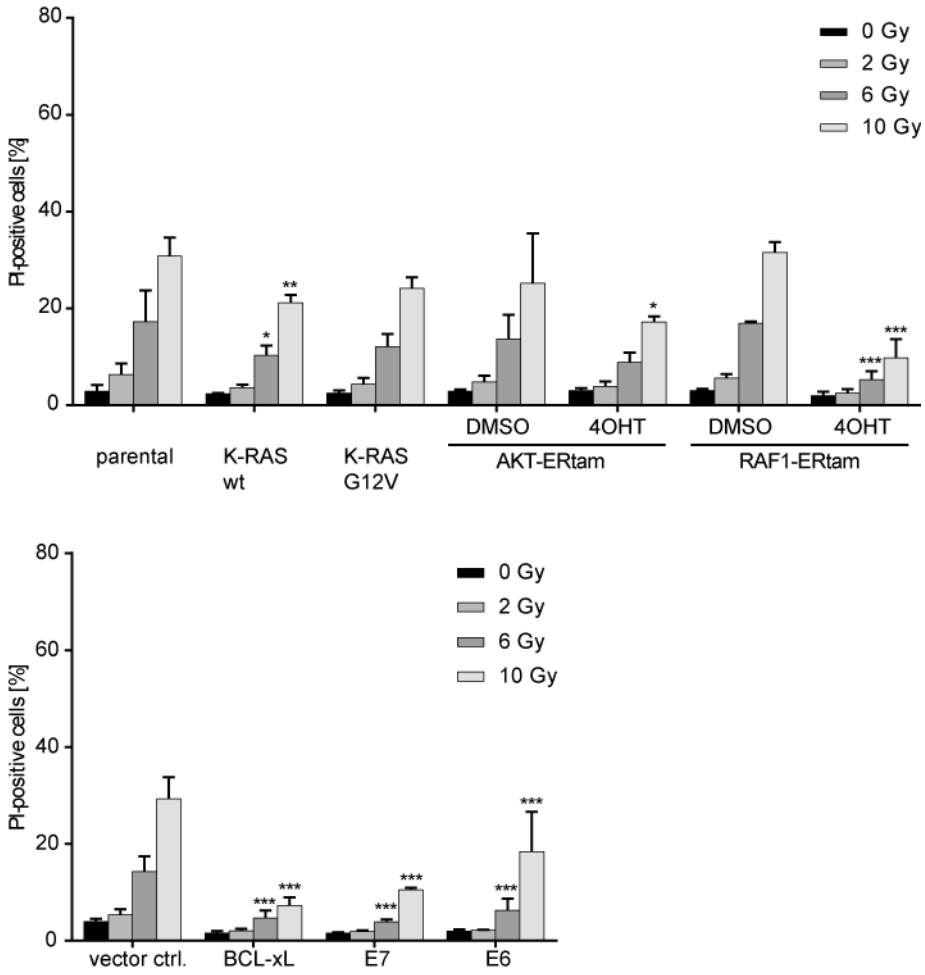

Figure S 1: Impact of different transgenes on irradiation-induced cell death (48 h). A431 cells stably expressing indicated transgenes were stained with PI 48 h after irradiation with indicated doses (0 – 10 Gy) and the fraction of PI-positive cells was determined by flow cytometry (mean + SD, n = 3). * p ≤0.05, ** p ≤0.01, *** p ≤0.001.

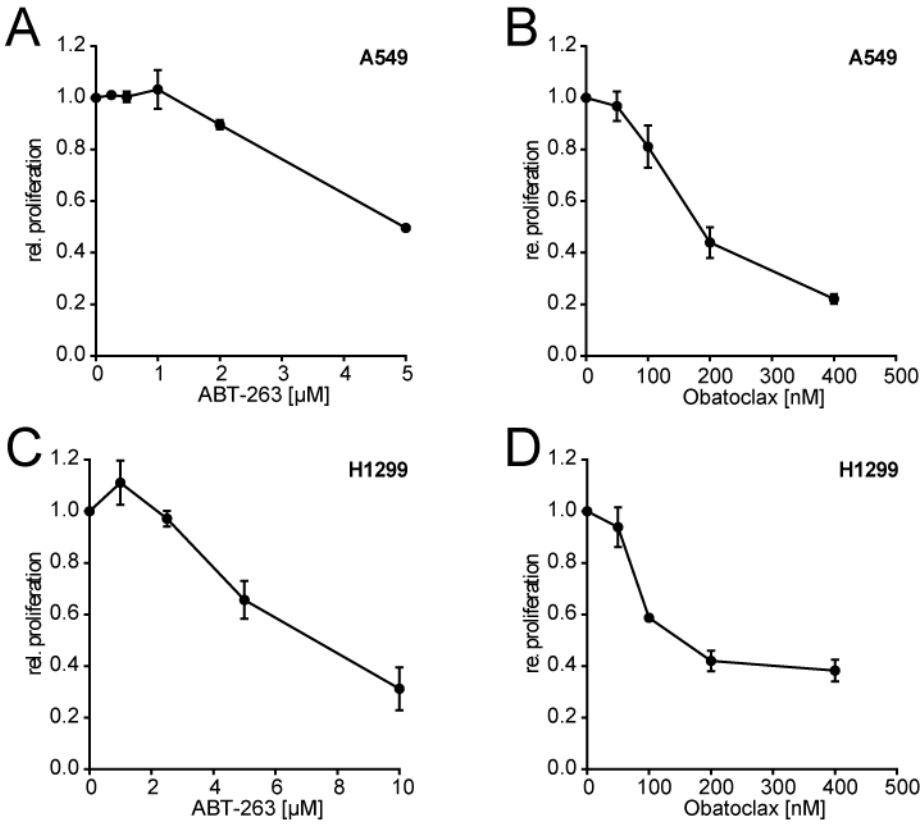

Figure S 2: Treatment with ABT-263 and Obatoclax. (A, B) Relative proliferation of A549 cells treated with different concentrations of ABT-263 (A) or Obatoclax (B) was measured by MTT assay in comparison to non-treated cells after 72 h (mean + SD, n = 2). **(C, D)** Relative proliferation of H1299 cells treated with different concentrations of ABT-263 (C) or Obatoclax (D) was measured by MTT assay in comparison to non-treated cells after 72 h (mean + SD, n = 2).

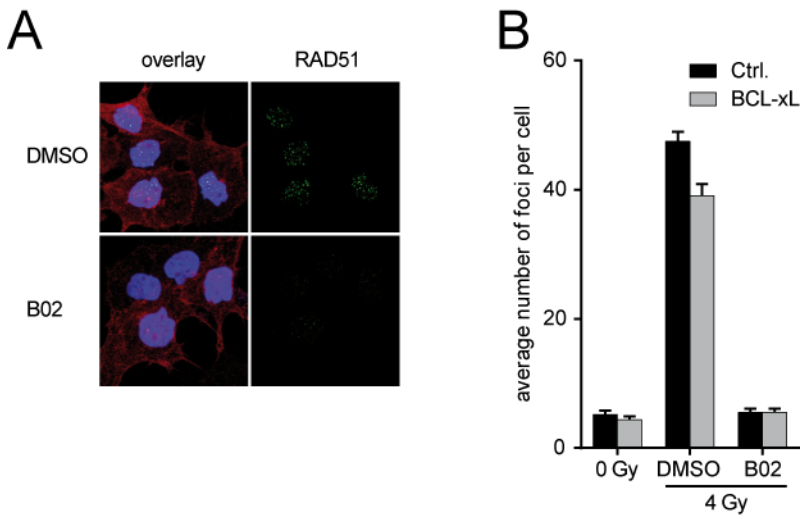

Figure S 3: Validation of decrease of RAD51 foci after B02 treatment. A431 cells stably expressing BCL-xL or empty vector control were pre-treated with 50 µM B02 or DMSO for 1 h before irradiation with 4 Gy. After 3 h, cells were fixed and immunostaining was performed to visualize RAD51 foci and Cyclin B1. **(A)** Representative images of control cells (blue: DAPI, red: Cyclin B1, green: RAD51). **(B)** Quantification of Rad51 foci in Cyclin B1-positive cells (S/G2 cells).

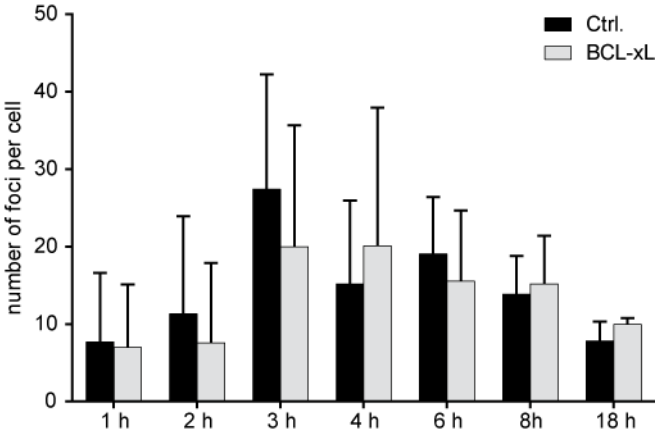

Figure S 4: RAD51 foci formation upon irradiation. A431 cells stably expressing BCL-xL or empty vector control were irradiated with 4 Gy or sham irradiation and fixed at indicated time points (1 – 18 h). Immunostaining was performed to visualize RAD51 foci and Cyclin B1. Numbers of Rad51 foci were only counted in Cyclin B1-positive cells (S / G2 cells).

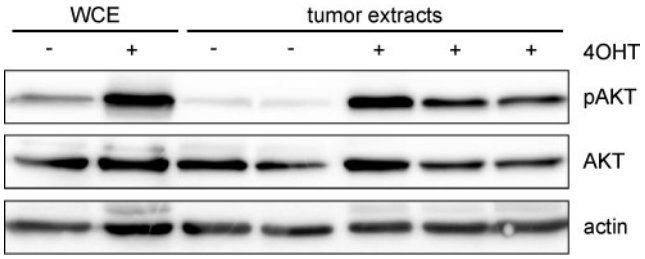

Figure S 5: AKT activation in tumor xenografts. NOD/SCID mice received subcutaneous injections of A431 cells stably transduced with AKT-1-ER^{tam} expression vector. At day 4 after injection, one group was fed with tamoxifen diet to induce AKT activation for 11 d. Expression of proteins in extracts from tumors was measured by immunoblotting and compared to whole cell extracts (WCE), actin served as a loading control.

8.2 Materials

8.2.1 Cell lines and bacteria

8.2.1.1 General cell lines

cell lines	source
A431	DSMZ, Braunschweig, Germany
A549	Schuler lab, University Hospital Essen, Germany
FNX	Nolan lab, Stanford University, USA
H1299	Schuler lab, University Hospital Essen, Germany
HEK293T	DSMZ, Braunschweig, Germany

8.2.1.2 Stably transduced cell lines

cell lines	abbreviation	source
A431 [pBabePuro]	A431 [Puro]	established in this project
A431 [pBabePuro_bcl-xL]	A431 [BCL-xL]	established in this project
A431 [pBabePuro_Δraf-1-Ertam]	A431 [Raf-1-Ertam]	established in this project
A431 [pBabePuro_K-RAS_G12V]	A431 [K-RAS_G12V]	S. Kasper
A431 [pBabePuro_K-RAS_WT]	A431 [K-RAS_wt]	S. Kasper
A431 [pLKO.1-puro_scrambled]	A431 [shRNA scr.]	established in this project
A431 [pLKO.1-puro_TRCN0000005514]	A431 [shRNA MCL-1_1]	P. Craigmile
A431 [pLKO.1-puro_TRCN0000005515]	A431 [shRNA MCL-1_2]	P. Craigmile
A431 [pLKO.1-puro_TRCN0000005516]	A431 [shRNA MCL-1_3]	P. Craigmile
A431 [pLKO.1-puro_TRCN0000005517]	A431 [shRNA MCL-1_4]	P. Craigmile
A431 [pLKO.1-puro_TRCN0000005518]	A431 [shRNA MCL-1_5]	P. Craigmile
A431 [pLKO.1-puro_TRCN0000033499]	A431 [shRNA BCL-xL_1]	established in this project
A431 [pLKO.1-puro_TRCN0000033500]	A431 [shRNA BCL-xL_2]	established in this project
A431 [pLKO.1-puro_TRCN0000033501]	A431 [shRNA BCL-xL_3]	established in this project
A431 [pLKO.1-puro_TRCN0000033502]	A431 [shRNA BCL-xL_4]	established in this project
A431 [pLKO.1-puro_TRCN0000033503]	A431 [shRNA BCL-xL_5]	established in this project
A431 [pMx-pie-Mcl-1]	A431 [MCL-1]	S. Kasper
A431 [pQC_HPV16-E7_IN]	A431 [E7]	M. Pogorzelski
A431 [pQC_mAkt-HA-Ertam_IP]	A431 [AKT-Ertam]	S. Kasper
A431 [QCXIN_HPV16_E6]	A431 [E6]	M. Pogorzelski

cell lines	abbreviation	source
A549 [pLKO.1-puro_scrambled]	A549 [shRNA scr.]	established in this project
A549 [pLKO.1-puro_TRCN0000005514]	A549 [shRNA MCL-1_1]	P. Craigmile
A549 [pLKO.1-puro_TRCN0000005515]	A549 [shRNA MCL-1_2]	P. Craigmile
A549 [pLKO.1-puro_TRCN0000005516]	A549 [shRNA MCL-1_3]	P. Craigmile
A549 [pLKO.1-puro_TRCN0000005517]	A549 [shRNA MCL-1_4]	P. Craigmile
A549 [pLKO.1-puro_TRCN0000005518]	A549 [shRNA MCL-1_5]	P. Craigmile
A549 [pLKO.1-puro_TRCN0000033499]	A549 [shRNA BCL-xL_1]	established in this project
A549 [pLKO.1-puro_TRCN0000033500]	A549 [shRNA BCL-xL_2]	established in this project
A549 [pLKO.1-puro_TRCN0000033501]	A549 [shRNA BCL-xL_3]	established in this project
A549 [pLKO.1-puro_TRCN0000033502]	A549 [shRNA BCL-xL_4]	established in this project
A549 [pLKO.1-puro_TRCN0000033503]	A549 [shRNA BCL-xL_5]	established in this project
A549 [pQC_rtTA-M2_IP, pRevTRE_BAK]	A549 [tet_BAK]	S. Hoffarth
A549 [pQC_rtTA-M2_IP]	A549 [rtTA]	S. Hoffarth
H1299 [pLKO.1-puro_scrambled]	H1299 [shRNA scr.]	established in this project
H1299 [pLKO.1-puro_TRCN0000005514]	H1299 [shRNA MCL-1_1]	P. Craigmile
H1299 [pLKO.1-puro_TRCN0000005515]	H1299 [shRNA MCL-1_2]	P. Craigmile
H1299 [pLKO.1-puro_TRCN0000005516]	H1299 [shRNA MCL-1_3]	P. Craigmile
H1299 [pLKO.1-puro_TRCN0000005517]	H1299 [shRNA MCL-1_4]	P. Craigmile
H1299 [pLKO.1-puro_TRCN0000005518]	H1299 [shRNA MCL-1_5]	P. Craigmile
H1299 [pLKO.1-puro_TRCN0000033499]	H1299 [shRNA BCL-xL_1]	established in this project
H1299 [pLKO.1-puro_TRCN0000033500]	H1299 [shRNA BCL-xL_2]	established in this project
H1299 [pLKO.1-puro_TRCN0000033501]	H1299 [shRNA BCL-xL_3]	established in this project
H1299 [pLKO.1-puro_TRCN0000033502]	H1299 [shRNA BCL-xL_4]	established in this project
H1299 [pLKO.1-puro_TRCN0000033503]	H1299 [shRNA BCL-xL_5]	established in this project

8.2.2 qPCR primers

gene	sequence (5' → 3')	supplier
Actin	sense: GGATTCCTATGTGGGCG antisense: GGCGTACAGGGATAGC	Eurofins MWG
E6	sense: TTGCTTTTCGGGATTTATGC antisense: CAGGACACAGTGGCTTTTGA	Eurofins MWG
E7	sense: CAGCTCAGAGGAGGAGGATG antisense: GCCCATTAACAGGTCTTCCA	Eurofins MWG

8.2.3 Plasmids

8.2.3.1 Packaging plasmids

plasmid name	function	origin
Hit60 (MLV gag-pol)	retroviral polymerase	C. Benedict
pCMV.VSV-G	retroviral envelope	W. Nishioka
pMD2	lentiviral envelope	Scholl/Fröhling – Ulm
pSPAX	lentiviral polymerase	Scholl/Fröhling – Ulm

8.2.3.2 Retroviral plasmids of interest

plasmid name	function	origin
pLPC_EGFP	GFP control	M. Schuler
pBabePuro	empty vector control	C. Benedict
pBabePuro_bcl-xL	BCL-xL overexpression	J. Goldstein
pBabePuro_Δraf-1-Ertam	conditional RAF1 activation	S. Cook

8.2.3.3 Lentiviral plasmids of interest

plasmid name	function	origin
pHRST-ires-GFP	GFP control	J.-S. Lee
pLKO.1-puro_scrambled	shRNA scrambled	Scholl/Fröhling – Ulm
pLKO.1-puro_TRCN0000005514	shRNA MCL-1_1	P. Hähnel
pLKO.1-puro_TRCN0000005515	shRNA MCL-1_2	P. Hähnel
pLKO.1-puro_TRCN0000005516	shRNA MCL-1_3	P. Hähnel
pLKO.1-puro_TRCN0000005517	shRNA MCL-1_4	P. Hähnel
pLKO.1-puro_TRCN0000005518	shRNA MCL-1_5	P. Hähnel
pLKO.1-puro_TRCN0000033499	shRNA BCL-xL_1	Sigma-Aldrich

plasmid name	function	origin
pLKO.1-puro_TRCN0000033500	shRNA BCL-xL_2	Sigma-Aldrich
pLKO.1-puro_TRCN0000033501	shRNA BCL-xL_3	Sigma-Aldrich
pLKO.1-puro_TRCN0000033502	shRNA BCL-xL_4	Sigma-Aldrich
pLKO.1-puro_TRCN0000033503	shRNA BCL-xL_5	Sigma-Aldrich

8.2.4 Antibodies

8.2.4.1 Primary antibodies for immunoblotting

antibody	species	dilution	source
anti-Mcl-1	rabbit	1:1000	EPITOMICS (#1239-1)
anti-phospho-Akt(Ser473)	rabbit	1:1000	Cell Signaling (#9271)
anti-Ras	rabbit	1:1000	Cell Signaling (#3965)
anti-cRaf	rabbit	1:1000	Cell Signaling (#9422)
anti-phospho-cRaf(Ser338)	rabbit	1:1000	Cell Signaling (#9427)
anti-AKT	rabbit	1:1000	Cell Signaling (#9272)
anti-BCL-xL (54H6)	rabbit	1:1000	Cell Signaling (#2764)
anti-actin (clone C4)	mouse	1:10000	MP Biomedicals (#69100)
anti-Bak	rabbit	1:1000	Upstate (#06-536)

8.2.4.2 Secondary antibodies for immunoblotting

antibody	dilution	source
anti-mouse-HRP	1:2000	Thermo Scientific
anti-rabbit-HRP	1:2000	Thermo Scientific

8.2.4.3 Primary antibodies for immunofluorescence

antibody	species	dilution	source
anti-Rad51 (14B4)	mouse	1:500	GeneTex (GTX70230)
anti-CyclinB1 (H433)	rabbit	1:150	Santa Cruz (sc-752)

8.2.4.4 Secondary antibodies for immunofluorescence

antibody	dilution	source
goat-anti-rabbit-Alexa568	1:400	life technologies
goat-anti-mouse-Alexa488	1:400	life technologies

8.2.5 Kits and Mixes

FITC Annexin V Apoptosis Detection Kit	BD Biosciences (US)
High Pure RNA Isolation Kit	Roche (CH)
Light Cycler ® 480 SYBR Green Master Kit	Roche (CH)
Plasmid Plus Maxi Kit	QIAGEN (NL)
Protein Assay Dye Reagent Concentrate	BioRad (US)
Sorenson's buffer	Gibco, life technologies (US)
Super Signal West Pico system	Thermo Scientific (US)
Transcriptor High Fidelity cDNA Synthesis Kit	Roche (CH)

8.2.6 Cell culture materials

ABT-263 (Navitoclax)	Cayman (US)
ABT-737	Abbott Laboratories (US)
B02	Calbiochem, Merck KgaA (D)
Colcemid	Biochrom, Merck KgaA (D)
Dimethyl sulfoxide (DMSO)	Sigma-Aldrich (US)
DMEM (high glucose, no glutamine)	Gibco, life technologies (US)
Doxycycline	Sigma-Aldrich (US)
DPBS (no calcium, no magnesium)	Gibco, life technologies (US)
FBS	Biochrom, Merck KgaA (D)
4-Hydroxytamoxifen (4OHT)	Sigma-Aldrich (US)
L-Glutamine (200 mM)	Gibco, life technologies (US)
Matrigel (growth factor reduced, phenol red-free)	Corning (US)
NU7441	Tocris Bioscience (US)
Penicillin-Streptomycin (10,000 U/ml)	Gibco, life technologies (US)
Puromycin, Dihydrochloride	Calbiochem, Merck KgaA (D)
RPMI 1640 (no glutamine)	Gibco, life technologies (US)
0.4% Trypan blue	Invitrogen, life technologies (US)
Trypsin-EDTA (0.05%, phenol red)	Gibco, life technologies (US)

8.2.7 Chemicals

3-(4,5-dimethylthiazol-2-yl)-2,5-diphenyltetrazolium bromide (MTT)	Sigma-Aldrich (US)
Acetic acid	Roth (D)
Acrylamide mix Rotiphorese® Gel 30 (37.5:1)	Roth (D)
Ammonium peroxodisulfate	Roth (D)
Boric acid	Roth (D)
Brilliant blue	Roth (D)
Bromophenol blue	Merck KgaA (D)
BSA fraction V	Roth (D)
Calcium chloride ($CaCl_2$)	Roth (D)
Circlegrow ® medium (Capsules)	MP Biomedicals (US)
cOmplete Protease Inhibitor Cocktail	Roche (CH)
Dry milk (blotting grade)	Roth (D)
Entellan®	Merck KgaA (D)
EDTA	Roth (D)
EGTA	Roth (D)
Ethidium bromide	Roth (D)
Gelatin from porcine skin	Sigma-Aldrich (US)
Gelatin from cold water fish skin	Sigma-Aldrich (US)
Giemsa	Roth (D)
Glucose	Roth (D)
Glycerol	Roth (D)
Glycine	Roth (D)
HEPES	Roth (D)
Nonidet® P40 Substitute (NP40)	Fluka, Sigma-Aldrich (US)
Low Melting Agarose	Roth (US)
2-Mercaptoethanol	Sigma-Aldrich (US)
Methanol	J. T. Baker, VWR (US)
N-laurylsarcosine	Merck KgaA (D)
PageRuler Prestained Protein Ladder	Thermo Scientific (US)
Paraformaldehyde	Roth (D)
Phosphatase Inhibitor Cocktail 2/3	Sigma-Aldrich (US)
Ponceau S	Roth (D)
Potassium chloride (KCl)	Roth (D)
PromoFluor Antifade reagent	PromoKine (D)
Propidium iodide	Fluka, Sigma-Aldrich (US)

RNAse A	Sigma-Aldrich (US)
SDS	Roth (Karlsruhe, D)
SeaKem LE Agarose	Lonza (CH)
Sodium chloride (NaCl)	Roth (D)
Sodium citrate	Roth (D)
Sodium hydrogen phosphate	Roth (D)
TEMED	Roth (D)
Tris	Roth (D)
Triton-X100	Roth (D)
Tween20	Roth (D)

8.2.8 Consumables and laboratory equipment

(standard equipment not listed)

ChemiSmart Imaging System	Vilber Lourmat (F)
Co-60 γ-ray machine	Philips (NL)
Countess™ Automated Cell Counter	Invitrogen, life technologies (US)
Countess™ Cell Counting Chamber Slide	Invitrogen, life technologies (US)
Coverslips (20 mm diameter)	VWR (US)
Coverslips (24 mm x 60 mm)	Roth (D)
FC500 Flow Cytometer	Beckman Coulter (US)
Gene Quant Pro spectrophotometer	GE Healthcare (GB)
glass slides (76 x 26 mm)	Roth (D)
microscope slides (cut, color frosted)	VWR (US)
Hybond ECL 0.45 µm nitrocellulose membranes	GE Healthcare (GB)
Leica DMR fluorescence microscope	Leica (D)
LightCycler® 480 System	Roche (CH)
MagNA Lyser Instrument	Roche (CH)
Mini-PROTEAN electrophoresis system	BioRad (US)
Mini-Trans Blot ® Cell tank blot system	BioRad (US)
Minisart ® 0.2 µm filter	Sartorius Stedim Biotech (D)
NanoDrop lite spectrophotometer	Thermo Scientific (US)
Nunc ® cell scraper	Thermo Scientific (US)
Olympus CKX41 microscope	Olympus (JP)
QuantiFire XI camera	Intas (D)
Trans-Blot® Turbo™ Transfer System	BioRad (US)

Typhoon 9410 Imager	GE-Healthcare (GB)
Vanix-T bright field microscope with Vimba Marlin F046B camera	Olympus (JP)
X-ray machine	GE Healthcare (GB)

8.2.9 Material for mouse experiments

Electronic Digital Caliper (VWRI819-0013)	Control Company (US)
NOD/SCID mice	Charles River Laboratories (US)
Tamoxifen Diet (2016, 400), Pellet, irradiated	Harlan (NL)

8.2.10 Software

Adobe Illustrator CS3	Adobe Systems (US)
Adobe Photoshop CS3	Adobe Systems (US)
GraphPad Prism (Version 6)	GraphPad Software (US)
ImageJ	Wayne Rasband (NIH, US)
Image-Quant	GE Healthcare (GB)
Imaris (8.0.2)	Bitplane (CH)
SigmaPlot (Version 13)	Systat Software Inc (US)

8.2.11 Standard buffers

5x transfer buffer

29 g	Tris
14.5 g	Glycine
1.85 g	SDS

adjust pH to 9.0
add A. dest. To 1 l
add 20 % methanol when diluting

5x SDS running buffer

15.1 g	Tris
72 g	Glycine
5 g	SDS

add A. dest. To 1 l

6x SDS loading buffer

600 mM	Tris-HCl, pH 6.8
24 %	SDS
20 %	glycerol
200 mM	2-Mercaptoethanol
0.2 %	Bromophenol blue

NP40 lysis buffer

1 %	NP40
150 mM	NaCl
50 mM	HEPES, pH 7.4
1 mM	EDTA
2 mM	EGTA

add 40 µl/ml cOmplete Protease Inhibitor Cocktail,
10 µl/ml Phosphatase Inhibitor Cocktail 2,
10 µl/ml Phosphatase Inhibitor Cocktail 3

2x HBS

280 mM	NaCl
10 mM	KCl
1.5 mM	Na_2HPO_4
12 mM	glucose
50 mM	HEPES

adjust pH=7.0
filtered with 0.22 µm filter

HFS buffer

5 mg	propidium iodide
100 mg	sodium citrate
100 µl	Triton-X100

add 100 ml A. dest.

Stripping Buffer

62.5 mM	Tris-HCl (pH 6.8)
2 %	SDS

MTT solubilization buffer

0.01 M	HCl (38 %)
10 %	SDS

8.2.12 Standard solutions

stacking gel solution

5 %	acrylamide mix
126 mM	Tris-HCl, pH 6.8
0.1 %	SDS
0.1 %	APS
0.1 %	TEMED

resolving gel solution

10 %	acrylamide mix
380 mM	Tris-HCl pH 8.8
0.1 %	SDS
0.1 %	APS
0.04 %	TEMED

Ponceau S

0.2 %	Ponceau S
5 %	Acetic Acid

Blotto

50 g	dry milk (fat free)
1 %	Tween 20

add 1 l PBS

10x NET-G

1.5 M	NaCl
50 mM	EDTA
500 mM	Tris-HCl, pH 7.5
0.5 %	Tween 20
0.4 %	Gelatin (from porcine skin)

Colony staining solution

0.25 %	Brilliant blue
10 %	Acetic acid
40 %	Methanol

8.2.13 Buffers for PFGE

lysis buffer

10 mM	Tris
100 mM	EDTA
50 mM	NaCl
2 %	N-laurylsarcosine

adjust pH to 7.6
add 0.2 mg/ml protease directly before use

washing buffer

10 mM	Tris
100 mM	EDTA
50 mM	NaCl

adjust pH to 7.6
add 0.1 mg/ml RNAse A directly before use, if necessary

5x TBE

445 mM	Tris
445 mM	boric acid
10 mM	EDTA

8.2.14 Buffers for immunofluorescence

P-Solution

100 mM	Tris-HCl, pH 7.4
50 mM	EDTA
0.5 %	Triton-X100

PBG

0.2 %	Gelatin (from cold water fish skin)
0.5 %	BSA fraction V
	PBS

8.2.15 Buffers for metaphase analysis

hypotonic solution

75 mM	KCl

Carnoy's fixative

3x	methanol
1x	acetic acid

8.3 List of figures

8.4 List of abbreviations

4OHT	4-hydroxytamoxifen
A. dest.	Aqua destillata
alt-EJ	alternative end-joining
ATM	ataxia telangiectasia mutated
ATR	ATM and Rad3-related
ATRIP	ATR-interacting protein
BAD	BCL-2-associated agonist of cell death
BAK	BCL-2 antagonist / killer
BAX	BCL-2-associated X protein
BBC3	BCL-2 binding component 3
BCL-2	B-cell lymphoma 2
BCL-xL	B-cell lymphoma extra-large
BER	base excision repair
BH	BCL-2 homology
BID	BH3 interacting domain death agonist
BLM	Bloom’s syndrome protein
BOK	BCL-2-related ovarian killer
BRCA1	breast cancer 1
CDK	cyclin-dependent kinase
cDNA	complementary deoxyribonucleic acid
c-NHEJ	classical non-homologous end-joining (DNA-PK-dependent)
CR	conserved region
CtIP	C-terminal binding interacting protein
ctrl.	Control
DDR	DNA damage response
DEQ	dose equivalent
D-loop	displacement loop
DMEM	Dulbecco’s modified eagle medium
DMSO	Dimethyl sulfoxide
DNA	deoxyribonucleic acid
DNA-PK	DNA-dependent protein kinase

DNA-PKcs	catalytic subunit of DNA-dependent protein kinase
dNTP	deoxynucleotide
Dox	doxycycline
DPBS	Dulbecco’s phosphate-buffered saline
DSB	double-strand break
EDTA	Ethylenediaminetetraacetic acid
EGFR	epidermal growth factor receptor
ER	estrogen receptor
Exo1	exonuclease 1
FBS	fetal bovine serum
FDR	fraction of DNA released
GFP	green fluorescent protein
GOI	gene of interest
Gy	Gray
H1	histone 1
HRR	homologous recombination repair
IR	ionizing radiation
LET	linear energy transfer
LigIV	ligase IV
MAPK	mitogen-activated protein kinase
MCL-1	myeloid cell leukemia 1
MOMP	mitochondrial outer membrane permeabilization
MRE11	meiotic recombination 11
mRNA	messenger ribonucleic acid
MTT	3-(4,5-Dimethylthiazol-2-yl)-2,5-Diphenyltetrazolium Bromide
NBS1	Nijmegen breakage syndrome 1
NER	nucleotide excision repair
NOD / SCID	non-obese diabetic severe combined immunodeficiency
NSCLC	non-small-cell lung cancer
PARP-1	Poly (ADP-ribose) polymerase 1
PFGE	pulsed-field gel electrophoresis
PI	propidium iodide
PIKK	phosphatidylinositol 3-kinase-related kinase

POI	plasmid of interest
PS	phosphatidylserine
qPCR	quantitative polymerase chain reaction
RAS	rat sarcoma protein
RPA	replication protein A
RPMI	Roswell Park Memorial Institute
RTK	receptor tyrosine kinase
SD	standard deviation
shRNA	short hairpin RNA
SSB	single-strand break
ssDNA	single-stranded DNA
TKI	tyrosine kinase inhibitor
TM	transmembrane
USP9x	ubiquitin-specific protease 9x
WCE	whole cell extract
WRN	Werne syndrome protein
wt	wildtype

9 Acknowledgement

The work reported here was supported by a grant from the *Deutsche Forschungsgemeinschaft* (DFG) within the Research Training Group GRK1739, “Molecular determinants of the cellular radiation response and their potential for response modulation” at the University Duisburg-Essen (Project 8).

I am very grateful to my supervisor, Prof. Dr. Martin Schuler, for giving me the opportunity to perform my PhD project in the Molecular Oncology group at the Department of Medical Oncology at the University Hospital Essen. I would like to thank him for sharing his expertise and knowledge as well as supporting me in scientific and personal matters throughout the last years.

Special thanks also go to Prof. Dr. George Iliakis for mentoring me within the GRK and sharing his brilliant expertise in radiation biology and DNA repair. This inter-professional collaboration really promoted the development of my PhD project.

I would also like to thank Dr. Frank Breitenbücher for his guidance and support in the lab as well as for the critical reading of this thesis. At this point, a great “Thank You” is additionally directed to all other colleagues of the Molecular Oncology group for providing the comfortable working atmosphere and their readiness to help. Especially, I have to mention Jeannette Phasue and Stephanie Meyer: Thank you girls that you did not only support me within all experimental aspects, especially the mouse experiments, but also on a personal level. You always listened to me and made me laugh. I will terribly miss you!

Additionally, I have to thank Phillip Craigmile, who joined my project within the DAAD RISE program for ten weeks in 2014. You helped me a lot to generate the BCL-xL and MCL-1 knockdown cells, which would have taken so much longer without you, and it was a lot of fun to have you in the lab.

Furthermore, I thank all members of the “Iliakis group”, especially Dr. Katja Paul-Konietzko, Dr. Aashish Soni, Vladimir Nikolov, and Marilen Demond, for being supportive in all DNA repair questions and for passing on their secrets in performing DNA repair experiments.

I am also indebted to Prof. Dr. Martin Stuschke and Dr. Ali Sak for giving me the opportunity to irradiate my cells and mice with the cobalt-60 γ-ray machine. Thank you, Michael Groneberg and Kristina Bannik, for giving up your time to supervise my irradiations.

I would also like to thank the speaker, Prof. Dr. Verena Jendrossek, and the coordination team, Dr. Gabriele Siedenburg and Ivonne Schulte, of the GRK1739 for organizing this excellent program. It was a good support to develop my project and I hope that the experiences within the program will be beneficial for my future career. I also thank all other graduate students of the program: it was a lot of fun with you and I wish you all the best for your future!

Above all, I thank my family and friends! Alina Kollmannsperger, thank you so much for always being there for me. I know that I can always rely on you in every aspect of my life and I am very proud of our friendship. And of course, I also thank you for the critical reading of this thesis. Marlene Kalthoff, I am very happy that our friendship exists since our childhood and I know that I can always count on you! Christina Wieczorek, thank you for always having a sympathetic ear for my questions, thoughts, fears, and happy moments. It was good to experience the same by writing our PhD thesis nearly in parallel, as it was always motivating to proceed. Nicolas Wieczorek, thank you for being my little brother, supporting me, and making me laugh. Mum and Dad, thank you for your encouragement, unconditional love, and unceasing support every day. You never gave up promoting me along the way!

10 Curriculum Vitae

Der Lebenslauf ist in der Online-Version aus Gründen des Datenschutzes nicht enthalten.

Der Lebenslauf ist in der Online-Version aus Gründen des Datenschutzes nicht enthalten.

Der Lebenslauf ist in der Online-Version aus Gründen des Datenschutzes nicht enthalten.

11 Declarations

Erklärung:

Hiermit erkläre ich, gem. § 6 Abs. 2, g der Promotionsordnung der Fakultät für Biologie zur Erlangung des Dr. rer. nat., dass ich das Arbeitsgebiet, dem das Thema „Assessment of the impact of deregulated signal transduction pathways on the radiotherapy response of non-small-cell lung cancer“ zuzuordnen ist, in Forschung und Lehre vertrete und den Antrag von Sarah Alexandra Wieczorek befürworte.

Essen, den _____ _____ _____

Name des wissenschaftl. Betreuers/Mitglieds der Universität Duisburg-Essen	Unterschrift d. wissenschaftl. Betreuers/Mitglieds der Universität Duisburg-Essen

Erklärung:

Hiermit erkläre ich, gem. § 7 Abs. 2, d und f der Promotionsordnung der Fakultät für Biologie zur Erlangung des Dr. rer. nat., dass ich die vorliegende Dissertation selbständig verfasst und mich keiner anderen als der angegebenen Hilfsmittel bedient habe und alle wörtlich oder inhaltlich übernommenen Stellen als solche gekennzeichnet habe.

Essen, den _____ _____

Unterschrift des/r Doktoranden/in

Erklärung:

Hiermit erkläre ich, gem. § 7 Abs. 2, e und g der Promotionsordnung der Fakultät für Biologie zur Erlangung des Dr. rer. nat., dass ich keine anderen Promotionen bzw. Promotionsversuche in der Vergangenheit durchgeführt habe, dass diese Arbeit von keiner anderen Fakultät abgelehnt worden ist, und dass ich die Dissertation nur in diesem Verfahren einreiche.

Essen, den _____ _____

Unterschrift des/r Doktoranden/in